Studies of Star Clusters and Stellar Evolution

A Thesis
submitted for the degree of
DOCTOR OF PHILOSOPHY

In
The Faculty of Science
Bangalore University
Bangalore

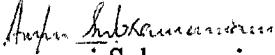By
Annapurni Subramaniam

Indian Institute of Astrophysics
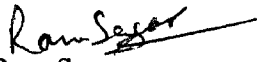## Bangalore 560 034
India

April 1996

Declaration

I hereby declare that the matter contained in this thesis is the result of the investigations carried out by me at the Indian Institute of Astrophysics, Bangalore, under the supervision of Professor Ram Sagar. This work has not been submitted for the award of any degree, diploma, associateship, fellowship, etc. of any university or institute.

Annapurni Subramaniam
(Candidate)

Bangalore 560034
1996 April 22

Certificate

This is to certify that the thesis entitled 'Studies of Star clusters and Stellar evolution' submitted to the Bangalore University by Ms. Annapurni Subramaniam for the award of the degree of Doctor of Philosophy in the faculty of Science, is based on the results of the investigations carried out by her under my supervision and guidance, at the Indian Institute of Astrophysics. This thesis has not been submitted for the award of any degree, diploma, associateship, fellowship, etc. of any university or institute.

Ram Sagar
(Supervisor)

Bangalore 560034
1996 April 22

Acknowledgments

It has been a pleasure to work under Professor Ram Sagar. I am grateful to him for giving me full freedom in research and for his guidance and attention throughout my doctoral work inspite of his hectic schedules. I am indebted to him for his patience in countless reviews and for his contribution of time and energy as my guide in this project. My sincere thanks to him. I am thankful to Dr. H. C. Bhatt for his keen interest in my work and for spending much of his valuable time on discussions and going through all the manuscripts, especially the thesis. I am thankful to Dr. T. P. Prabhu for sharing his knowledge on subtler aspects of observation and reduction techniques.

I am grateful to the Director of the Institute for providing all the facilities needed to complete this project. The computer staff were very helpful and I am grateful to Mr. A. V. Ananth and Mr. J. S. Nathan for allowing me to use ample disk space to store and reduce all the data files. The library personnel were very helpful in providing me with the books and journals that were needed and I am thankful to them. The observing assistants at the 1.02 m and 2.34 m telescopes at the Kavalur Observatory were very helpful during my observing runs and I am grateful to all of them in helping me to collect data, especially, Mr. A. Muniandi and Mr. G. Selvakumar. Mr. S. Perumal was of great help in the computer center at Kavalur and I am grateful to him for all the help extended by him.

I am extremely thankful to Prof. B. C. Chandrasekhara and Prof. C. Raghavendra Rao for their help as the Chairmen of the Physics Department of Bangalore University in speeding up the administrative procedures of the University.

During the early part of this work Y. D. Mayya was of great help and I received many tips about the observations and data reductions. I am thankful to him for this and also for all the useful discussions. I am thankful to G. C. Anupama for her helping me understand the various aspects of spectroscopic reductions, in the early part of this work. I am using this opportunity to thank two of my batchmates Uma Gorti and B. E. Reddy. I have learned a great deal from working with Uma and she had been a good support and friend. So, this is the time to say, "Thank you!". Reddy has been a friend to fight with and to shout at, and I am thankful to him for tolerating my idiosyncracies. Uma and Reddy, thanks for everything. I have enjoyed the company of P. Bhaskaran, R. D. Prabhu,

Abstract

Studies of star clusters are important as they contain valuable information regarding the processes of star formation, stellar evolution and the properties of the host galaxy. Star clusters are the best testing ground for stellar evolutionary theories. We have studied one young and 4 intermediate age open star clusters, NGC 1907, NGC 1912, NGC 2383, NGC 2384 and NGC 6709 in our Galaxy and 4 young populous clusters in the Large Magellanic Cloud (LMC), NGC 1711, NGC 2004, NGC 2164 and NGC 2214. We compare their colour-magnitude diagrams (CMDs) with the theoretical stellar evolutionary models. These were used to find if the inclusion of overshooting in the convective cores of intermediate to high mass (3.0–14.0 $M_\odot$) stars in the stellar evolutionary models is necessary.

The photometric observations of the open clusters are done using the 1.02m and the 2.34m telescopes at the Vainu Bappu Observatory (VBO), Kavalur, India. The clusters NGC 2383 and NGC 2384 are observed in B, V, R and I; NGC 1912 and NGC 6709 in B, V and I and NGC 1907 in B and V passbands. The spectra of some bright stars in four clusters are obtained using the 1.02m telescope. Charge Coupled devices (CCDs) have been used as the detector for both photometric and spectroscopic observations. The initial processing of the CCD data is carried out using the software package, Image Reduction and Analysis Facility (IRAF). The magnitude estimations and transformations to the standard system are done using Dominion Astrophysical Observatory Photometry routine, DAOPHOT II. The spectroscopic data is reduced using IRAF. The spectra are classified with the help of the digital spectral library from Jacoby et al. (1984).

The first CCD photometric observations of the five open clusters are presented here, which consist of magnitude estimates of ~ 3320 stars reaching down to V$\sim$20 mag and spectroscopic observations of 37 stars in 4 open clusters put together. We obtain the cluster CMDs from the photometric observations, which are used to estimate the values of distance and reddening to the clusters. This is done by fitting zero-age main-sequence (ZAMS) to the unevolved main-sequence (MS) of the clusters. The present estimates of reddening are similar to the values

i

obtained by earlier studies, but we estimate larger distances to the clusters. The present data reaches up to ~ 20.0 mag in V, whereas the earlier studies were limited to about ~ 16.0 mag in V. This enables us to fit the ZAMS in a wide range (~ 6 mag) of the cluster MS. Therefore our distance estimates are more accurate. The spectroscopic data are used to identify the probable members from their estimated spectral types and luminosity classes and also to determine the reddening and distance modulus. The present spectroscopic observations identify the presence of an H_α emission line star in NGC 2383, for the first time.

The observations are compared with the stellar evolutionary models from Castellani et al. (1990), Schaller at al. (1992) and Bressan et al. (1993), which consists of two classical and two overshoot models. The comparison of observed CMDs with the models are done in three ways: isochrone fitting, comparison of observed CMDs with the synthetic CMDs and comparison of observed luminosity functions with the ones computed from synthetic CMDs. The isochrones are used to estimate the ages of the clusters and also to compare the fitting of the isochrones to the features of the observed CMDs. The classical models estimate younger ages whereas the overshoot models estimate older ages for the clusters. A code is developed to generate synthetic CMDs from the evolutionary models, which consists of randomly generated stellar masses, weighted by the power law mass function. The stars are assigned the age of the cluster under study and the luminosity and the effective temperature of each star corresponding to its mass, are found from the evolutionary models. The absolute magnitudes and colours are obtained using bolometric corrections and colour transformations. The effects due to binary stars and photometric errors are also included in the code. The synthetic CMDs generated using this code are used to compare the number of stars present in the observed CMDs of open clusters and LMC clusters with the number predicted by the models in various evolutionary phases. The number of stars present in any evolutionary phase is proportional to the time-scale of evolution in that phase. Thus, we compare the ratio of the helium burning to the hydrogen burning time-scale by comparing the integrated luminosity function (ILF) normalised to the number of evolved stars obtained from the cluster CMDs with the ones obtained from the synthetic CMDs.

The clusters studied here consist of intermediate age open clusters and young LMC clusters which corresponds to the turn-off mass in the range 2.8–4.0 $M_\odot$ for 3 open clusters; $\sim$ 12 $M_\odot$ for one cluster and 6.0–14 $M_\odot$ in the case of LMC clusters and hence the evolutionary scenarios discussed here correspond to the above mentioned masses. In the case of intermediate mass range, the differences between the classical and the overshoot models are not very apparent from the isochrone fitting method. The comparison of synthetic CMDs indicates that the overshoot models ought be preferred, but the distinction between the two overshoot models couldn not be made. The comparison of ILFs shows that the value of the time-scale ratio given by the model from Schaller et al. (1992) comes close to the observed one. In the case of high mass stars the method of isochrone fitting does not favour any model, whereas the comparison of the observed CMDs with the synthetic CMDs favours the overshoot models from Bressan et al. (1993). The comparison of ILFs does not favour any model as the computed ILFs could be matched with the ones observed using various combinations of mass function slope and percentage of binary stars. The estimation of mass function slopes shows that the open clusters, NGC 1912 and NGC 6709 and the LMC cluster, NGC 1711, seem to have a steeper value of mass function slope, (x=1.7) compared to the Salpeter value (x=1.35); the open cluster, NGC 2383 and the LMC clusters, NGC 2004, NGC 2164 and NGC 2214 have mass function slopes close to the Salpeter value and the open cluster NGC 2384 has shallower value of mass function slope (x=1.0). The steeper value of NGC 1711 may be due to the presence of slight mass segregation.

The molecular clouds, which are the formation sites of open clusters are known to form more than one cluster in their lifetime. The existence of double/binary clusters in the Magellanic Clouds is fairly well established, whereas only one such pair, h+χ Persei, is known in the Galaxy. From the catalogues of open clusters of the Galaxy, we have identified 18 probable pairs of clusters (with known distances), with spatial separations less than 20 pc. The tidal disruption time-scales for these pairs, due to Galactic differential rotation are calculated, using cluster data where available or by assuming typical values. In some cases, these time-scales are larger than the average open cluster lifetime, $\approx 10^8$ yr. About

8% of open clusters appear to be members of binary systems, and hence binary cluster systems may not be very uncommon in the Galaxy. The clusters, NGC 2383+NGC 2384 are found to be situated at the same distance within the errors of distance estimation. The present age estimates show that they have very dissimilar ages and hence may not be born together. In the case of NGC 1907+NGC 1912, the cluster distances are close and ages are very similar indicating that they might be born together, as their metallicity and radial velocities are also similar. We suggest that this pair is a potential candidate for a double open star cluster.

Contents

Chapter 1

Introduction

A star cluster is a group of dynamically associated stars, presumably created from the same material at about the same time, and consequently, located at the same distance. Star clusters have a major contribution to the understanding of the structure and evolution of the galaxies in the present universe. This mainly came about by the use of star clusters in understanding the theory of stellar evolution and vice versa. Not only did this study lead to the knowledge about star clusters, but also the properties of the stars within a given cluster, taken as a group, indicated surprising new features of individual stars, i.e., how they evolve. Cluster colour-magnitude diagrams (CMDs) are the best testing ground for the stellar evolutionary models. On the other hand, the use of stellar models has improved the understanding of stars in different evolutionary stages in the cluster, like RR Lyrae stars and Cepheids and also in the determination of ages of clusters, which has made it possible to use them as indicators of structure and evolution of our Galaxy. These objects are found to have considerable information regarding the formation and evolution of the host galaxy, for example, the study of globular clusters has revolutionised the understanding of our Galaxy. The star clusters help us to understand external galaxies, where it is not possible to resolve and hence observe the individual stars. In these cases, the integrated properties of the clusters are used to understand the structure, formation and evolution of these galaxies. This has made it possible to extend our knowledge of the star cluster systems in external galaxies. This is a much needed input to understand

1

the processes of star formation and the influence of environment in forming star clusters. Thus the study of star clusters has an important role in the astrophysical research.

1.1 Classification of star clusters

The star clusters, as the name suggests are aggregates of stars. They are identified by the sudden enhancement in the stellar number density compared to the field. Their characteristics mainly depend on the host galaxy. Star clusters are found in all the three components, halo, disk and bulge of our Galaxy. The clusters in our Galaxy can be classified into three types, based on their appearance.

1.1.1 Globular clusters

The clusters which have spherical appearance are called globular clusters. These are very old objects, presumed to be formed first in the Galaxy. Hence the stars populated in these systems are also old and belong to the class known as Population II, which are very metal poor compared to the Sun. Majority of the globular clusters are distributed in a spherical volume around the center of the Galaxy, constituting the halo and the bulge. These contain 10^4–10^5 stars within a diameter of 50–100 pc. The typical stellar density being, 10^3 pc^{-3} at the densest core to 0.5 pc^{-3} in less denser regions. Ages of these objects are about 10–15 billion yrs and hence the mass of individual stars present in them is less than a solar mass. Globular clusters are the ideal objects to study the evolution of Population II stars. Shapley found the distribution of the globular clusters in the Galaxy with the help of RR Lyrae stars in 1915. This led to the realisation of the actual dimensions of the Galaxy (Shapley 1918). Thus these objects are ideal to understand the structure of our Galaxy. The luminosity function (LF) of the integrated magnitudes of globular clusters exhibits a Gaussian LF with a dispersion $\sigma \sim 1.3$ mag (van den Bergh & Lafontaine 1984). This property has been found to be characteristic of the globular cluster systems, irrespective of the host galaxy.

1.1.2   Open clusters

This classification of star clusters is also from their appearance. These are the open clusters, which are moderately denser than the surrounding field. These objects are situated in the disk of the Galaxy and hence are part of the recent activities in the Galactic disk. The stars present in them belong to the Population I class of objects. The first comprehensive study of open clusters and their distribution in the Galaxy was made by Trumpler (1930). The open clusters have a very wide range of age, ranging from almost as old as the disk (a few times 10^9 yr) to 10^6 yr, the age of the new born star cluster from the molecular cloud. As the spiral arms constitute the major part of present day star formation, the very young star clusters are generally found in these regions. Becker (1963b) pointed out the similarity between the distribution of young open clusters in our Galaxy and the appearance of spiral structure in NGC 1232 (Lyngå 1979). Since then many attempts have been made at getting a better picture of the galactic spiral arms by adding more young clusters to the material and by including other types of objects. The old clusters do not seem to occupy any preferred location. There are about 1400 open star clusters known in our Galaxy. These objects contain 50–1000 stars located within a diameter of 5 pc. Typical number density is 0.1–10 pc^{-3}. As the number density suggests, they don't have a core region like globular clusters and in fact it is often difficult to find the center of these objects. The open star clusters house intermediate to low mass stars and are ideal to study the evolution of these stars. The intermediate mass stars are responsible for the chemical enrichment of the interstellar medium (ISM) through their stellar winds and the low mass stars are important as they lock up the mass for longer time-scales. The LF of the integrated magnitudes of open clusters has a form $N(M_V) \propto 10^{0.2M_V}$ (van den Bergh & Lafontaine 1984), where, $N(M_V)$ is the number of clusters with integrated magnitude M_V .

Classification of Open clusters

The open star clusters, also known as galactic clusters as they populate the galactic disk, are further classified by Trumpler (1930) and Ruprecht (1966) according

to their appearance. They used a combination of roman numerals I to IV to indicate decreasing central concentration, the numbers 1 to 3 to indicate the range of brightness of stars found in the clusters and the letters p, m and r to indicate the richness class of the cluster. In detail, I indicates that the cluster has a strong concentration with respect to the surrounding field, whereas IV means that it is just a chance clustering. The number 1 means that all stars have approximately equal brightness, 2 means that stellar magnitudes are distributed uniformly over a large range and 3 means that apart from a few bright stars, most of the stars are faint. The letters are used to indicate the number of stars present in the cluster: p (poor) stands for less than 50 stars, m (moderate) for 50–100 stars and r (rich) for more than 100 stars. This classification criterion has a dependence on distance, to the extent that for similar exposure times, a distant cluster would show up with fewer faint stars. On the other hand, the open clusters are also classified according to their Hertzsprung–Russell (H-R) diagram, by Trumpler (1925, 1930). He used the numbers 1 to 3 to quantify the relative proportion of the late type giants, e.g., 1 for clusters with no giants and only main-sequence (MS) stars, 2 for those with small number of giants and mostly MS stars and 3 characterises clusters with most of their bright members in the giant branch. The letters are used to show the earliest spectral type in the MS, i.e., o, b, a and f stands for O, B, A and F spectral types respectively. A slight modification to this classification is introduced by Trumpler & Weaver (1953), by adding the spectral subclass information to the spectral type. This criterion does not depend on the distance and hence is a better classification of the galactic clusters.

1.1.3   OB Associations

The third classification is called the OB associations. These objects are loose groups of massive O and B stars. As these are found very close to the star formation activity, they are excellent tracers of the spiral arms. Many of the open clusters that contain O-type stars also appear to be the nuclei of OB associations. Ambartsumian (1947) was the first to identify these objects. The space density of OB stars in the associations is much less than the gravitational binding mass and thus these are not bound systems. The lifetimes of these systems are only

about 10 Myr due to their loose gravitational binding and the short lifetimes of the constituent O and B stars. On a galactic time-scale, the birth, evolution and death of these O and B stars occur almost instantaneously. Successive generations of these stars are responsible for the rapid alteration of the ISM. These stars destroy the giant molecular clouds (GMCs) through the action of stellar winds and supernova (SN) explosions, and eject processed elements into the ISM. The enrichment of iron peak elements and oxygen in the ISM is mainly due to these stars. In general, these associations have HII regions around them and are therefore easy to identify in the external galaxies.

1.2 H-R diagram and star clusters

It is well known that star clusters are born from molecular clouds and a star cluster is formed out of a single clump in a molecular cloud. This means that all the stars in a cluster are born from the same material. The star formation process lasts for a few million years to form the cluster. For clusters older than about 50 Myr this time-scale can be neglected and hence one can safely assume that all the stars are formed at the same time. Though this is a valid assumption for old to intermediate age clusters, this is not valid for young clusters (age $< 10^7$ yrs). Thus formed clusters have diameter typically of the order of 5 pc. This is quite small compared to the cluster distances of about hundreds of parsecs. Thus all the stars in a cluster can be considered to be located at the same distance. They, thus suffer the same amount of interstellar absorption and reddening. In short, the stars in a cluster can be considered to have the same age, chemical composition and located at the same distance, the only differing parameter being the individual stellar mass. This makes these objects ideal to study the processes of stellar evolution.

The basic lessons of stellar evolution are from the Hertzsprung-Russell (H-R) diagram which was developed independently by the Danish astronomer E. Hertzsprung in 1911 and the American astronomer H. N. Russell in 1913. H-R diagram displays the relationship between the stellar spectral types and luminosities in a two dimensional plot. The most convenient form of the H-R diagram
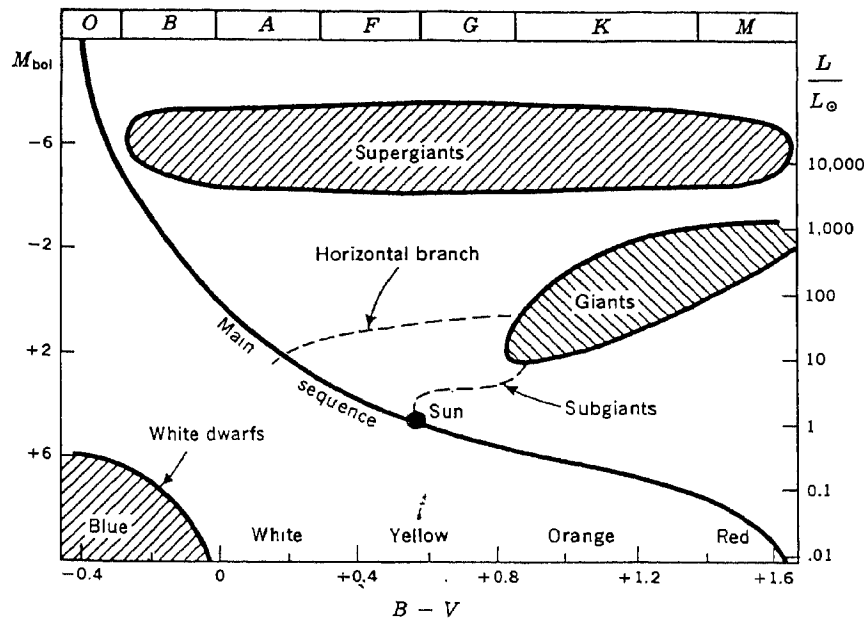
Figure 1.1: *The H-R diagram showing the location of stars in various evolutionary phases.*

for evolutionary analyses is a plot of log $(L/L_\odot)$ versus log (T_{eff}) and this is usually called the theoretical H-R diagram. On the other hand, its most useful observational form is the colour-magnitude diagram (CMD) which is a plot of magnitude versus colour index. The main feature of this diagram is that the stars in different evolutionary stages occupy specific regions in the diagram. This can be seen in Figure 1.1. This figure tell us that the stars are not scattered at random in the H-R diagram. The majority of the stars are found to lie along the MS, which stretches from luminous O stars to cool M stars and these stars are often called dwarfs (MK luminosity class V). The next prominent sequence is the giant branch, which stretches from spectral type G0 at a luminosity about three times brighter than the MS stars of the same type, towards cooler and brighter stars. These stars are called red giants, which correspond to the MK luminosity class III. A few stars seen on top of the diagram are extremely bright stars in all spectral types. These are the supergiants, corresponding to the MK luminosity class I. The region between the MS and giant branch, which is devoid of stars is known as the Hertzsprung gap. A few stars can be seen about 10 mag below the
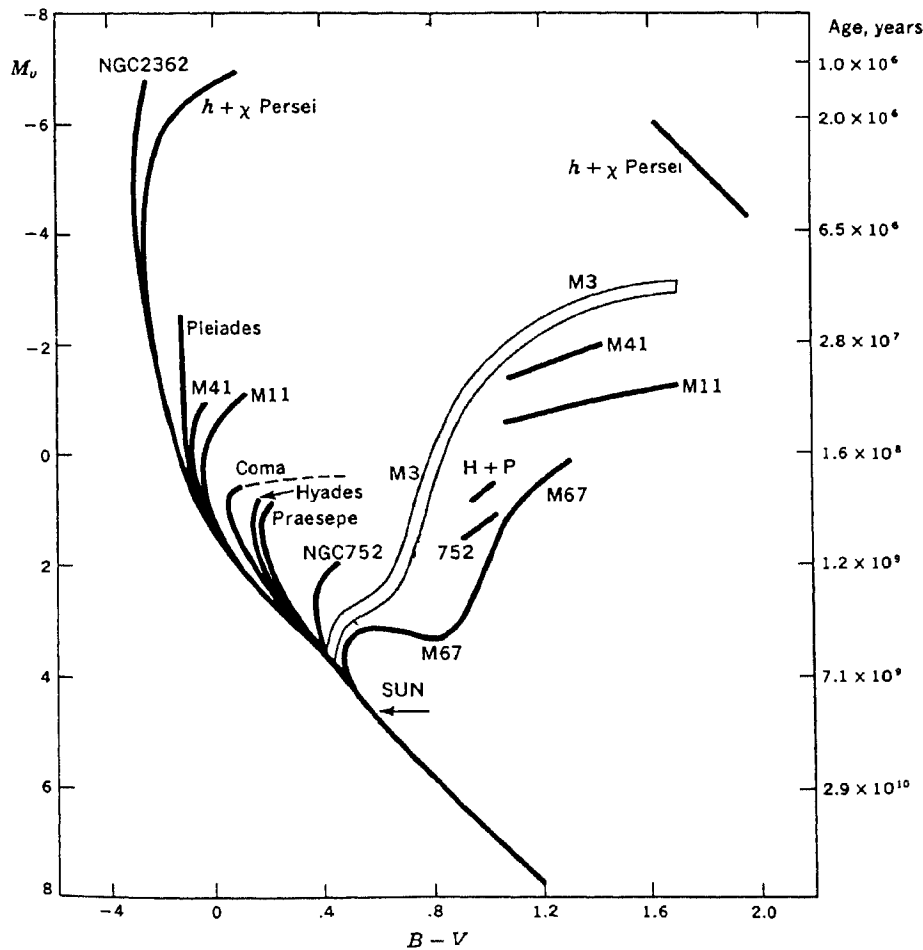
Figure 1.2: *This shows the composite open cluster CMDs of various ages. It can be seen that the turn off magnitude decreases as the age increases.*

MS, these are the hot and faint stars called white dwarfs. H-R diagram thus helps in understanding the evolutionary status of a star once its location in the CMD is known and hence its age. It is thus, one of the best tools to check the stellar evolutionary theories. The evolutionary theory predicts the location of stars in various evolutionary stages in this plane. In order to check the theory, one needs to compare the diagram calculated from the theory with the one obtained observationally. For this, one needs to observe very many stars, find their individual values of distance, reddening, metallicity and place them in the H-R diagram. This is not an easy task as the distance, reddening and metallicity estimates of individual field stars are difficult.

The cluster CMDs have a well defined MS extending up to an upper limit of brightness (see figure 1.2). This upper limit is created by the evolution of stars brighter than the limit on to the red giant phase. In young clusters, one can see a few supergiants across a wide Hertzsprung gap and a group of M supergiants. In intermediate age clusters, the MS terminates at a lower brightness and a red giant branch can be seen separated from the MS by a narrower Hertzsprung gap and no supergiants. Thus, what a cluster CMD presents is a snapshot of stellar evolution at different time-scales. This is what is actually needed to test the stellar evolutionary theories. The stellar evolutionary theories predict the luminosities and the effective temperatures of a star of mass m, at different ages. These are called the stellar evolutionary tracks. Now, if we find the locus of stars with different masses having the same age, it is called an isochrone. Isochrones thus define the locus of stars with different masses for a particular age. Thus, the cluster CMD is nothing but an isochrone corresponding to the cluster age.

1.3   Stellar evolution

The stars as they are born from the molecular cloud, are initially in the state of contraction on Kelvin-Helmholtz time-scale. In this stage the star is fully convective and occupies the right side of the H-R diagram. Once the central region of the star attains the temperature high enough to start the fusion reactions of hydrogen, it settles on the left hand side of the H-R diagram. This is the MS location of the star. Normally the time-scale needed to reach the MS is very small compared to its lifetime as a MS star. For high mass stars, this time-scale is very less ($< 10^6$ yr), whereas that for low mass stars are more ($> 10^7$ yr). At the same time, the MS lifetimes of low mass stars are much higher than the high mass stars. Thus the stars in the MS can be considered as new born or having age equal to zero. The location of stars of all masses in the MS is therefore called the zero-age MS (ZAMS).

1.3.1 Low mass stars

The MS stars have a core where the hydrogen fuses to form helium and the temperature is of the order of a few 10^6 K. The temperature of the material surrounding the core drops towards the surface of the star. The energy generated in the core is transported to the surface mainly through radiative energy transfer. The MS star is in hydrodynamic equilibrium. Though most of the energy transport is through radiation, in many conditions and in different regions of the star, convective energy transport also takes place. At any given point inside the star, one needs to know when the material in that region is unstable to convection. In general, at a given point, if the radiative temperature gradient (∇_{rad}) exceeds the adiabatic temperature gradient (∇_{adb}), then it is unstable to convection. This happens in stars of all masses due to different reasons. In the case of cool stars, the convective instability occurs in the envelopes resulting in convective envelopes. Here, the (∇_{rad}) increases due to the sudden increase in the absorption coefficient of hydrogen, as the temperature there is just right for the hydrogen to start ionising. In the core of these stars, most of the energy production is due to the proton-proton (PP) chain reaction. The convective instability also occurs in the core of stars more massive than about 1.3 $M_{\odot}$. For stars more massive than this limit, the carbon-nitrogen-oxygen (CNO) cycle starts operating in the core of the star. As the CNO cycle is highly dependent on the temperature, approximately to the 16th power, the energy generation is highly concentrated towards the center of the star. The energy at the very center is produced by both cycles and hence the central temperature rises, thereby increasing the ∇_{rad}. This results in a convective core. These stars have a radiative envelope.

In the convective region, the material is unstable against convection. A small bubble kept in this region rises up to a certain height and mixes with the surrounding, and the height it travels before mixing with the surroundings is called the mixing length l. The parameter used to characterise the pressure gradient is the pressure scale height H, which is the length scale on which the pressure falls by a factor of e. These are the two main parameters used in mixing length theory (MLT) to characterise convection in a given region. The actual value of the ratio l/H is to be determined by the comparison of stellar models with real stars. But,

at the boundary of the convective region, the convective elements reaching the boundary will still have a positive velocity though the force acting on it upwards is zero. Thus the convective elements move a little more into the outer layer before getting decelerated. This is called the convective overshoot. The length scale of overshoot will depend on the temperature gradient and the stability of the outer region. The overshoot of the convective bubbles into the overlying stable region is the reason why we see granulation in the convectively stable solar photosphere. In the case of stars with convective cores, a similar prescription of MLT is used to quantify the mixing in the core. As hydrogen is transformed into helium in the core, the convection mixes the material and keeps the chemical composition uniform. Overshoot of the convective region as mentioned above happens in the convective cores also. Here, the overshoot distance is very important as this determines the mixing of material from outside the convective boundary into the convective core.

As the nuclear fusion continues in the core, more and more hydrogen is converted into helium, resulting in a helium rich core, pushing the fusion to a ring outside the core. This makes the helium rich core shrink and heat up. This state continues till the core becomes a pure helium core containing more than 10 % of the stellar mass. The gravitational contraction of the helium core releases energy, which heats up the base of the nuclear burning shell. This raises the temperature and the CNO cycle becomes more active. The excess pressure thus created lifts the envelope of the star and the star expands. Such an expansion starts while the star is already on the MS, but it becomes more noticeable when the core mass exceeds 10% of the stellar mass (Böhm-Vitense 1992). The expansion of the hydrogen envelope terminates the MS lifetime. The luminosity remains essentially constant while the envelope expands. With increasing radius at constant luminosity, the effective temperature must decrease. The star then moves on to the right side of the H-R diagram along the giant or subgiant branch depending upon the stellar mass. During this time, the shell source is further driven out and a small increase in the mass of the helium core causes a relatively large expansion of the envelope. The star then has a fully convective envelope which extends deep into the stellar interior. The total energy transport in the outer layer is

increased because of the convective energy transport, which is more efficient than the radiative transport by the diffusion of photons. With the increased energy transport outwards, the star is able to keep its surface temperature constant and the star moves up the red giant branch close to the Hayashi track. The luminosity of the star increases, the envelope expands and the helium core grows in mass. During these low surface temperatures in the red giant phase, the convective zone may finally reach down into layers with nuclear processed material and bring it up to the surface. This is called the first dredge up. In stars more massive than the Sun, this dredge up brings out the processed material due to CNO cycle. Enlarged ratios of $^{14}N/^{12}C$ and $^{13}C/^{12}C$ can be expected in the atmosphere of such stars. In this phase these stars loose mass through stellar wind.

When the helium core reaches a size of about 0.45 $M_\odot$, the star appears at the top of the red giant branch in the H-R diagram. At this point the central temperature of the helium core reaches a value of 10^8 K and this is high enough for the triple alpha reaction to take place, where three ^{4}He nuclei combine to form one ^{12}C nucleus. When stars with mass less than 2.25 $M_\odot$ reach the tip of the red giant branch, the helium core becomes completely degenerate. This means that the pressure is due to the degenerate electron pressure and is temperature independent. When the triple alpha reaction starts in the core, it heats up the core whereas the pressure remains the same. This leads to a thermal runaway until the degeneracy is lifted by what is called a helium flash. At this point, the star finds a new equilibrium configuration with an extended non-degenerate helium burning core. This expands the hydrogen burning shell, lowering its temperature. This makes the star shrink and the surface becomes hotter. In the H-R diagram, the star ends up in the lower part of the giant branch, where such stars form the so called clump stars. Stars stay for a relatively longer time in this phase, while they burn helium in their core. This explains the occurence of a number of stars in this phase, resulting in the formation of a clump.

For stars less massive than 0.5 $M_\odot$, the helium core never becomes hot enough to start fusing helium. These stars end up as helium white dwarfs. For stars more massive than about 3 $M_\odot$ the helium core never becomes very degenerate and the helium burning starts slowly in a quasi-equilibrium configuration. These

stars do not experience the helium flash. The helium burning through triple alpha reaction would lead to a carbon core. This pushes the helium burning to a shell and causes the envelope to expand and pushes the star up the red giant branch once again. These stars are called asymptotic giant branch (AGB) stars. During this phase, the stars loose mass on a very large scale, which results in loosing their envelopes at the tip of the AGB phase resulting in the formation of planetary nebulae. The central core becomes a carbon white dwarf.

1.3.2 Intermediate and High mass stars

Just as for low mass stars, the evolution of intermediate and high mass stars is caused by the change in chemical composition when hydrogen fuses to helium. These stars have a convective core such that the newly formed helium is evenly mixed throughout the core. The degree of mixing of helium enriched material to the outer layers is rather uncertain because of semi-convection as well as the unknown amount of convective overshoot and possible other mechanisms. It is important to know the expected changes in stellar evolution if the degree of mixing is larger than that assumed in the model calculations. The stellar evolutionary models incorporating no overshoot mixing outside the convective core and assuming a abundance stratification in the semi-convection zone is called the classical or standard models. The evolutionary models which incorporate the overshooting of the convective core and the resultant increase in the mixing are known as core overshoot models. For increased mixing:

(i) The MS lifetime of a star with a given mass becomes longer because a large amount of hydrogen is fueled into the core due to overshoot mixing, before the shell source develops.

(ii) The luminosity of the giant branch is increased relative to the MS star of a given mass.

(iii) The luminosity of the blue loop is increased even more than the luminosity of the giant branch.

This is explained using the evolutionary tracks in Figure 1.3, where the different evolutionary stages for a star of $5M_\odot$ are computed using overshoot model and
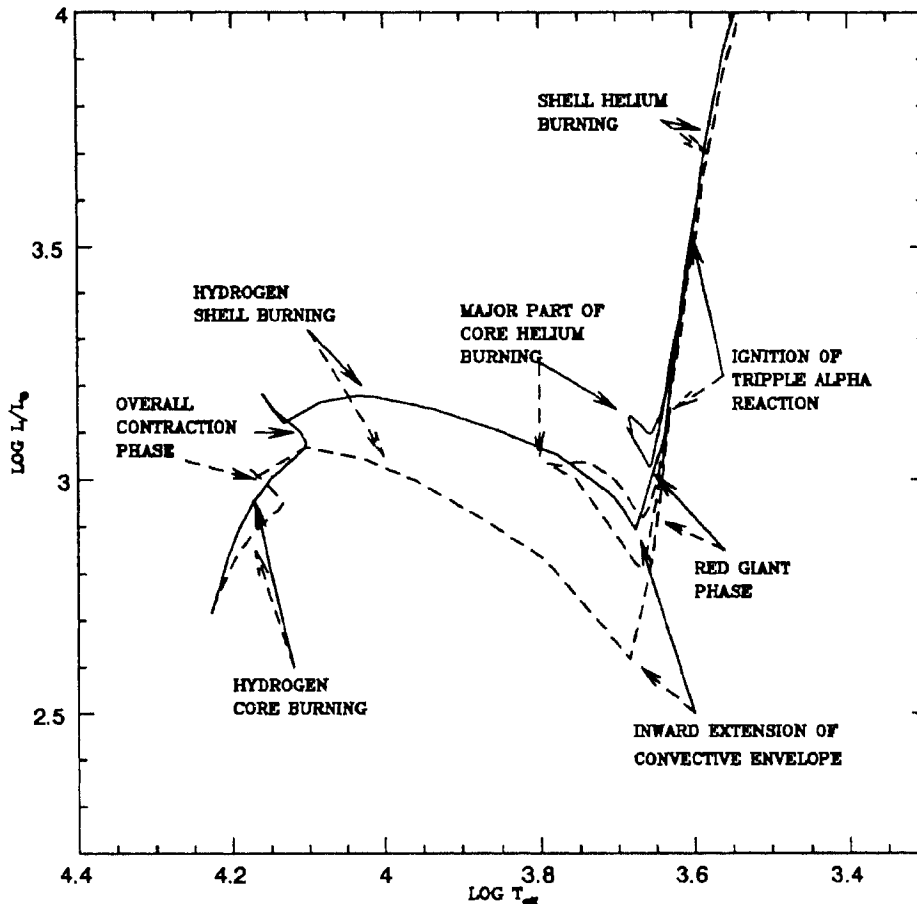
Figure 1.3: *The evolutionary track of a 5 $M_\odot$ star is shown here. The continuous line corresponds to the track with overshooting in the convective core and the dashed line is assuming classical model. Each evolutionary phase is marked in the figure.*

classical model (Bressan et al. 1993) are shown. For overshoot mixing to about 1 scale height above the convective core, the expected mass of a star in a particular evolutionary phase would be lower by about 20 % (Böhm-Vitense 1992). The reduction in the mass increases with the extent of the overshoot.

During the MS phase, while hydrogen is consumed, the convective core contracts and also shrinks in mass. This results in a region outside the convective core, which is slightly enriched in helium and also in the $^{14}N/^{12}C$ and $^{13}C/^{12}C$

ratios. The stars massive than $\sim$ 10 $M_\odot$ loses mass while they are in the MS itself. This is of the order of $\sim$ 10^{-7} $M_\odot$ /yr and results in the decrease of the mass of the star. The life-time of the star increases with increasing mass loss rate (Chiosi & Maeder 1986). As the star develops a hydrogen burning shell around the helium core, just like for the low mass stars, the envelope expands and the star moves in the H-R diagram towards the red giant region. At this phase, an outer convection zone develops and reaches into the deeper layers containing processed materials. This dredges up the processed material to the surface. During the red giant phase, these stars loose large amount of mass and their further evolution depends on the rate of mass loss.

In massive stars, the central densities are lower than in low mass stars, so that even during core contraction, the core does not become degenerate. Therefore, the triple alpha reaction starts smoothly. During these phases, unlike the low mass stars, these stars do not increase their luminosity very much. The helium burning starts in the center, when the helium core contains more than about 0.47 $M_\odot$. At this stage, core expands, the envelope contracts and the T_{eff} increases, resulting in a blue loop in the H-R diagram. Since the conversion of helium to carbon is a slow process, the evolution from the red giant phase to the tip of the blue loop is much slower than the evolution from the MS to the red giant phase. The life time in the central helium burning stage is only few percent of the MS life time. For higher temperatures in the core, carbon can combine with helium nucleus to form ^{16}O. Therefore they have a carbon and oxygen core in the center surrounded by helium burning shell and an outward hydrogen burning shell. For stars in the mass range, 2.25–5 $M_\odot$, the contraction of the core leads to central densities high enough to start electron degeneracy. The onset of ^{12}C burning then leads to a runaway energy generation, until the temperature becomes high enough to remove the degeneracy. It is not yet clear whether the degenerate burning of the carbon could perhaps lead to explosion of the star.

After the carbon is exhausted in the interiors of massive stars, the core further contracts and heats. Nuclear reactions between nuclei with increasing Z can take place, building up heavier and heavier elements, until elements of the iron group like Ni, Fe, Co are formed. At this stage, a star of initial mass $\sim$ 10 $M_\odot$ would

have a central core of iron, surrounded by concentric shells containing silicon, oxygen, neon, carbon, helium and hydrogen. When the mass of the iron core exceeds 1.4 $M_\odot$, the core begins to collapse. This results in the explosion of the star called Supernova (SN). In this process, the matter around the core is thrown out and the central core ends up becoming a neutron star. If the mass of the collapsing core is more than the upper limiting mass of the neutron star (3–5 $M_\odot$), the central core is expected to become a black hole.

1.4 Dynamical evolution of star clusters

The stars in a cluster can be assumed to have been born with virial velocities and the system left to itself will evolve. An isolated system of stars undergoes dynamical evolution, in quasi-equilibrium, due to gravitational encounters between the members. The stars exchange energy through gravitational interactions, and after a certain period of time, the velocity distribution of the system approaches close to a maxwellian distribution. The time-scale over which sum of the changes in the velocity of a typical member becomes of the order of the velocity itself, is called the relaxation time-scale of the star cluster. The relaxation time can be expressed as

$$\tau_{rel} = \frac{8.9 \times 10^5 N^{1/2} r_c^{3/2}}{m^{1/2} log(0.4N)}$$

where N is the number of cluster stars and r_c is the radius containing half of the cluster mass in parsecs (Spitzer & Hart 1971). The relaxation time-scale is larger for large N systems, and smaller number clusters relax in shorter time-scales. The multiple gravitational encounters of the cluster members result in an exchange of energy between them, with the entire cluster evolving towards equipartition. This normally occurs on a relaxation time-scale of the cluster, and the total kinetic energy of the cluster gets redistributed more or less equally among the individual stars. Relaxation also results in the formation of a central dense region and a outer expanding envelope, with further evolution making the core more and more compact and a corresponding expansion of the outer members. The system thus gradually expands with time. In this process, some stars attain velocities more than the escape velocity and they leave the system. Thus the

system loses stars continuously. For a system with a spectrum of stellar masses, equipartition has the additional consequences on the spatial distribution of stars. As all stars have approximately the same kinetic energy, the more massive stars have correspondingly lower velocities while lower mass stars have higher velocities on an average. Thus, the massive stars occupy positions closer to the center of the system. Lower-mass stars on the other hand, move on more extended orbits owing to their larger velocities and thus a spatial segregation of mass is established in the system. Evolved clusters have a central dense concentration of high-mass stars, and an outer envelope of low-mass stars. Mass segregation is in fact observed in all old Galactic clusters, and in globular clusters. Recent observations of young star clusters indicate mass segregation in clusters which are too young to have relaxed dynamically (e.g., Trapezium, NGC 2024, NGC 2071; McCaughrean et al. 1991, Lada 1991: NGC 6530, IC 1805, NGC 6913; Sagar et al. 1988). This could be a consequence of the star formation process itself, which ends in the formation of massive stars closer to the center of the cluster. Gorti & Bhatt (1995) suggest that the mass segregation seen in young protostar clusters is caused by mass dependent dynamical friction acting on the protostellar clumps in molecular clouds, from which they form.

The open clusters lie in the galactic disk and move in circular orbits around the galactic center. Apart from the cluster potential, the individual stars are acted upon by the galactic potential as well. This results in a limiting radius of the cluster, where the gravitational attraction due to the galactic potential exceeds that of the cluster, known as tidal radius. As the cluster expands due to relaxation, the stars with orbital radius more than the tidal radius then do not belong to the cluster anymore. Therefore the cluster loses stars. Among the cluster members, the stars which lie closest to the galactic center move faster while the stars farthest move slower with respect to the center of mass velocity, due to the differential rotation of the galactic disk. This results in the stretching of the cluster and over a time-scale the cluster disrupts. Apart from the galactic tidal forces and the relaxation, other important destruction processes are tidal shocks by interstellar cloud complexes, tidal shocks as clusters pass through the galactic disk and mass loss from evolved stars (Wielen 1975, King 1979). The

approximate lifetime of an open cluster in the galactic disk is estimated to be $\sim 10^8$ yr (Wielen 1984). The age distribution of open clusters (Wielen 1971, VandenBerg 1983) indicates that only about 50% of the clusters survive to an age of $\sim 10^8$ yr, while less than 5% live as long as 10^9 yr. This age distribution of the open star clusters can be satisfactorily explained by a combination of the above mentioned processes (Wielen 1971).

1.5 Mass function

In many applications, as the integrated appearance and effects of a large number of stars are of primary interest, it is important to specify the relative fraction of stars in different mass intervals. The frequency distribution of stellar masses at birth is called the initial mass function (IMF). The IMF can be expressed as a power law by

$$\frac{dN}{dM} = AM^{-(1+x)}$$

where dN is the number of stars in the mass interval dM at mass M and x is the slope of the mass function. Observational determinations of the IMF and its possible variations in space and time provides the fundamental constraint on the theories of star formation. Most stars form in groups within large interstellar cloud structures and the observed IMF constraints information on how mass is partitioned and possibly redistributed among the protostellar cloud fragments, and on the manner in which these processes depend on local and global conditions. A primary method for estimating the stellar mass function is to determine the frequency distribution of luminosities for field stars in the solar neighbourhood, convert this to a mass distribution by adopting a mass-luminosity relation and then correct the distribution for the stars which have died during the history of the disk. This approach was used in the pioneering paper by Salpeter (1955) and he found the value of mass function slope, x to be 1.35.

Star clusters present an excellent opportunity to study the IMF, its possible variations on small spatial scales and with time, possible differences between different types of clusters and between clusters and the field star IMF. The usefulness of clusters arises primarily because all stars are at the same distance and

have the same age. If the formation time is less than the age of the cluster, then their observed LFs below the MS turn-off, directly reflect the IMF without the necessity for birthrate history corrections or stellar lifetimes. For clusters with ages less than the relaxation time-scale, the LFs can be used directly without correcting for the escape of stars due to dynamical evolution. One doesn't need to assume a time-independent IMF as in the case of field stars and in fact, the only way to determine the time-dependence of IMF is to look at star clusters of different age. Thus, most of the numerous problems associated with the field star IMF can be avoided for clusters.

The open star clusters which span a wide range of stellar mass in the MS presents a problem of small number of stars. One way out of this, is to construct composite LFs by combining the data from various clusters. There has been many attempts in this direction, one of them being the LF of 62 clusters by Taff (1974) which spans a mass range of 1–10 $M_\odot$. He finds a value of 1.8 for x. Taff's cluster IMF fits the field star IMF very well in the same mass range. Piskunov (1976) also constructed a composite cluster IMF, using 7000 members of 61 clusters to derive a mean IMF slope of 1.3±0.14 in the mass range 1–25 $M_\odot$ with no evidence for large cluster to cluster differences. Burki (1977) did a similar analysis for 27 open young open clusters. He divided the clusters according to their diameter into small, intermediate and large clusters. The mean slopes of mass functions range between 1.2 to 1.7. A more recent of estimate of the slope of the composite mass function of 8 open clusters by Kjeldsen & Frandsen (1991) find the value to be 1.3±02, which is very close to the Salpeter value.

Among the mass function determinations of individual clusters, Sagar et al.(1986) presented an investigation of 11 young open clusters and the main results were that the average value of the slope is 1.4±0.3 in the mass range 1.25–60 $M_\odot$ and no significant cluster to cluster variation in the value of slope. It thus appears that the young clusters and associations agree fairly well among themselves and with the Taff composite and field star IMF between about 3 and 10 $M_\odot$, but most of the young cluster IMFs are flatter than the adopted field star IMF for $M \geq$ 10 $M_\odot$ (Scalo 1986). In the case of intermediate to old clusters, differences in the slopes as well as turn over in some masses are seen. According to Tarrab

(1982) if one considers only clusters with more than 60 members (10 clusters), the averaged slope is 1.7 in the mass range 1.25–14 $M_\odot$. This is similar to the indices of the field star IMF, Taff's (1974) composite cluster IMF and Burki's (1977) composite IMF for small clusters, for the same mass range. A recent study by Phelps & Janes (1993) on the mass function of 8 clusters show that the average value of the slope is, x = 1.4±0.13 over the mass range 1.4–7.9 $M_\odot$, which is very close to the Salpeter value, but slightly flatter than the slope of Tarrab (1982). The differences among the individual clusters must be a combination of real variations, statistical uncertainties and systematic errors. The establishment of reliable LFs for open clusters is not very easy, incompleteness, contamination by non-members, and radial mass segregation are the most severe effects to content with. To get reliable estimates, much more work on proper motions, radial velocities, and photometry to very faint limits will be required. There may exist variations among the IMFs among clusters and between clusters and field stars and such variations might be expected if the IMF represents a stochastic process.

1.6 Clusters in Magellanic Clouds

Earlier in this chapter, we classified the clusters based on their appearance and properties in our Galaxy. It is worthwhile to look at the clusters in the nearby galaxies also. Such a study might throw light regarding the physical factors which favour the formation of star clusters. Let us consider the Magellanic Clouds (MCs) which belong to the irregular class of galaxies. The advantage with MCs is that we can resolve the individual stars in a cluster in the MCs which is not possible in the case of the other far away neighbouring galaxies. MCs consists of two galaxies, the Large and the Small Magellanic Clouds, situated $\sim$ 50 and 63 kpc away from the Galaxy, respectively.

The MCs provide evidence for the conclusion that mass spectrum of cluster formation differs in different galaxies. In our Galaxy, there exists a clear-cut dichotomy between massive globular clusters and much less massive open clusters. The MCs contain a class of populous star clusters, with masses that are typically an order of magnitude smaller than those of the average globular clusters, but an

order of magnitude larger than those of the most Galactic open clusters, this class is rare or absent in our Galaxy. The old globular clusters seen in MCs are very few and have ages greater than 10 Gyr. The mean absolute magnitude of these objects is identical to that for true globulars in M31 and our Galaxy (van den Bergh 1991). This indicates that the old globulars in MCs are objects of the same type as those in giant spirals. Therefore, the MC clusters either contain three distinct type of clusters - globular clusters, populous clusters and open clusters - of which globular and open clusters are exact counterparts to similar objects in our own Galaxy, or, the globular clusters are physically similar objects in the Galaxy and in the LMC, but the LF (mass spectrum) of open clusters extends to higher luminosities and masses in the Clouds than it does in the Galaxy. The second alternative seems to be probable as the LF of the populous clusters is similar to that of the open clusters in our Galaxy. Both old and young clusters in the MCs have radii, which contains half of the cluster light in projection, typically 3–4 times larger than those of their Galactic counterparts. The Galactic open star clusters are also generally more compact than those in MCs. Many young clusters in MCs are embedded in rich unbound stellar coronae. Stellar coronae around clusters can survive longer in the Clouds than in the Galaxy, because tidal forces are much lower in the Clouds than in the Galaxy. Since the overall density of the MCs is lower than that of the Galaxy, the most plausible explanation of the above observation may be that clusters with small radii are preferentially formed in regions of high density.

Studies of the populous clusters in the MCs are particularly important as they allow one to study the rapid evolutionary phases in the H-R diagram due to their richness, which are unlikely to be observed in the sparser Galactic open clusters. Also most of the cluster in MCs populate a region of age-metallicity plane that is not populated in the open clusters. Hagen & van den Bergh (1974) have pointed out that the stars in the old open clusters in SMC lie on evolutionary tracks that differ systematically from those of stars in Galactic open clusters of similar age. Open clusters in LMC have metallicities and giant branch colours that are intermediate between those of clusters in the Galaxy and in the SMC.

1.7   Aim of the present study

There are two main schemes in theoretical stellar evolutionary models, the classical and the core overshoot. These two schemes predict different sets of evolution for stars due to different input physics. In brief, while classical models possess standard convective cores during the central H-burning phase and may undergo mixing processes like semi-convection and so-called breathing convection only during the central He-burning phase (see Renzini & Fusi Pecci 1988), models allowing for overshoot possess larger convective cores all over their evolutionary history. The differences would affect the evolutionary paths, lifetime ratios among various phases, hence relative number of stars in different areas of the CMD and different LFs for the MS stars (Chiosi et al. 1989). In order to resolve the issue, the predictions by these two schemes should be compared with the observations. The CMDs of star clusters are the classical template to which the stellar models are compared and the CMDs of star clusters of any age prove to be the most direct means of testing stellar models.

Even though the main properties of the CMDs of the star clusters are accounted for by theoretical models, still there are several aspects which are not easily fitted by the evolutionary schemes. In fact, there are clusters that, on the basis of the turn-off mass (1.6–1.8 $M_\odot$), should develop extended red giant branches, whereas they exhibit a red giant population which is characteristic of the turn-off of a more massive star (Barbaro & Pigatto 1984). Furthermore, for a turn off mass of 4–5 $M_\odot$ and canonical efficiency of mass loss, the cluster CMD instead of having a well populated luminous asymptotic giant branch, has few AGB stars (Becker & Mathews 1983). The overall morphology of the CMDs of Galactic clusters in the age range of Pleiades to Hyades (Mermilliod 1981) and of rich young LMC clusters seem to indicate that the relative number of evolved to MS stars and the ratio of blue to red giants are at variance with theoretical expectations (Chiosi et al. 1989). Thus the debate of whether one needs to include a fair amount of overshoot from the convective cores, in the stellar evolutionary models is still on.

The present study aims at getting a set of homogeneous data of intermediate

age, rich open clusters of our Galaxy in order to compare their CMDs with those from the stellar models. The richness of the cluster is important as we need the stars to be populated in various evolutionary stages. In order to identify the observational features sensitive to the core overshooting in the CMDs of star clusters, turn-off masses of stars should lie in the mass range, 1.5–10 $M_\odot$. The effects of core overshoot are difficult to identify in stars with mass less than 1.5 $M_\odot$, due to their very small core and stars with mass above 10 $M_\odot$ loose mass in the MS itself, making a direct comparison between the observation and theory difficult. If we consider very young clusters (age $\leq 10^7$ yr), we encounter problems of low mass stars still in the pre-MS phase and the presence of differential reddening across the cluster. The old clusters (age $\geq 10^9$ yr) have dynamical relaxation times smaller than their ages and hence would have lost stars due to relaxation. In the case of intermediate age clusters (age around 10^8 yr), they would not have relaxed dynamically and these clusters are not generally seen to have differential reddening. Consequently, we have chosen, NGC 1912, NGC 1907, NGC 2383 and NGC 6709 for the present study. The cluster NGC 2384 lies very close to NGC 2383, which prompts us to include this young cluster also, in the present study.

The simplistic way to compare the observations with models is to compare the cluster CMDs with the isochrones from the stellar models. This relates the shape of the MS turn-off, red giant branch etc., of the observed CMDs with the isochrones. A better way is to compare the ratios of evolutionary time-scales, which is not possible through isochrones. The method we have adopted for this purpose is to compute synthetic CMDs from the stellar models. A computer code has been developed for constructing synthetic CMDs and luminosity functions as a function of cluster age, chemical composition, initial mass function and total number of stars. The algorithm allows for age dispersion, fluctuations in the stochastic nature in the IMF, binary stars and observational errors in magnitudes and colours.

The comparison of the synthetic CMDs and the open cluster CMDs can be done only to a limited extent due to the poor number statistics in various evolutionary phases. The LMC clusters contain more stars and therefore good number of stars can be seen in various evolutionary phasea, thereby reducing the effects

due to statistical fluctuations. We extend the comparison of stellar models to the young LMC clusters, NGC 1711, NGC 2004, NGC 2164 and NGC 2214.

1.8 Outline of the present study

Though there are about 1400 open star clusters known in our Galaxy, the clusters with distances known are only about 400 (Lyngå 1987), and similar is the state with the other cluster parameters like age, reddening etc. Also, most of the clusters studied are through photographic or photoelectric photometry which have their own limitations. The CMDs thus obtained terminate at relatively large brightness levels and hence the evolutionary features may not be brought out properly, especially in the case of old clusters. Thus a deeper and systematic study of galactic open clusters is attempted here in view of comparing with the stellar evolutionary models. We present here the first CCD observations of five open clusters, NGC 1912, NGC 1907, NGC 2383, NGC 2384 and NGC 6709. These clusters are observed using 102cm and 234cm telescopes at Vainu Bappu Observatory in Kavalur. The clusters NGC 2383 and NGC 2384 are observed in B, V, R and I; NGC 1912 and NGC 6709 are observed in B, V and I and NGC 1907 in B and V passbands. Low resolution spectra ($\sim$ 250 Å /mm) of some of the bright members are obtained using these telescopes. The details of the detectors, observations and reductions are described in Chapter 2. The observed CMDs of the clusters are presented in Chapter 3. The CMDs in the V vs (B$-$V), V vs (V$-$R) and V vs (V$-$I) are used to estimate the cluster distance and reddening. Spectra of the some bright members are also presented, which are used for spectral classification and to identify probable members

The ages of these clusters are determined with the help of isochrones from Castellani et al.(1990), Schaller et al.(1992) and Bressan et al. (1993). To compare the evolutionary time-scales in different phases of stellar evolution, we make use of the synthetic CMD created from the evolutionary models. The prescription for obtaining the synthetic CMDs is presented in chapter 4. The open cluster CMDs and LFs are compared with the ones obtained from the synthetic CMDs. As the LMC star clusters are better suited for the comparison with theories, we

extend our comparison to four young LMC clusters NGC 1711, NGC 2004, NGC 2164 and NGC 2214 in the LMC. All these are also presented in chapter 4.

The existence of double/binary clusters in MCs is fairly well established, whereas only one such pair, h+χ Persei, is known in the Galaxy. We find 18 probable pairs of binary clusters in the Galaxy. We have observed two pairs of clusters from this and we find that these pairs are physically close. This forms the contents of chapter 5. The main conclusions of the present study are summarised in chapter 6, with some discussion on future work.

Chapter 2

Observations and reduction techniques

This chapter consists of a brief description on the telescopes and filter systems used to obtain the data, the photometric reduction and calibration methods, followed by the spectroscopic reduction techniques used in the present study. A discussion on the observations and reductions is mandatory as the results are preceded by these processes.

The open star clusters chosen for the present study are observed using the 1.02m and 2.34m telescopes at the Vainu Bappu Observatory (VBO) in Kavalur (78° 50' E longitude, 12.5° N latitude, 2340 ft altitude). The Cassegrain focus of the 1.02m Carl-Ziess reflector and the prime focus of the 2.34m reflector were used for CCD imaging of open clusters. A set of filters coated to get the required responses in B, V, R and I passbands are used. The Cassegrain focus of 1.02m along with the Universal Astronomical Grating Spectrograph (UAGS) is used for acquiring spectroscopic data. The details of the focal planes, image scales and the filter systems used for both the telescopes are given in Table 2.1.

2.1 Charge Coupled Devices

The detectors used for this study are the Charge Coupled Devices (CCDs). The operation of a CCD is quite simple and can be explained using an elegant analogy, as given in Figure 2.1. The CCD as a detector performs four tasks to generate

Table 2.1: *Details of the focal planes, image scales and the filter systems for the 1.02m and 2.34m telescopes at VBO. The filter specification is the same for the filter sets in both the telescopes.*

F ratio	Image scale	Filter system	
	arcsec/mm	Passband	$(\lambda_0/\delta\lambda)$
1.02m (Cassegrain)		B	4400/1050
f/13	15.6	V	5425/1050
2.34m (Prime)		R	6550/1300
f/3.23	27.5	I	8150/1700

an image. These operations are:

(a) Photo electron generation (rain)

(b) Electron collection (buckets)

(c) Charge transfer (conveyor belts)

(d) Readout (metering station)

When a pattern of light from an astronomical object falls on the CCD, the photons that constitute the incoming image are absorbed by the silicon lattice of the chip resulting in the production of free electrons. These are then collected in each storage unit called pixel. In the figure, buckets represent the pixels. After the exposure is over, the charge in each pixel is read out. This is done by shifting the charge from one pixel to the other in the first row to the output amplifier, from where, it is digitised and displayed or stored. The conveyor belts and measuring station in the figure depicts this. Then the charge in the second row is shifted to the first and the process is continued till the last row is read out.

The CCDs have revolutionised the modern astronomy due to the following reasons. The output from the CCDs are in digital form, that can be easily stored, copied and transported. These digital images can be easily manipulated by computers enabling one to bring out the subtleties not obvious in the original image as well as allowing one to process and analyse the images automatically.
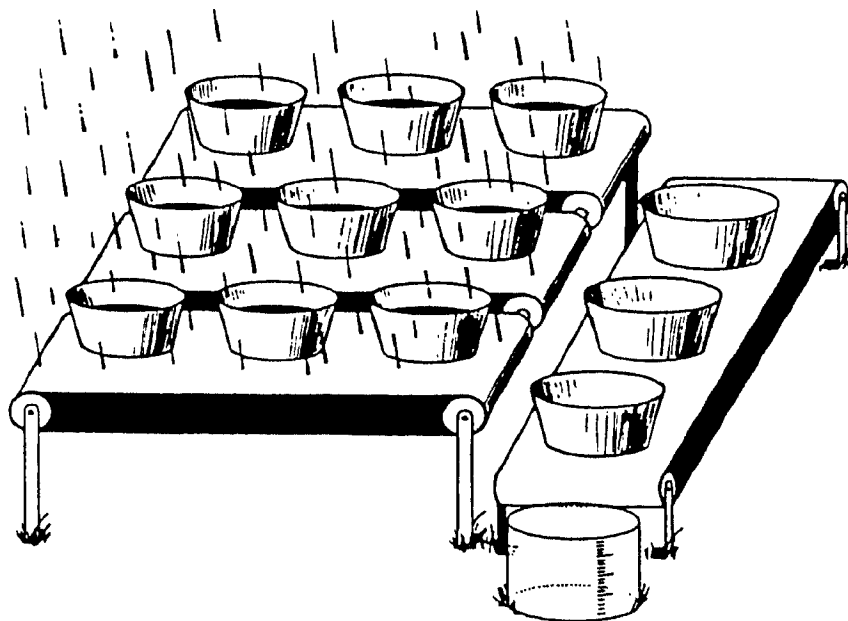
Figure 2.1: *Determining the brightness distribution of an astronomical object with a CCD can be likened to measuring the rainfall at different points is a field with an array of buckets. Once the rain has ceased, the buckets in each row are moved horizontally across the field on conveyor belts. As each one reaches the end of the conveyor, it is emptied into another bucket on a belt which carries it to the metering station, where its contents are measured. (Figure from Janesick & Blouke 1987)*

Another breakthrough is that we are able to reach limiting magnitudes $\sim$ 25 mag in V, which has helped in a better understanding of the globular cluster ages and Hubble constant. Finally CCDs have made it possible to make valuable contribution from small to moderate size telescopes. Large quantum efficiency has made a 1m telescope + CCD approximately equivalent to 4m + photographic plate. With the help of CCDs, one is able to reach limiting magnitudes of $\sim$ 20 mag with moderate size telescopes. Since the accessibility is more for these telescopes, long term projects like surveys are possible. These have given new life to many of the smaller facilities.

The CCDs used in the present study are listed in the Table 2.2. Their characteristics, sizes and the total field covered by the chip are also tabulated. All the

Table 2.2: *The details of the CCD detector systems used in the two telescopes are tabulated here. RN is the read out noise in electrons and gain is in electrons/ADU.*

CCD	size	Tel.	image scale arcsec/pix	Total field	RN	gain
CSF TH 7882 Photometrics Inc.	23μ 384×576	1.02m	0.36	137×206 arcsec^2	8	27
GEC P8603 Astromed Inc.	23μ 385×578	2.34m	0.63	4.0×6.1 arcmin^2	9	4
TK 1024AB2 Photometrics Inc.	24μ 1024×1024	2.34m	0.63	10.75×10.75 arcmin^2	4	4

chips used are coated for enhancement of the sensitivity in the UV region.

2.2 Photometric reductions

The CCD data obtained from the telescope has the CCD characteristics present in them, so the first step in the reduction procedure of the data is the removal of CCD dependent parameters. We list the different parameters and the procedure used to correct them are discussed below:

Bias The CCD has a d-c offset voltage which gets recorded along with the image. Bias frame is an image frame with exposure time equal to zero and this contains information of the d-c voltage applied to the CCD chip. Bias frames are acquired at regular intervals during the observations. To remove the d-c voltage from the object frames, the bias frame is subtracted from the object frames. The subtraction is done pixel by pixel. A closer look at the bias frames may reveal the presence of a few pixels, either in the beginning or at the end of the rows or columns, with abnormally high or low bias counts. These pixels are removed by trimming them from all the frames.

Flat Fielding The different pixels in a CCD chip may have slightly different sensitivity, though ideally all pixels are supposed to have the same sensitivity. In order to correct this non-uniformity, uniformly illuminated frames called flats are obtained. The flats are taken during the evening and morning

twilights. First, all the frames were bias subtracted and the flats for each night were combined to produce a master flat of better S/N ratio for each filter. These master flats are then used to flat field the object images. This is done by dividing each object image by the master flat of the corresponding filter.

Dark The CCD generates some charge because of thermal fluctuations. The counts registered on the CCD with its shutter closed are called the dark counts. This can be minimised by operating the CCD at a lower temperature. The CCD is kept in a evacuated dewar, which is cooled by liquid nitrogen to $\sim -120°C$. At this temperature, the dark is found to be less than a few counts for an exposure of 30 min, which is negligible. Therefore, the dark correction is not applied.

Since the bias is noticed to vary across the night in the case of CSF chip (Mayya 1991), the bias frames are acquired at regular intervals. The bias frame closer to the observed images is used for bias subtraction. During each observing run, the flats are obtained in all filters in the evening as well in the morning. These flats are first bias subtracted and trimmed before stacking using median to obtain master flat for each filter. These master flats are used to flat field the cluster images. All these processes are done using the package CCDPROC in IRAF.

2.2.1 DAOPHOT II

After the CCD characteristics are removed, we proceed to do the photometry of the stars in the object frame. The software package, DAOPHOT II is used for the estimation of magnitudes of stars present in the frames and to transform the instrumental magnitudes to the standard system. This program is the revised version of DAOPHOT (Stetson 1987). This is written and continues to be developed at the Dominion Astrophysical Observatory. A brief description of the methods DAOPHOT uses to carry out the tasks required to get the instrumental magnitudes are described here. The primary tasks performed by DAOPHOT II on the object frames are: (1) find star like objects above a certain detection

threshold, rejecting bad pixels, rows and columns etc, (2) derive concentric aperture photometry for these objects, estimating a local sky brightness for each star from a surrounding annulus of pixels, called aperture photometry, (3) obtain a point-spread function (PSF) for the frame from several stars, in an iterative procedure intended to fit and subtract faint neighbour stars which contaminate the profile, (4) compute precise positions and magnitudes for the program stars by fitting the PSF to a group of stars and (5) erase stars from the frame subtracting appropriately scaled PSF functions corresponding to the positions and magnitudes derived for stars during the photometric reductions. Thus the first job is to find the stars in the object frame. This involves:

1. detecting and locating small, positive brightness enhancements within an image;

2. distinguishing stellar images from

a.random noise peaks in the data,

b.images of galaxies or other extended objects

c.cosmic rays or any high energy particles

3. recognising when a seemingly extended object consists of two or more overlapping stellar images.

The star-finding algorithm in DAOPHOT is the FIND routine and it needs the following information: (1) gain and read-out noise of the CCD, (2) the number of electrons corresponding to one ADU (3) the maximum count beyond which the CCD fails to respond linearly, (4) the full width at half maximum (FWHM) of the stellar image and (5) the lowest count to be considered as the peak of a stellar image. FIND then attempts to locate a star in a pixel by fitting an analytic Gaussian profile to the brightness values of the surrounding subarray of pixels. A location in the image where the central height of the best-fitting model Gaussian profile achieves a large, positive value probably lies near the center of a star image. The non-stellar detections like the cosmic rays are narrower than the seeing-broadened stellar images. A criterion called sharpness parameter is introduced, which is the ratio of the height of two dimensional delta function to the height of the Gaussian function. For the cosmic ray event, this value will be grater than one, and for spurious detections around low valued pixels,

sharpness falls close to zero. The criterion used by us for the detection of real stars is $0.2 < sharp < 1.0$. Another class of false detections arises in the charge overflow columns and rows from grossly overexposed objects in the frame. The roundness criterion compares the peak of the Gaussian in x-direction, h_x to that in the y-direction, h_y such that $round = 2(h_x - h_y)/(h_x + h_y)$. It is evident that the stars will have roundness close to zero and for overflow rows or columns, it will be around 2. The roundness criterion used for the detection of real stars is $-1.0 < round < +1.0$.

Once the stars are identified by their x and y positions in the frame, the next job is to do the photometry. In the case of a well isolated star, the instrumental magnitude can be found by the synthetic aperture photometry. This is done as follows: The program allows one to specify radii for 12 concentric apertures and an annulus to evaluate the sky. The sky value per pixel determined is an estimate of mode of the intensity values of pixels in the annulus. The magnitude of the star corresponding to any aperture is determined by summing the data inside that aperture and from the relation, $m = zpt - 2.5 logI$, where zpt is the arbitrary zero-point and $I = \Sigma I_{ij} - n_{pix}i_{sky}$. In the expression, n_{pix} is the number of pixels in the aperture for the star and i_{sky} is the intensity of sky per pixel. The magnitude of the star thus obtained for the first aperture specified is used as the preliminary estimate for the next routines. The magnitudes from the rest of the apertures can be used to determine the stellar brightness growth curve on the CCD frame.

The aperture photometry is good enough for isolated stars. In the case of clusters, one can find two or more stars inside the first aperture itself. Therefore the above method does not hold good. In these cases, one sets to determine the PSF of a star on the frame. The basic principle of the technique is that all images on a CCD frame have the same form and thus differ from one another only in intensity by a scaling ratio. King (1971) estimated an empirical determination of the radial density profile of a stellar image. He showed that next to the central core, the image is approximately Gaussian in form, the tail region has an inverse square law and in between part is best represented by an exponential. This profile is further complicated by telescope aberrations, tracking errors, camera optics

etc. Three mathematical functions in particular have been found to be useful in describing the stellar brightness profile (Stetson et al. 1989) . They are:

$$\text{Gaussian:} \quad G(r;\alpha) \quad \propto \quad e^{-r^2/2\alpha^2}$$

$$\text{Lorentzian:} \quad L(r;\alpha,\beta) \quad \propto \quad \frac{1}{1+(r^2/\alpha^2)^\beta}$$

$$\text{Moffat:} \quad M(r;\alpha,\beta) \quad \propto \quad \frac{1}{(1+r^2/\alpha^2)^\beta}$$

where, α and β are the free parameters. In addition, it is possible to simply store the observed profile of the sum of several bright stars as a data array $O(i,j)$ and to use an interpolation technique to estimate the brightness observed.

$$\text{Empirical:} \quad E(x_i,y_i) \quad \propto \quad O(i,j)$$

The analytical method has the advantage of integrating numerically over the entire stellar image, but the problem being that the functions used fit the profile only approximately. The epirical method has the advantage that it uses the observed profile, but the drawback in this case is that, near the central regions of the stellar image, the brightness varies too rapidly between the adjacent pixels to be interpolated correctly. Therefore, better results can be obtained by combining the two methods.

DAOPHOT uses the sum of a Gaussian and a look-up table with bicubic interpolation. This combines the advantages of analytical and empirical methods. In the new version, DAOPHOT II, six functions are available, which being Gaussian, Lorentzian, Moffat with two options and Penny (a sum of Gaussian and Lorentzian) with two options. The Penny function (Penny & Dickens 1986) is given by:

$$P \propto (1 - \alpha_4)exp[-\frac{1}{2}(\alpha_1 x^2 + \alpha_2 y^2 + \alpha_3 xy)] + \frac{\alpha_4}{1 + (\alpha_1 x^2 + \alpha_2 y^2 + \alpha_3 xy)^2}$$

In the present study, the option 5 is used for the PSF function, which is the Penny function having four free parameters. As the cluster regions are not crowded, fitting of this function does not take much of the CPU time and the chi value for fitting is found to be less than 0.02. To determine the PSF for a CCD frame, the brightest few stars, which are fairly isolated in the frame are identified. Finding the PSF is an iterative process, since the neighbours if present inside the PSF radius has to be subtracted from the frame. The process of detecting and deleting

the neighbours is repeated till all such neighbours are deleted from the frame. Once the chosen stars are devoid of neighbours, they are used to determine the final PSF. This PSF is applied to all the stars with aperture photometry using the routine ALLSTAR. The output of this routine gives the final x and y positions of the stars, their magnitudes and errors along with sharpness, roundness values and chi values of PSF fitting. The estimated errors in the magnitude determination are used to reject the bad measurements.

2.2.2 Transformation to the standard system

In the PSF magnitude determination, we assume a fixed aperture and scale the peak of the PSF for different magnitudes. This magnitude is restricted to the aperture chosen and has to be corrected for the counts left out in the wings of the stellar profile. Most of the profile-fitting photometry routines rely on two additional reduction steps, synthetic aperture photometry followed by a growth curve analysis, to measure the total stellar magnitudes. The mean difference between these magnitudes and the relative PSF magnitudes for the stars is needed to find the actual magnitude. This is achieved by the growth curve analysis. The aperture photometry values obtained for an increasing set of apertures is used to find the growth curve, which in turn gives the aperture correction. This correction is applied to the PSF magnitudes to get the actual magnitudes. This is done using the DAOGROW routine. The next process is to transfer the observed instrumental magnitudes to the standard system.

To get a good transformation, the first and the foremost requirement is that the observed night should be a photometric. As all the nights of observation are not photometric, one or two regions in the center of the cluster are observed on a photometric night along with the standard stars. The rest of the regions of the cluster are observed in overlap with these central regions, so that the transformation can be extended to the other regions of the cluster. This is the method followed in all the clusters observed. To find the transformation coefficients, we use the standard stars and to extend the transformation to the cluster, we choose a set of $\sim$ 20 secondary standards in the central regions of the cluster. These stars are used to determine the aperture correction and later on as standards

to transform the rest of the cluster stars. Usually the PSF stars are chosen as secondary standards.

The standard stars observed are the stars in the dipper asterism region of M67 (NGC 2682). The usefulness of this region in M67 in calibrating CCDs is discussed by several authors (Schild 1983; Sagar & Pati 1989; Joner & Taylor 1990; Chevalier & Ilovaisky 1991). This region contains 16 stars within a magnitude range of 9.7 to 14 mag in V and -0.09 to 1.35 mag in (B$-$V) . It is observed in all filters at different airmass to obtain a reliable estimate of the atmospheric extinction coefficients. Brightest two stars in the frame are used for this purpose. Ten stars in the region are used to estimate the zero-points and the colour coefficients. The frames with the dipper asterism region are also reduced using DAOPHOT II with the help of PSF, and the aperture corrections are done as explained earlier. All the observed frames are transformed to a single co-ordinate system using which the magnitudes of each star in various frames and filters could be identified. The magnitudes and colours of standard stars are taken from Chevalier & Ilovaisky (1991). The transformation equations to the standard system are of the form,

$$B_{std} = b_{inst} + a_0 + a_1(B - V)_{std} + a_2 X + a_3 X(B - V)_{std}$$

$$V_{std} = v_{inst} + b_0 + b_1(V - I)_{std} + b_2 X$$

$$R_{std} = r_{inst} + c_0 + c_1(V - R)_{std} + c_2 X$$

$$I_{std} = i_{inst} + d_0 + d_1(V - I)_{std} + d_2 X$$

where a_0, b_0, c_0 and d_0 are the zero-points, a_1, b_1, c_1 and d_1 are the colour coefficients and a_2, b_2, c_2 and d_2 are the extinction coefficients, *std* stands for the starndard magnitudes and *inst* for the instrumental magnitudes. In the estimation of B magnitudes, we use the second order term, as the extinction varies rapidly across this bandpass and a_3 is the corresponding coefficient. The zero-points should be stable within a run as there is no reason to expect the overall sensitivity of the CCD/telescope system to change on a nightly basis. On the other hand it is quite likely that the extinction will change from night to night as the atmospheric conditions vary, hence a nightly determination of the

Table 2.3: *The transformation coefficients to Johnson-Cousins system. The values are for the 1.02-m system.*

Passband	zero-point	colour coeff.	ext. coeff.
9th March 1992			
B	7.614	0.348	0.685
V	7.071	0.037	0.540
R	6.755	0.027	0.408
I	7.334	0.007	0.295
10th March 1992			
B	7.455	0.303	0.807
V	6.997	0.025	0.598
R	6.661	0.005	0.485
I	7.148	0.036	0.394
19th March 1993			
B	7.738	0.308	0.550
V	7.179	0.018	0.455
R	6.805	0.008	0.404
I	7.311	0.064	0.236

extinction coefficient is necessary. These transformation equations are used to estimate the values of the coefficients, with the help of the estimated values of extinction coefficients and the previously estimated value of a_3 (= 0.036). The values of the coefficients obtained for the three photometric nights are given in Table 2.3. It can be seen that the values of extinction coefficients are larger on the 9th and 10th of March 1992, compared to those found in the previous months, but is consistent with the values for 7th and 8th of March 199 2, obtained by Mayya (1993). This may be because of the volcanic activity in Philippines during this time (!). The colour coefficients are seen to remain more or less constant. The tabulated values are obtained for the 1.02-m system. The filters used in the 2.34m are identical to the ones in 1.02-m and colour coefficients for both the filter sets are similar, (see Mayya 1993), we therefore used the same colour coefficients for both the sets of filters.

These estimated values of the colour coefficients are used to determine the zero-

points, as listed in the table 2.3 and to transfer the observed M67 magnitudes to their standard values and along with that, the secondary standards in the cluster frames are also transferred to the standard system. A library of the secondary standards are created to transform the cluster stars. The final transformation of all the cluster stars is done by the FINAL routine. We have modified this routine to include stars for which V magnitude and at least one colour could be estimated.

The open clusters in this program are observed on non-photometric nights as well, as explained earlier. The regions which are calibrated on a photometric night are then used to transform the rest of the cluster stars. This is done with the help of DAOMATCH and DAOMASTER. The regions having the direct overlap are transferred to the coordinates of the calibrated frame. The stars which are in common are used to find the zero-point shift and the stars in the overlapping region is transferred to the standard system. Then the library file is extended to include the stars which are in the region outside the calibration frame. This method is extended to cover the entire field. The zero-point errors for the cluster stars are uncertain by ~ 0.01 mag in B, V, R and I filters. The various exercises explained in this section are done using the routines available in DAOPHOT II.

2.3 Spectroscopic reductions

The spectral classification can be done based on the temperature and luminosity sensitive line ratios or with the help of the continuum flux. The former classification needs a spectra of intermediate resolution (~ 50 Å /mm) and the latter method can be adapted for low resolution (~ 200 Å /mm) spectra. Here, we try to identify the spectral types and luminosity class of some bright members in the open clusters using low resolution spectra. This needs an accurate determination of the continuum flux distribution in the wavelength covered. This technique is usually called as spectrophotometry. The observed spectrum is a combination of the source, wavelength dependent atmospheric extinction, telescope optics, spectrograph response and the detector response. To obtain the source spectra, we need to deconvolve these contribution from the observed spectra.

The low resolution spectra of some bright members of four clusters are observed using the 1.02-m telescope. We used the Carl-Ziess Universal Astronomical Spectrograph (UAGS) with 150 lines/mm grating giving a dispersion of 6 Å /pixel and a net resolution of 9 Å /pix. The grating is blazed at 5000 Å giving a wavelength coverage of 3700–6700 Å . The CCD described earlier is used as the detector. The spectrophotometric standards are observed in all nights. The Iron-Argon spectra is used for wavelength calibration.

The dome flats are taken after each observing run. The spectra are bias subtracted using the bias taken at regular intervals in the night. After obtaining the master flat as explained earlier, it is normalised and fitted with a sixth degree polynomial. This function is then used to flat field the object spectra. The comparison Iron-Argon spectrum is wavelength calibrated and that is applied to the object spectra. The standard stars observed on each night are used to find the sensitivity function. The average extinction for the sight as a function of wavelength is used for atmospheric extinction correction. The sensitivity function is applied to the object spectra along with the atmospheric extinction correction, thereby flux calibrating the observed stellar spectra. These flux calibrated spectra are then used for spectral classification.

Chapter 3

Observations of Open star clusters

In this chapter, we present the photometric observations of 5 and spectroscopic observations of 4 open star clusters. The distances and reddening to these clusters are determined using the cluster CMDs as well as the spectra of the members.

3.1   Introduction

From the catalogue of Lyngå (1987), we have chosen the clusters, NGC 1912, NGC 6709, NGC 2383, NGC 2384 and NGC 1907, for the present study. These clusters have only photographic or photoelectric data available and that too only for the bright stars in the cluster. The cluster parameters given in the catalogue are based on such photometric measurements and hence may not be very accurate. The CCD observations of these clusters are carried out to render CMDs with better photometric accuracy and MS extending up to fainter magnitudes. These help in the precise determination of cluster parameters and yield a good CMD for comparison with stellar models. We next discuss the different methods generally used to determine the various cluster parameters with details about the methods used in the present study.

3.2 Membership determination

It is well known that one of the major problems posed by open clusters is the difficulty in identifying the cluster members from the field stars. There are different methods for estimating the membership and we discuss each of them below.

3.2.1 Kinematic membership

As all the stars in a cluster are born together, they are supposed to have the same motion. Their velocities perpendicular to the line of sight are given by the proper motion and the velocity in the line of sight by the radial velocity. The radial velocity determinations are available for a few bright star in open clusters. This is a difficult criterion as the spectroscopic binaries will have varying velocity and hence different from the cluster, keeping in mind the fact that the clusters are known to house a substantial number of binaries (e.g., NGC 2287–Harris et al. 1993; IC 4665–Crampton et al. 1976). These values are used for the membership criterion wherever available. The proper motion data is available only for nearby clusters as the nearby stars move more in the perpendicular direction compared to the distant ones in a given amount of time. Wherever the proper motion data is available, it is used to identify the members. This method holds good only when the cluster stars have a very different motion compared to the nearby field stars (Vasilevskis 1962, Mathieu 1983).

3.2.2 Photometric criterion

All the stars belonging to the cluster should fall on a well defined evolutionary sequence in the cluster CMD, if the assumption of coeval nature of star formation holds good. Then, the stars falling away from the expected sequence can be considered as non members. This works well, if the field stars have a different age with respect to the cluster, as well as different distance and reddening. This method is generally used, except in the case of very young clusters (age ≤ 10 Myr), where the stars still reaching the MS fall scattered on to the right side of the MS, where they could be mistaken for field stars. Spread in the cluster MS as well as in the later evolutionary phases is created by binaries, contact binaries,

probable blue stragglers etc. Any differential reddening present across the phase of the cluster can also create spread in the evolutionary sequences. As the present study is on intermediate age clusters, the stars sufficiently far away from the MS towards the right can be considered as field stars.

3.2.3 Statistical criterion

This method assumes the fact that in the cluster region as well as in the near neighbourhood of the cluster, the field star density is same. One can estimate the number density of stars in various magnitude and colour bins from a region close enough for the approximation to hold good, but far enough to exclude the possible members. This field star number density can be used in the cluster region to get the cluster number density in various magnitude and colour bins. This method gives the true number of cluster stars present, but will not identify them individually, as this is a statistical method.

3.2.4 Spectroscopic membership

This method is based on the determination of the spectral type and luminosity class of individual stars from their spectra. The comparison between the spectral information and the photometric information will give an idea about the evolutionary status of the star and the distance. If the star has a different evolutionary status from the one expected from its position in the cluster CMD, or if the spectroscopic distance is different from the one obtained from the cluster CMD, then the star is not a member. This method is applicable only to the bright members as it is difficult to get good spectra of faint members. In this study, the spectra obtained for the cluster stars are used to estimate their membership.

3.3 Earlier studies

The parameters of the 5 clusters as catalogued in Lyngå (1987) are given in Table 3.1. Earlier studies of the individual clusters are discussed below:

Table 3.1: *Basic cluster parameters of the five open cluster as given the catalogue Lyngå (1987).*

Parameter	Value				
	NGC 1912	NGC 6709	NGC 2383	NGC 2384	NGC 1907
R A(1950.0)	5^h 25.3'	18^h 49.1'	7^h 22.6'	7^h 22.9'	5^h 24.7'
Dec. (1950.0)	$+35°$ 48'	$+10°$ 17'	$-20°$ 50'	$-20°$ 56'	$+35°$ 17'
Gal. longitude	$172°.27$	$42°.16$	$235°.26$	$235°.39$	$172°.62$
Gal. latitude	$0°.70$	$4°.70$	$-2°.44$	$-2°.41$	$0°.30$
Tr. cl.	II 2 r	IV 2 m	II 3 m	IV 3 p	I 1 m n
Ang. dia.(arcmin)	14	14	5.0	5.0	5.0
Distance(pc)	1320	950	2000	2000	1380
E(B−V)(mag)	0.24	0.30	0.27	0.29	0.42v
log(age)	8.35	7.89	7.40	6.00	8.64
[Fe/H]	−0.11	⊣	−	−	−0.10
Rad. velocity(km/s)	−	-13	−	31	−
No. of pec. mem. stars	−	1 Be star	−	−	~
Galactic R & z(pc)	9720; 15	7860; 72	9750; −83	9690; −137	9820; 6
Linear diameter(pc)	8.1	3.7	3.5	1.5	2.8

NGC 1912 This is an open cluster situated in the anticenter direction of the Galaxy. Its Trumpler classification is II 2 r, which means that the cluster has moderate concentration with respect to the field and it contains more than 100 stars with magnitudes distributed over a large range. This cluster lies in the constellation of Auriga and the field of the cluster is shown in Figure 3.1. This cluster is also designated as M38 in the Messier catalogue. Though this is a rich cluster, it is not studied much in detail. Johnson (1961) estimate the distance to be 1320 pc and the reddening, E(B−V) to be 0.27 mag. Becker (1963a) finds the distance and E(B−V) as 1415 pc and 0.24 mag respectively. The detailed photometric study is by Hoag et al. (1961), where photoelectric photometry of 28 stars and photographic photometry of 137 stars were obtained in U, B and V passbands. The follow up paper by Hoag & Applequist (1965) find 870 pc and 0.27 mag as the distance and the E(B−V) values respectively. A wide range in the distance modulii (8.7–10.6 mag) has been found for the stars in this cluster by Hoag (1966). There is proper motion information available for about 383 stars (Mills 1967). Spectroscopic information is available only for a few stars in this cluster (Hoag & Applequist 1965, Hiltner 1956 and Sowell 1987) and the radial
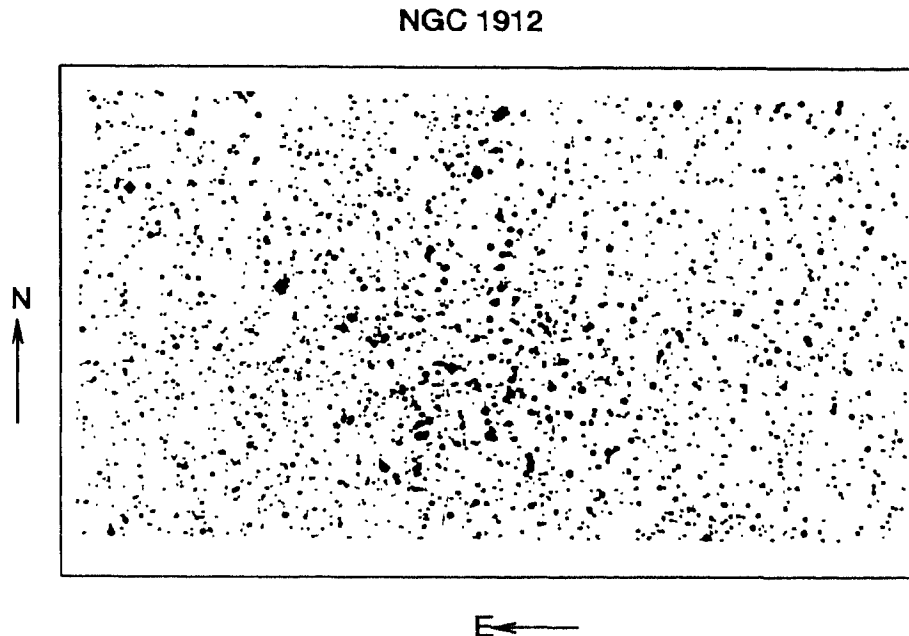
NGC 1912

Figure 3.1: *The field of NGC 1912 taken from Palomar Chart.*

velocity of 7 stars are determined by Glushkova & Rastorguev (1991).

NGC 6709 This is a moderately rich cluster situated towards the center of the Galaxy and lies in the constellation of Aquila. Trumpler classifies this cluster as IV 2 m, which means that the cluster has a low concentration with more than 50 stars whose magnitudes are distributed uniformly over a large range. The field of the cluster is given in Figure 3.2, which is taken from the Palomar chart. The cluster has received a lot of attention in the early part of the century. Among the more recent studies, Johnson (1961) finds a distance of 910 pc and E(B−V) value of 0.30 mag. The study by Becker (1963a) estimates a distance of 930 pc and E(B−V) of 0.34 mag. Hoag et al. (1961) have determined photoelectric photometry of 30 stars and photographic photometry of 80 stars in U, B and V passbands. Hoag & Applequist (1965) find a value of 9.8–10.2 mag for the distance modulus. The proper motion probabilities of around 500 stars in the cluster field are available from Hakkila et. al. (1983). Spectroscopic studies show
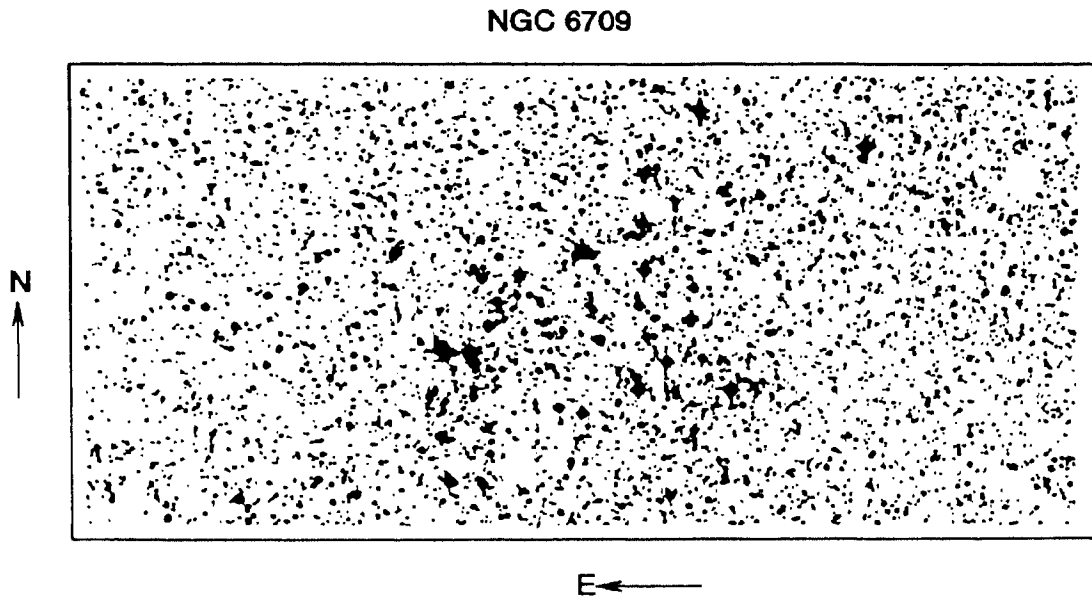
NGC 6709

Figure 3.2: *The cluster region of NGC 6709 as taken from Palomar.*

that this cluster contains two Be stars (Schild & Romanishin 1976), and one of them is found to be a shell star (Sowell 1987).

NGC 2383 This is a compact and moderately rich cluster in the constellation of Canis Major. The trumpler class is II 3 m, which means that the cluster has a fair amount of concentration containing around 50 stars mostly faint, barring a few bright ones. The field of the cluster is shown in Figure 3.3 and the cluster lies in the north-western region of the figure. To the south-east of this cluster, another star cluster is seen, which is identified as NGC 2384. The proximity of these two clusters in the plane of the sky, encourages us to find whether these two are located at the same place in the Galaxy or just a projection effect. NGC 2383 is a very poorly studied cluster. The only single photometric study is by Vogt & Moffat (1972), where the photoelectric photometry in U, B and V pass bands is available for 11 stars in the cluster field. They estimate the reddening, $E(B-V)$ and distance to the cluster as 0.27 mag and 1.97 kpc respectively. Spectral information of three stars are available in Fitzgerald et. al. (1979).
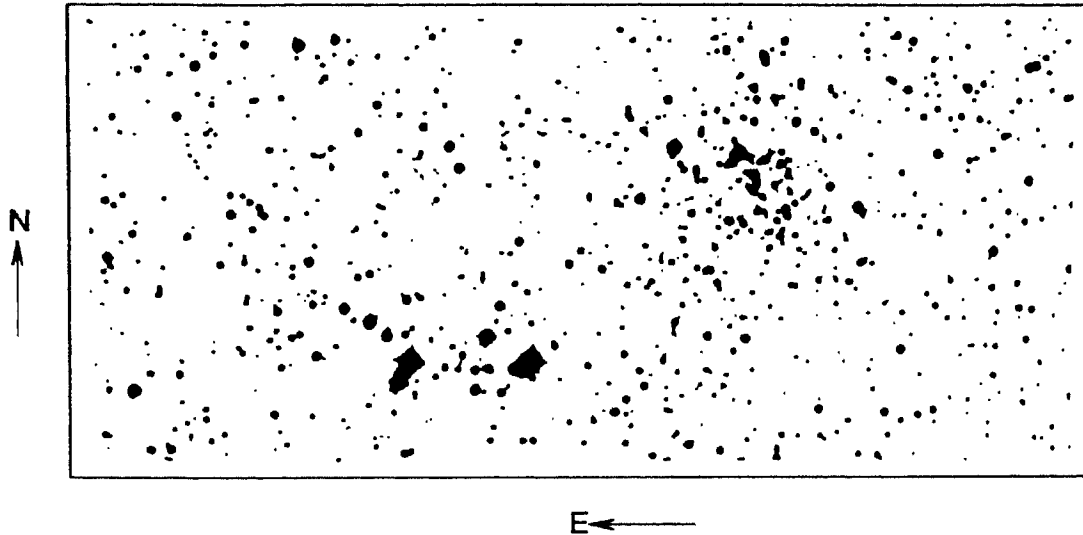
NGC 2383 & NGC 2384

Figure 3.3: *The region containing NGC 2383 and NGC 2384 is shown here, which is taken from SERC chart.*

NGC 2384 This cluster lies within 5 arcmin from NGC 2383. This is classified as IV 3 p indicating that there is very little concentration and there are about 50 stars mostly faint, barring a few bright ones. The cluster field along with the field of NGC 2383 is shown in Figure 3.3, which is obtained from SERC charts. The earliest study of this cluster is by Trumpler (1930) and he finds the distance as 2.6 kpc. Collinder (1931) finds the distance to the cluster to be 4.55–4.75 kpc. The first photometric study is by Vogt & Moffat (1972) where they have obtained photoelectric measurements of 15 stars in U, B and V passbands. They find a distance of 3.28 kpc and E(B−V) of 0.29 mag. Babu (1985) obtained photoelectric photometry in V passband for 20 stars and spectral types of 18 stars from objective grating spectra. The photographic study is done by Hassan (1984) where 49 stars are observed in U, B and V passbands. The main interest here is to know whether this cluster and NGC 2383 lies on different arms of the Galaxy as indicated by Vogt & Moffat (1972) or they lie physically close.

NGC 1907 This cluster is situated close to NGC 1912, in Auriga. The Trumpler class is I 1 m, indicating that the cluster has a strong concentration with about 50 stars, all in the same magnitude range. The cluster field is shown in the
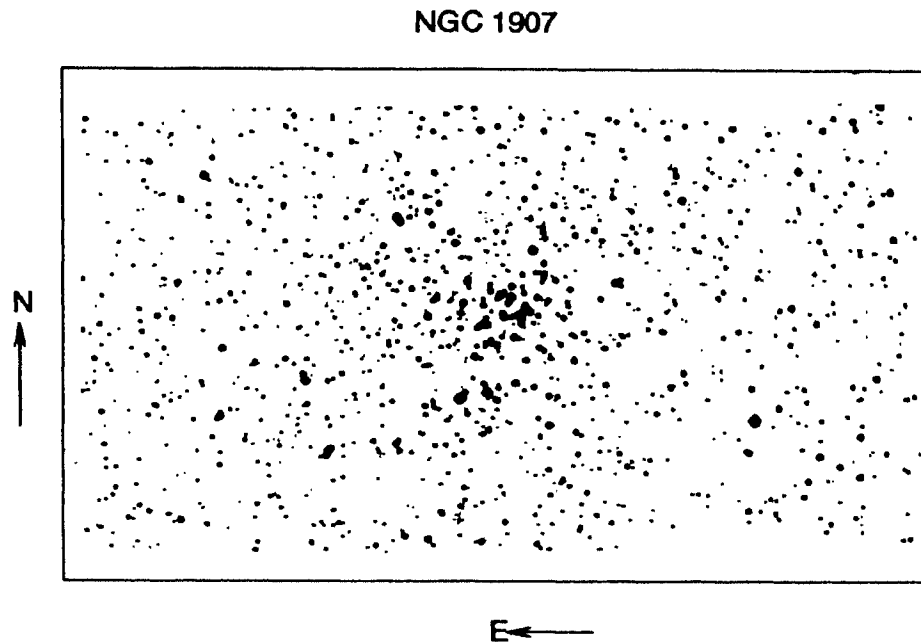
NGC 1907

Figure 3.4: *The field of NGC 1907 is shown here. It is taken from the Palomar charts.*

Figure 3.4. A number of studies have been made about this cluster in the early part of the century. Trumpler (1930) finds a distance of 2750 pc, Collinder (1931) finds it to be 4750 pc and Becker (1963a) obtains 1380 pc as the distance. The U, B and V photoelectric photometry of 27 stars and photographic photometry of 24 stars are available from Hoag et al. (1961). Hoag (1965) finds the distance as 1380 pc and the colour excess as 0.38 mag, but Hoag & Applequist (1965) find the distance as 1200 pc, but same reddening. Hoag (1966) finds that the distance modulus range from 10.4 to 11.2 mag. Strobel (1991) finds that the cluster has a metallicity [M/H] = −0.20.

All these studies discussed for the five clusters are restricted to stars brighter than 16 mag in V and also restricted to a few stars in the cluster field. For an accurate determination of the cluster parameters, a complete and deeper CMDs of these clusters are required.

Table 3.2: *The log of photometric Observation of the 5 open clusters*

Date	Telescope	Clusters	# of regions
11th February 92	1.02m	NGC 1912	3
9th March 92	1.02m	NGC 1912	3
10th March 92	1.02m	NGC 1912	2
28th December 92	1.02m	NGC 1912	2
29th December 92	1.02m	NGC 1912	4
30th December 92	1.02m	NGC 1907	2
20th January 93	1.02m	NGC 1907	4
21st January 93	1.02m	NGC 1907	2
23rd February 93	1.02m	NGC 1912	1
		NGC 2383	1
24th February 93	1.02m	NGC 1912	1
		NGC 2383	1
19th March 93	1.02m	NGC 2383	3
		NGC 6709	1
20th March 93	1.02m	NGC 2383	1
23rd May 93	1.02m	NGC 6709	1
24th May 93	1.02m	NGC 6709	4
17th June 93	1.02m	NGC 6709	4
18th June 93	1.02m	NGC 6709	5
15th January 94	1.02m	NGC 1907	3
19th March 94	1.02m	NGC 6709	2
21st March 94	1.02m	NGC 6709	2
12th April 94	1.02m	NGC 2383	1
6th March 92	2.34m	NGC 1912	2
7th March 92	2.34m	NGC 1912	1
20th April 93	2.34m	NGC 6709	3
13th February 94	2.34m	NGC 1912	1
14th February 94	2.34m	NGC 1912	2
13th January 96	2.34m	NGC 2383	1
13th January 96	2.34m	NGC 2384	1

3.4   Photometry

The photometric CCD data for the five clusters are acquired from the 1.02m and 2.34m telescopes and the the summary of the observation is given in Table 3.2.
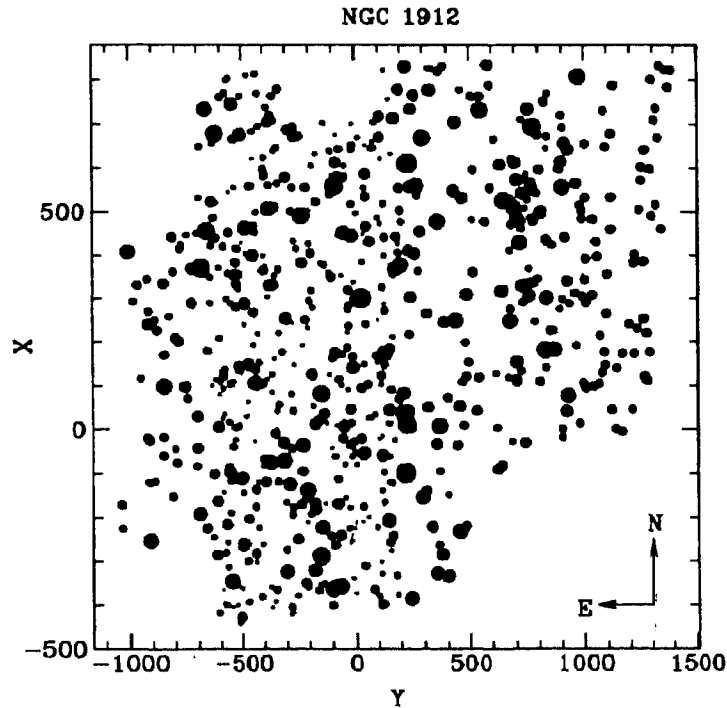
NGC 1912

Figure 3.5: *The stars observed in the cluster region are shown in the X-Y plot.
The coordinates are interchanged to get North towards up and East towards the
left. The size of the circle is proportional to the magnitude such that brighter the
star, bigger the circle.*

NGC 1912   We have obtained photometry for $\sim$ 740 stars in the field of NGC
1912 in B, V and I passbands. The standards are observed on two nights, 9
and 10th of March 92. The night used for calibration is 9 March 92. We have
obtained 140 frames in 22 overlapping regions of the cluster. The identified stars
are plotted on Figure 3.5. The V vs (B—V) and V vs (V—I) cluster CMDs
are shown in Figure 3.6. It can be seen from both the CMDs that the MS is
very broad. As the photoelectric and the photographic data (Hoag et al. 1961),
are available in V mag and in (B—V) colour, we compare our photometry with
these data. The differences in the magnitude and colour are shown in Figure
3.7. The difference is calculated as the Hoag et al. (1961) data subtracted from
the present data. The mean values and standard deviations of the differences in
V and (B—V) are —0.02±0.005 and 0.01±0.005 respectively. This tells us that
present photometry agrees well with that of Hoag et al. (1961).

NGC 1912

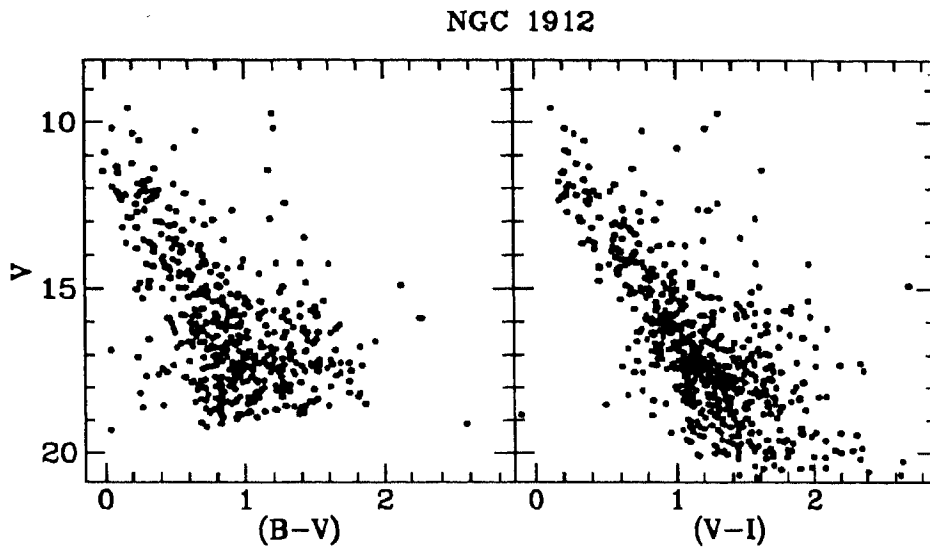Figure 3.6: *The V vs (B—V) and V vs (V—I) CMDs of the cluster NGC 1912 are shown here.*
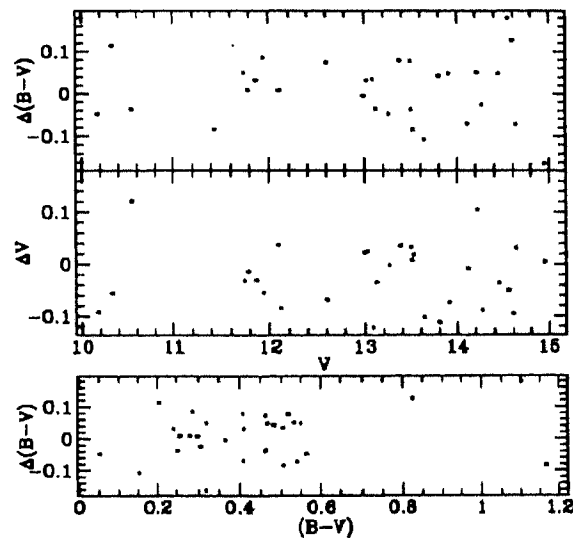
Figure 3.7: *The present data is compared with the photographic data by Hoag et al. (1961). The difference in magnitudes and colours is taken as Δ = present— Hoag et al.(1961).*

We used the proper motion probability from Mills (1967) to identify the members from our data and also from the photoelectric and photographic data. A
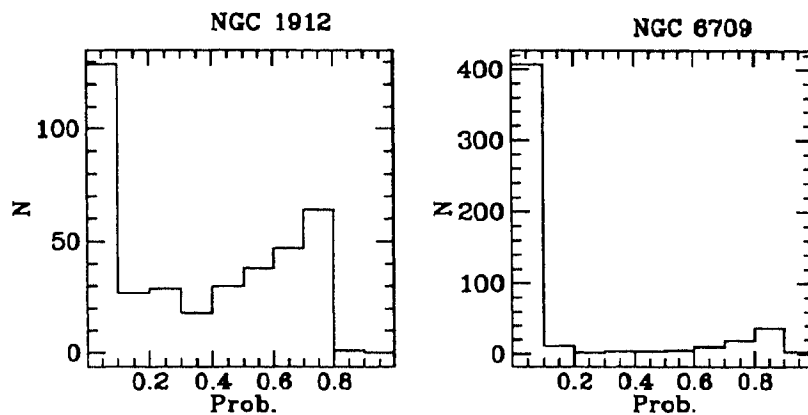
Figure 3.8: *The figure for NGC 1912 contains the histogram of the membership probability data of Mills (1967). The figure for NGC 6709 contains the probability distribution from the data of Hakkila et al. (1989).*

NGC 1912
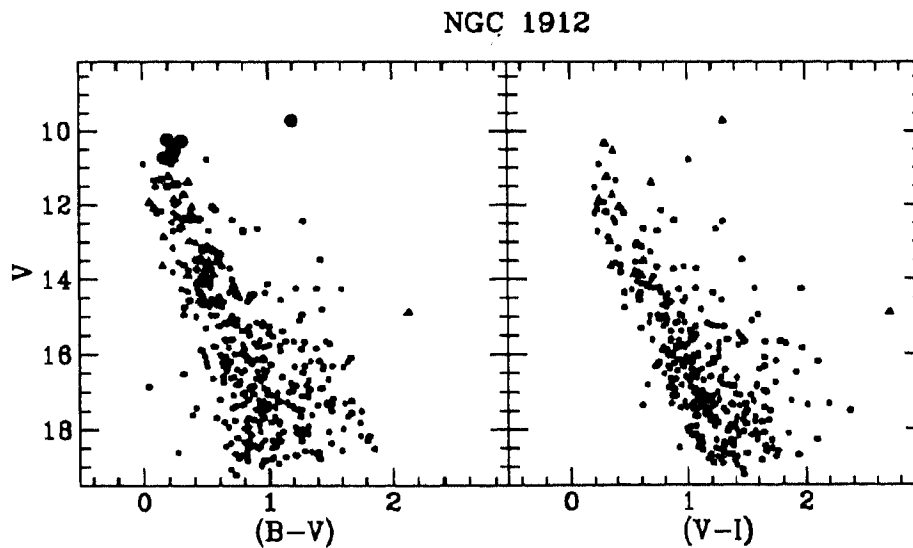
Figure 3.9: *The cluster CMD with the known non-members removed is shown here. The probable members of the present determinations are denoted by triangle, the members included from the photographic data of Hoag et al. (1961) is denoted by 'star' and the open circles around these points denote that spectra are obtained for these stars in the present study.*

histogram plot of the probability vs the number of stars using the data in Mills (1967) is given in Figure 3.8. This tells us that there is a clear demarcation between the cluster members and the field stars and the cluster population has a

Table 3.3: *The photometric errors obtained for NGC 1912 are tabulated here.*

Magnitude range	σ_B	σ_V	σ_R	σ_I
≤ 15.0	0.013	0.015	0.010	0.015
15.0–16.0	0.022	0.027	0.013	0.029
16.0–17.0	0.025	0.036	0.051	0.063
17.0–18.0	0.070	0.095	0.063	0.11
18.0–18.5	0.10	0.24	0.14	0.28

membership probability greater than 0.40. Hence we have considered stars with probability values greater than 0.40 as members. The photometric determinations with errors more than 0.02 mag in V and 0.05 mag in (B−V) are not included. The final CMDs, V vs (B−V) and V vs (V−I) are shown in Figure 3.9. The CMDs now present a well defined turn-off and MS in comparison with the ones shown in figure 3.6. It is very clear from the above exercise that the membership information is very important to identify the cluster sequence.

Photometric errors and data completeness The photometric errors are found by the method of artificial adding of stars and this is done using the routine ADDSTAR in DAOPHOT. As the number density of stars does not vary much in the field of the cluster, the add star experiment is performed on one region of the cluster for which exposure times in various filters are longer. We have added about 10% to 15% stars to each frame and these are recovered along with the observed stars. The photometric errors are estimated from the added stars and these values for magnitudes in various filters are tabulated in Table 3.3. The photometric errors are a function of crowding of stars and the exposure times (e.g., Sagar et al. 1991). As these two are very similar for all the five clusters studied here, these photometric errors can be considered typical for the rest of the four clusters also. This method also helps to estimate the incompleteness of stars with respect to magnitude. The method for determining the completeness of the photometric data on the CCD frames using DAOPHOT is discussed by several authors (e.g., Stetson 1987, Mateo 1988, Sagar & Richtler 1991 and references

NGC 6709
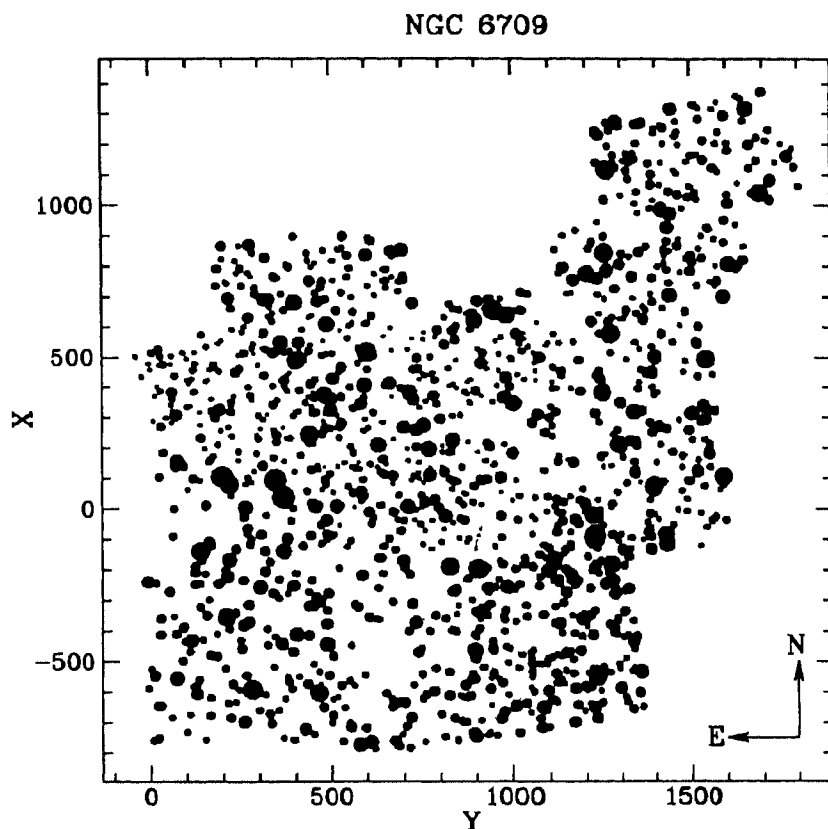
Figure 3.10: *The cluster stars for which photometry is done are shown. The orientation is changed to make the north pointing up and east pointing left.*

therein). From this method, we find that the data is 100% complete up to 16.0 mag, ∼ 95% complete upto 17.0 mag and 80% complete upto 17.5 mag in all the filters. Thus, the data incompleteness correction need not be applied upto a limiting magnitude of 16.0.

NGC 6709 We have observed about 22 overlapping cluster regions in 81 frames in B,V and I filters. All the frames are merged together to get the final cluster region, as shown in Figure 3.10. The X and Y positions are interchanged to get the directions as shown in the figure. The V vs (B−V) and V vs (V−I) CMDs are shown in Figure 3.11, where all the detected stars are shown. The present data has 10 stars in common with the photoelectric data and 23 stars in common with the photographic data of Hoag et al. (1961) and these data are compared as

NGC 6709
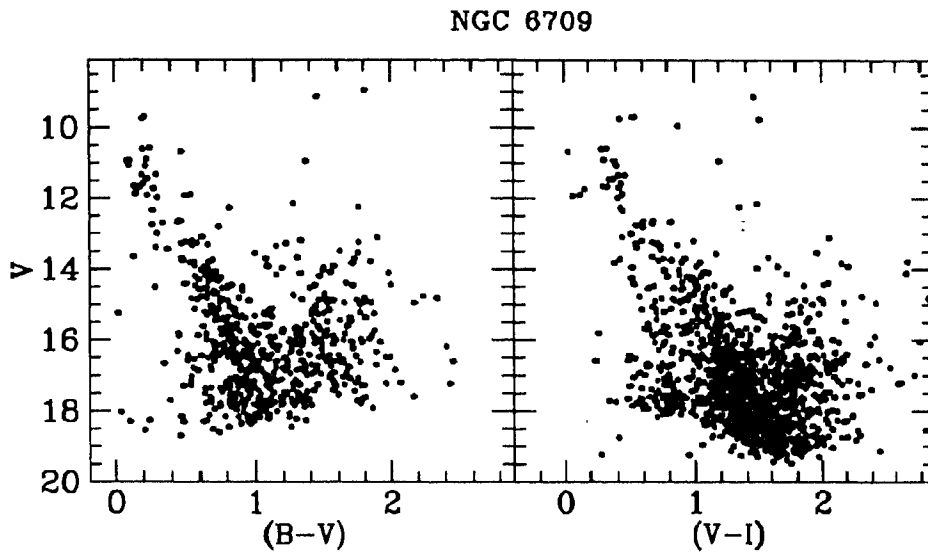
Figure 3.11: *The V vs (B—V) and V vs (V—I) are shown here. All the stars identified within the region shown in figure 2 are plotted.*
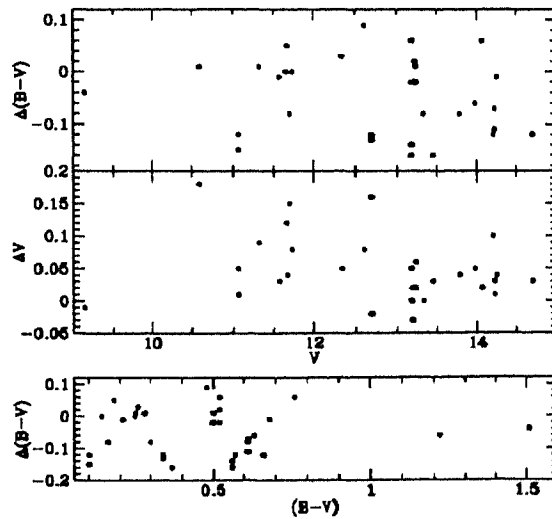
Figure 3.12: *The common stars observed in Hoag et al.(1961) and Hoag et al.(1961) are compared with the present photometry. The values on abscissa are the present value and the difference is Δ = present—literature.*

shown in Figure 3.12. The photometric data of Hoag et al. (1961) are subtracted from the present data for the comparison and the mean and standard deviation

NGC 6709
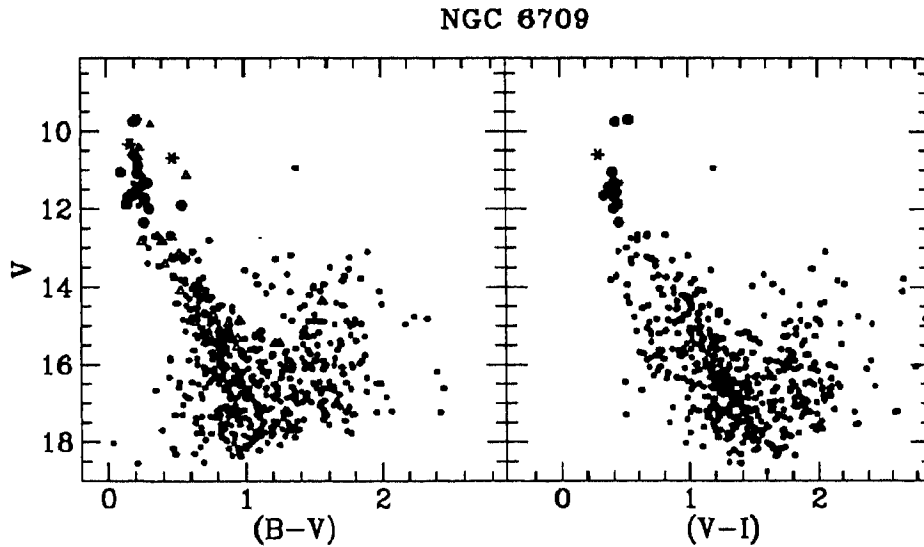
Figure 3.13: *The final V vs (B—V) and V vs (V—I) are shown here. The filled circles are the present data, the filled triangles are the photoelectric data, open triangles are the photographic data, the open circles around filled circles indicate that they are proper motion members, and the star symbol for member stars with spectra.*

and standard deviation of the differences in V and (B—V) are 0.05±0.003 and —0.05±0.005 respectively. This shows that the data agree in general and no systematic trend is seen. We include the stars which are not observed here, but for which photoelectric or photographic measurements are available. With the help of the proper motion information available from Hakkila et. al. (1983), probable members are identified. We plot the probability distribution as given by Hakkila et. al. (1983) and it is shown in Figure 3.8. This shows that there is a strong field population near the proper motion probability 0.0 and the cluster members generally lie above the probability of 0.60. Thus we consider stars with probability greater than 0.60 as members. The stars thus identified as members from photoelectric and photographic data are plotted together with the present data in Figure 3.13. The stars identified as members in the present data are shown by different symbol in the figure and the non-members are excluded. Also, stars with errors more than 0.02 mag in V and 0.05 mag in (B—V) are not included. Different symbols are explained in the figure caption.
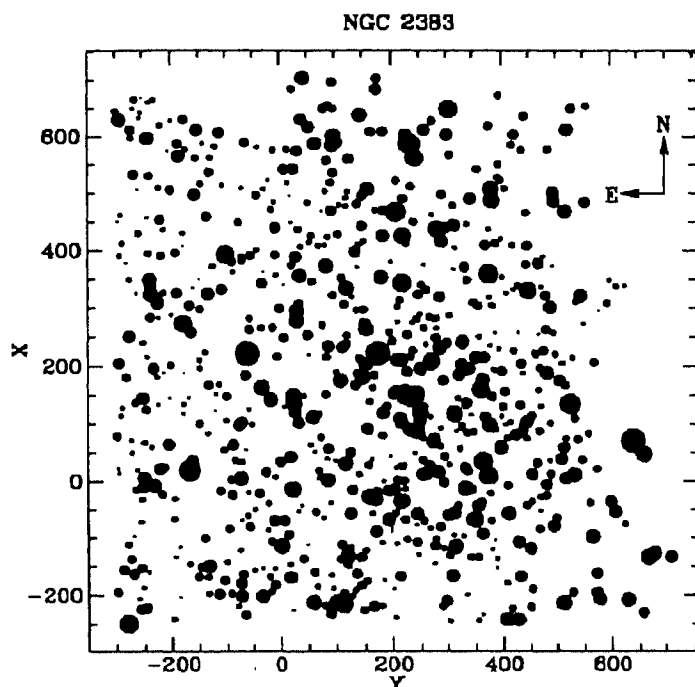
Figure 3.14: *The stars observed in the field of NGC 2383 are shown here.*

NGC 2383 We have obtained photometric measurements in B, V, R and I passbands for 353 stars. The X-Y plot of the stars observed are plotted in Figure 3.14. All the observed stars are shown in the V vs (B—V), V vs (V—R) and V vs (V—I) CMDs presented in Figure 3.15. The stars for which spectra are obtained are shown with open circles around them. Stars with errors more than 0.02 mag in V and 0.05 mag in (B—V) are not included. We have identified the 11 stars observed by Vogt & Moffat (1972) and compare with our photometry. The results of comparison is presented in Figure 3.16. The mean values and standard deviation of the differences in V and (B—V) between the present data and those from Vogt & Moffat (1972) are −0.04±0.009 and −0.03±0.003 respectively. The data is in good agreement, except in one case where the difference is more. In this case, the present determination is fainter, indicating that the photoelectric measurement may not be of a single star, but two or more, due to crowding.
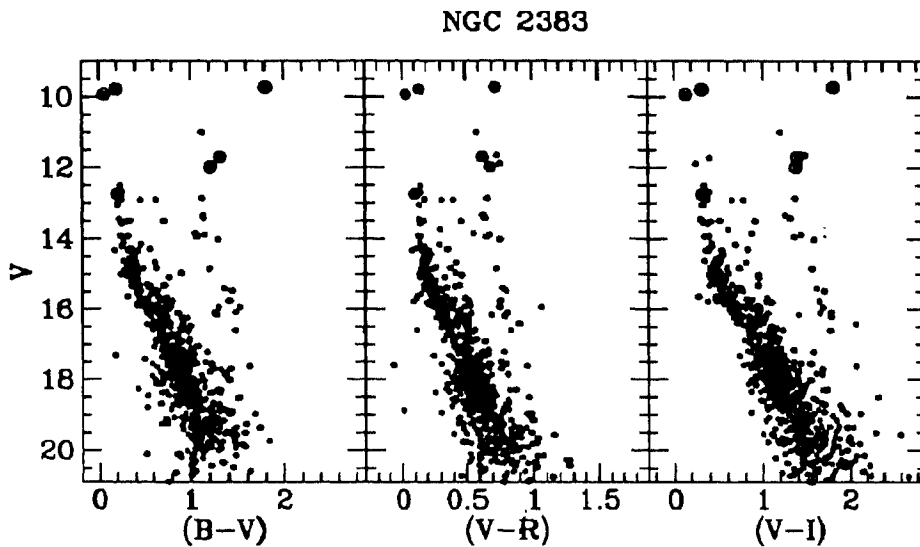
NGC 2383

Figure 3.15: *The cluster CMDs with all the stars observed are shown in the V vs (B−V), V vs (V−R) and V vs (V−I) planes. The stars with spectra are indicated with circles around them.*
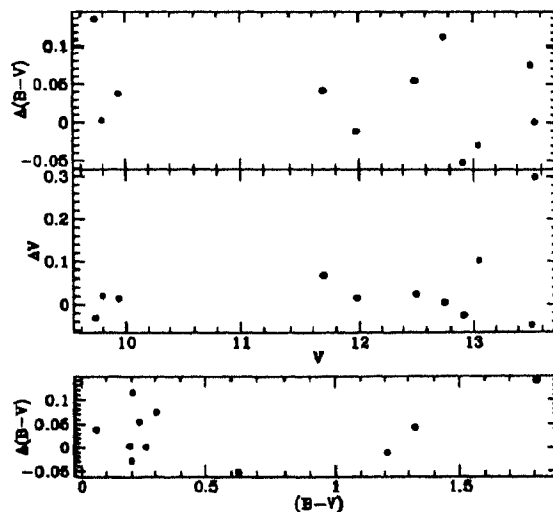
Figure 3.16: *The data for NGC 2383 is compared with Vogt & Moffat (1972) for the 11 common stars. The abscissa is the present data and the difference is calculated as Δ = present− Vogt & Moffat (1972).*

NGC 2384 We have obtained photometry of 304 stars in B, V, R and I pass-bands. The field observed for this cluster covers this cluster and part of NGC
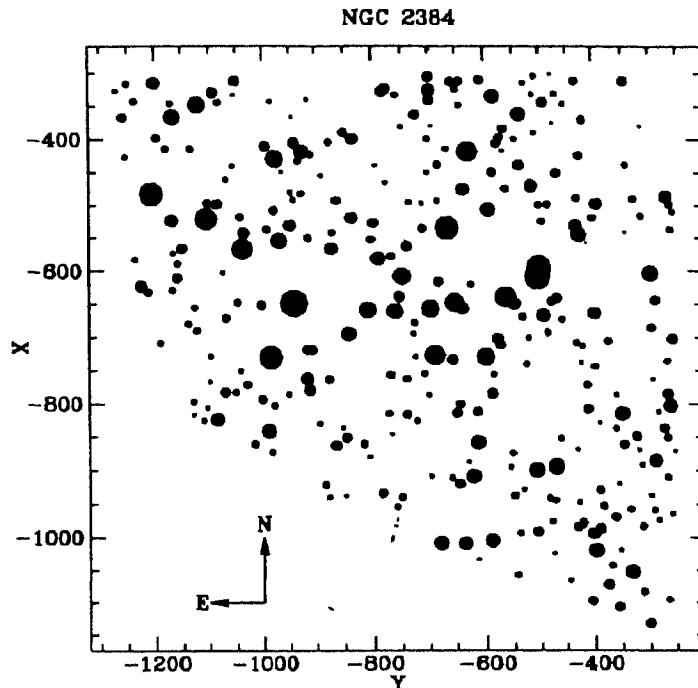
NGC 2384

Figure 3.17: *The cluster region observed is shown here. The stars for which photometry is obtained is shown here. North is up and East towards left.*

2383. The stars in NGC 2383 are used as standard stars to transfer this cluster stars to the standard system. The cluster region observed is shown in Figure 3.17. The common stars with the photometry of Vogt & Moffat (1972) and Hassan (1984) are identified and compared, the results are shown in the Figure 3.18. The mean values and standard deviations of the differences in V and (B−V) between the present data and Vogt & Moffat (1972) data are −0.06±0.002 and 0.05±0.001 respectively and in the case of present and Hassan (1984), the values are −0.03±0.004 and 0.002±0.005 respectively. The present data is in good agreement with both the earlier photometries. The cluster CMD in V vs (B−V), V vs (V−R) and V vs (V−I) planes are shown in Figure 3.19. Stars with errors more than 0.02 mag in V and 0.05 mag in (B−V) are not included. The stars with spectra are marked with open circles around the points.
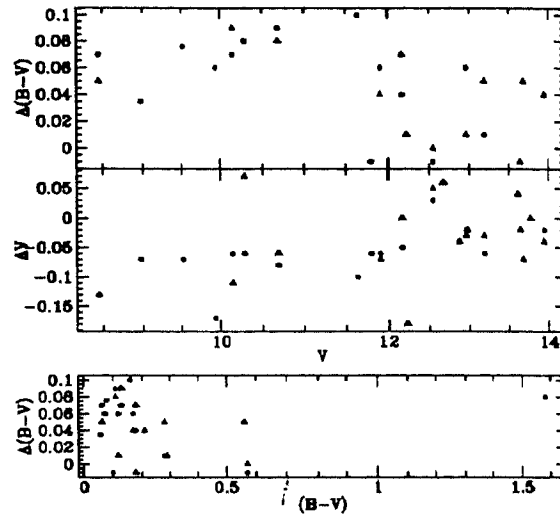
Figure 3.18: *The present photometry for NGC 2384 is compared with those of Vogt & Moffat (1972) (filled circles) and Hassan (1984)(triangles). The difference is calculated such that* Δ = *present—earlier photometry.*

NGC 2384
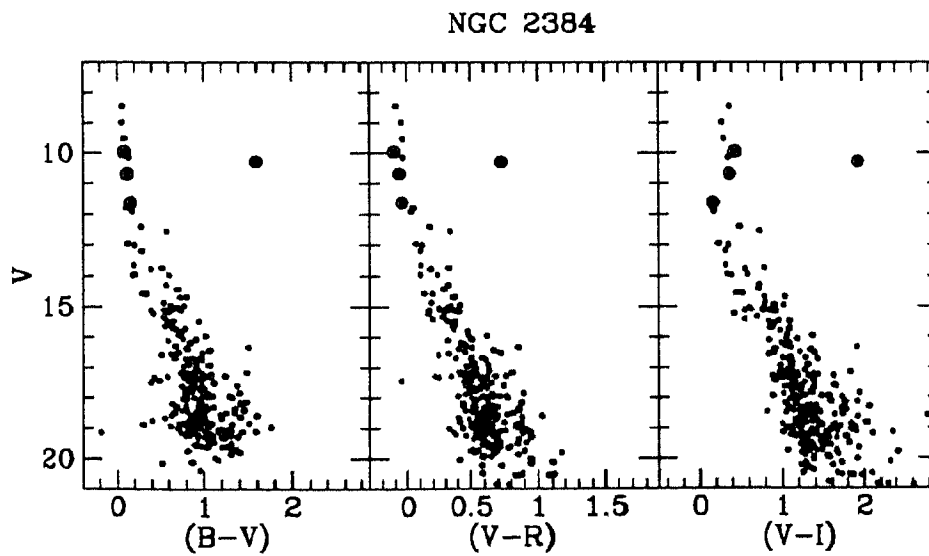
Figure 3.19: *The V vs (B–V), V vs (V–R) and V vs (V–I) CMDs are shown here. The stars with circles around them have spectroscopic data.*

NGC 1907 The cluster is observed in B and V passbands and the V and (B–V) magnitudes from Hoag et al. (1961) is used to convert the present data to the
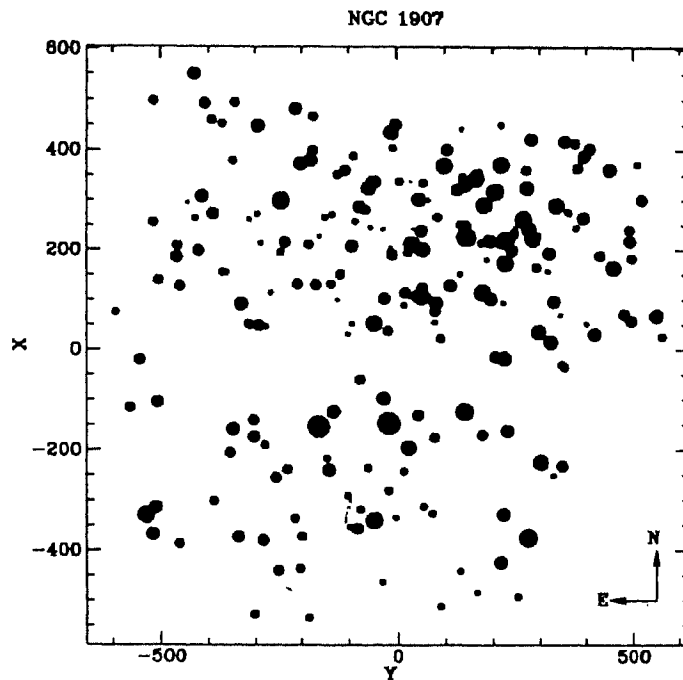
Figure 3.20: *The cluster region observed is shown here, the stars for which photometry is obtained is plotted here. The North is up and East is left.*
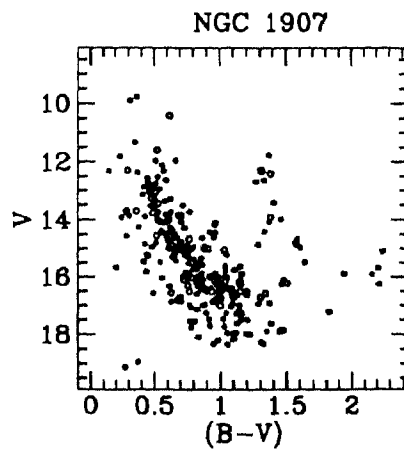
Figure 3.21: *The V vs (B—V) CMD of NGC 1907 is shown here, the number of stars present is 221. The stars denoted by filled circles are from present photometry and open circles are from Hoag et al. (1961).*

standard system. The field of NGC 1907 is shown in Figure 3.20 and the stars
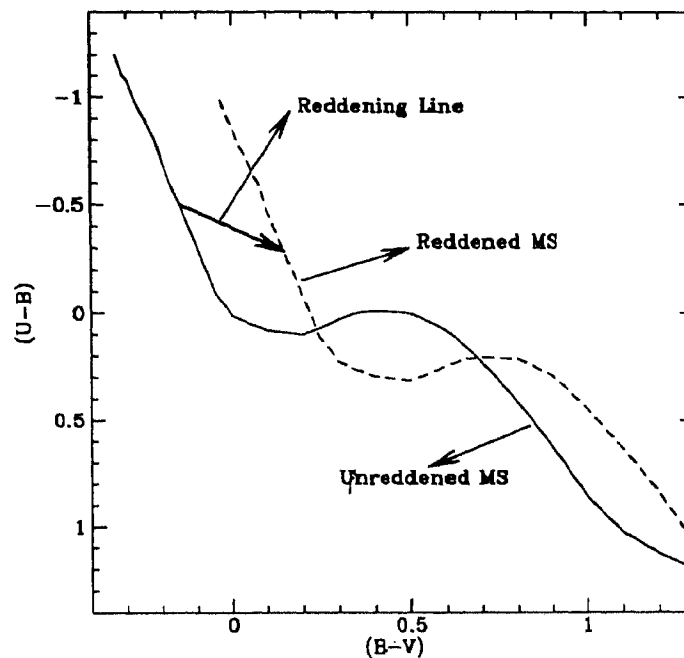
Figure 3.22: *The (U—B) vs (B—V) colour-colour diagram is shown here.*

observed are shown in the V vs (B—V) CMD in the Figure 3.21. Stars with errors more than 0.02 mag in V and 0.05 mag in (B—V) are not included in this figure. The stars which are not observed, but present in Hoag (1961) are included in this figure. There seems to be a lot of spread in the cluster MS, suggesting large amount of differential reddening. The Lyngå's catalogue also notes this by the letter v next to the reddening value of 0.42. The (U—B) vs (B—V) diagram using the U, B and V data of Hoag et al. (1961) does not have enough stars above the clump to determine the differential reddening. The MS as seen in Figure 3.21 has a denser region, which can be considered as the cluster sequence.

3.5 Reddening and Distance

The usual method to determine interstellar reddening of an open cluster is with the help of (U—B) versus (B—V) colour-colour diagram (Becker & Stock

1954). The stars of a given cluster in the colour-colour diagram will be reddened in comparison to the unreddened sequence, in a line parallel to the reddening line, as shown in the Figure 3.22. The slope of the reddening line is given by the ratio of the colour excesses, $E(U-B)/E(B-V) = 0.72$ (Johnson & Morgan 1953). Since we do not have magnitude of the stars in the U pass band, we use the data available in the literature. This method of reddening also helps in determining the differential reddening, if present, across the face of the cluster. This is our first method to determine the reddening.

The another method used to determine the reddening and distance from the present photometric data is by the fitting of ZAMS to the MS of the cluster CMD. We have the cluster CMDs in V vs $(B-V)$ and V vs $(V-I)$ and in some cases, V vs $(V-R)$ also. The simultaneous fitting of same distance modulus, $(V-M_V)$ to all the CMDs give the value of reddening $E(B-V)$, $E(V-R)$ and $E(V-I)$. This is our second method to determine the reddening, which estimates the distance modulus also.

The third method we adopted to determine the reddening $E(B-V)$ is from the colour-colour plot of $(B-I)$ vs $(B-V)$. The method is discussed in Natali et al. (1994) and presents a parameter which can be used to determine the interstellar reddening. The plot of $(B-I)$ vs $(B-V)$ turns out to be a straight line with a slope larger than for plots of $(B-V)$ with respect to other colours in B, V, R and I bands. This larger value is due to the large difference between the central wavelength of B and I bands. The relation between $(B-I)$ and $(B-V)$ is then $(B-I) = \beta (B-V) + C$, where, β is the slope and C is the y-intercept. The interstellar absorptions in B and I, referred to the V band, are $A_B = 1.324$, $A_I = 0.48$ (Rieke & Lebofsky 1985). The ratio between the two colour excesses will be $E(B-I)/E(B-V) = 2.64$. Therefore the relation between $(B-V)$ and $(B-I)$ becomes,

$$(B - I) = \beta(B - V) + E(B - V)(2.64 - \beta)$$

Therefore,

$$E(B - V) = \frac{C}{(2.64 - \beta)}$$

Once the reddening is estimated, the extinction in the V magnitude can be determined using the relation $A_V = R \times E(B - V)$. The value of R is assumed to

be 3.1. The intrinsic V magnitude then becomes $V_0 = V - A_V$. The distances to the clusters are found from the estimates of distance modulus, which is obtained in the second method. The distance modulus is related to distance by the relation, $(V_0 - M_V) = 5 \log D - 5$. From this relation, the distance to the cluster, D in parsec, can be computed.

3.5.1 Estimation of errors

The uncertainties associated with the reddening and distance determinations using the methods described above are discussed below.

Reddening The errors in the determination of the reddening mainly arise from the uncertainties in the intrinsic colours of the star which constitute the unreddened MS. In the method 1, if the uncertainties in $(U-B)_0$ and $(B-V)_0$ are $\sigma_{(U-B)_0}$ and $\sigma_{(B-V)_0}$ and the systematic uncertainty in $E(B-V)$ is given by,

$$\sigma^2_{E(B-V)} \sim \sigma^2_{(U-B)_0} + \sigma^2_{(B-V)_0}$$

Schmidt-Kaler (1982) have estimated that $\sigma_{(B-V)_0} \sim 0.04$ mag and $\sigma_{(U-B)_0} \sim 0.03$ mag. Therefore, the systematic error in $E(B-V)$, $\sigma_{E(B-V)} \sim 0.05$ mag.

The reddening estimated using method 2 is by visual fitting of ZAMS to the cluster MS and the uncertainty in the visual estimate is ~ 0.02 mag. Therefore, the uncertainty in $E(B-V)$ is

$$\sigma^2_{E(B-V)} \sim 0.02^2 + \sigma^2_{(B-V)_0}$$

The uncertainty corresponding to the second term is 0.04 mag as mentioned above. Thus, in the case of second method, the uncertainty in $E(B-V)$ is, $\sigma_{E(B-V)} \sim 0.05$ mag.

The third method uses the relation,

$$E(B-V) = \frac{C}{(2.64 - \beta)}$$

The uncertainty in $E(B-V)$ is,

$$\sigma^2_{E(B-V)} \sim \sigma^2_C + \sigma^2_\beta$$

The values of σ_C and σ_β are evaluated in individual cases.

The distances are estimated using the fitting of ZAMS to the cluster MS. The problem of fitting a fiducial ZAMS to an observed CMD is a pattern-matching process, which does not lend itself to a quantitative determination of the uncertainty in the derived distances. A detailed analysis of the uncertainty in the distance estimate is done by Phelps & Janes (1994). They estimate that the uncertainty in the determination of distance modulus, $\sigma_{(V_0-M_V)}$ is mainly dominated by the error in the calibration of M_V, which is $\sigma_{M_V} \sim 0.3$ mag, and the total uncertainty in the distance modulus is, $\sigma_{(V_0-M_V)} \sim 0.32$ mag. This gives rise the uncertainty in the distance,

$$\sigma_D^2 = 0.213 D^2 \sigma_{(V_0-M_V)}^2$$

where, D is in parsec. The uncertainty in the relative distances is much less if the fitting of ZAMS are used for all the clusters in the sample. In this case, the systematic error in distance modulus reduces to $\sigma_{(V_0-M_V)} \sim 0.10$ mag. As the uncertainty in distance is a function of distance, the errors are determined, when the individual cluster distances are estimated.

3.5.2 Method 1

We use the photographic data from Hoag et al. (1961) for NGC 1912 to obtain the (U−B) vs (B−V) colour-colour diagram shown in Figure 3.23. The unreddened MS is shifted in (B−V) and (U−B) to fit observed MS. There are only very few stars in the region above the clump. The unreddened sequence is shifted by 0.2 mag in (B−V) to match the cluster sequence and thus the reddening towards the cluster NGC 1912 is 0.20 mag. A few stars are seen to the left of the cluster sequence and we estimate a reddening of 0.40 mag for these stars. This indicates that there is a spread of ~ 0.20 mag in (B−V). The spread in the (B−V) of the cluster members are produced due to the presence of binaries and stars with high rotational velocities (Maeder 1974). These produce an intrinsic spread in the reddening, E(B−V) of the cluster, which is $\Delta E(B-V) \leq 0.12$ mag. The spread in E(B−V) estimated for this cluster is more than the intrinsic spread by 0.08 mag, which is almost equal to the error in the determination of E(B−V) .
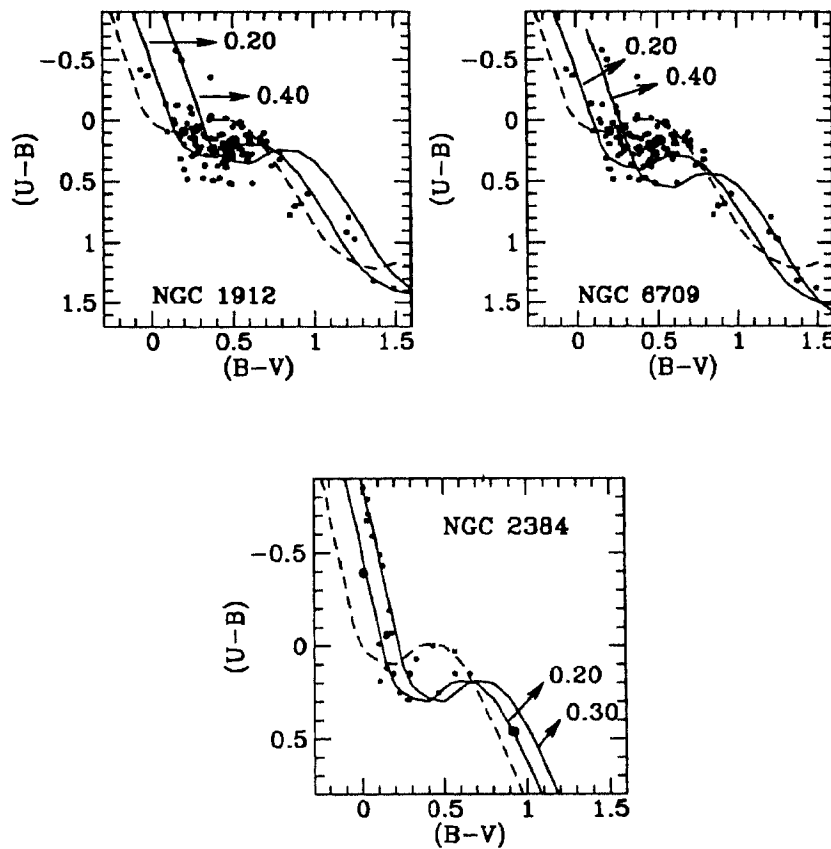
Figure 3.23: *The figure shows the (U—B) vs (B—V) diagrams for the clusters NGC 1912, NGC 6709, NGC 2384. For NGC 1912 and NGC 6709 we have used the photographic data of Hoag et al. (1961). In the case of NGC 2384, photographic data from Hassan (1984) are used. The dashed line is the unreddened MS and the amount of shift in (B—V) for the continuous lines are shown.*

Therefore, we conclude that there is very little differential reddening across the cluster phase of NGC 1912.

The photographic data from Hoag et al. (1961) is used for NGC 6709 and the (U—B) vs (B—V) diagram is shown in Figure 3.23. The unreddened MS is shifted by 0.20 to match the cluster sequence and therefore, the cluster reddening, E(B—V) = 0.20 mag. A spread of 0.2 mag in E(B—V) is seen in the cluster stars. This spread in E(B—V) is similar to the value obtained for NGC 1912 and therefore, the differential reddening is almost negligible.

In the case of NGC 2384, the U, B and V data of Hassan (1984) is used to

NGC 1912
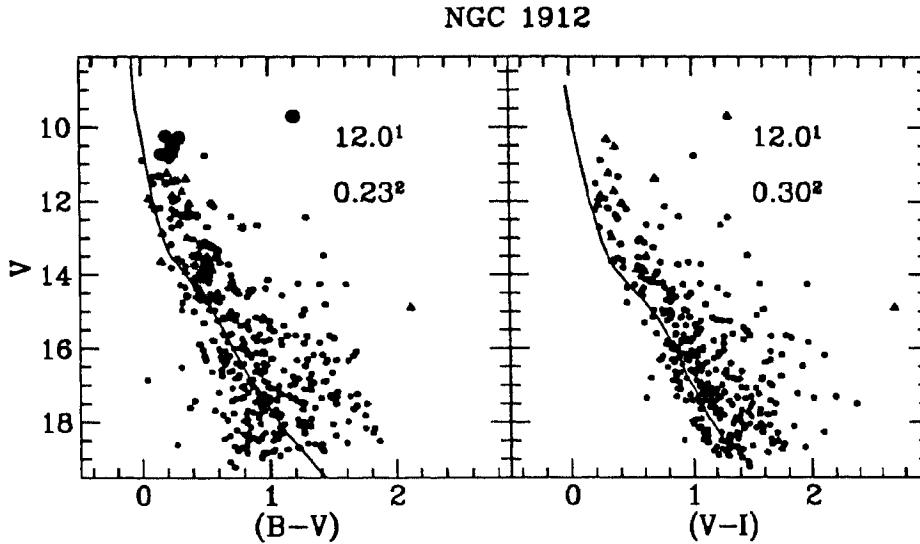
Figure 3.24: *The CMDs are shown in the 3 figures. The values of distance modulus are shown with superscript 1 and the reddening with superscript 2.*

find the reddening. The (U—B) vs (B—V) plot is shown in Figure 3.23. The reddening line is shifted by 0.20 mag in (B—V) to match the cluster sequence. Another sequence shifted by 0.30 mag is also seen in the figure. The stars marked with circles around them are non-members, the bluer one is star 4 and the redder one is star 14. The stars in the clump indicate that the reddening for one set of cluster stars is 0.20 mag. The brighter stars are thus a little more reddened, that is 0.30 mag. Apart from this, the cluster does not seem to have any differential reddening.

3.5.3 Method 2

NGC 1912 The simultaneous fitting of ZAMS to the V vs (B—V) and the V vs (V—I) CMDs estimate the value of distance modulus as 12.0 mag, as shown in the Figure 3.24. The reddening then turns out to be 0.23 mag and 0.33 mag for E(B—V) and E(V—I) respectively. This will give rise to a value of 1.44 for the ratio, E(V—I) /E(B—V). Then the value of A_V becomes $A_V = 3.1 \times$ E(B—V), which is 0.71 mag. This leads to a value of 11.29 for $(V_0 - M_V)$ and 1810 ± 265 pc for distance.

NGC 6709
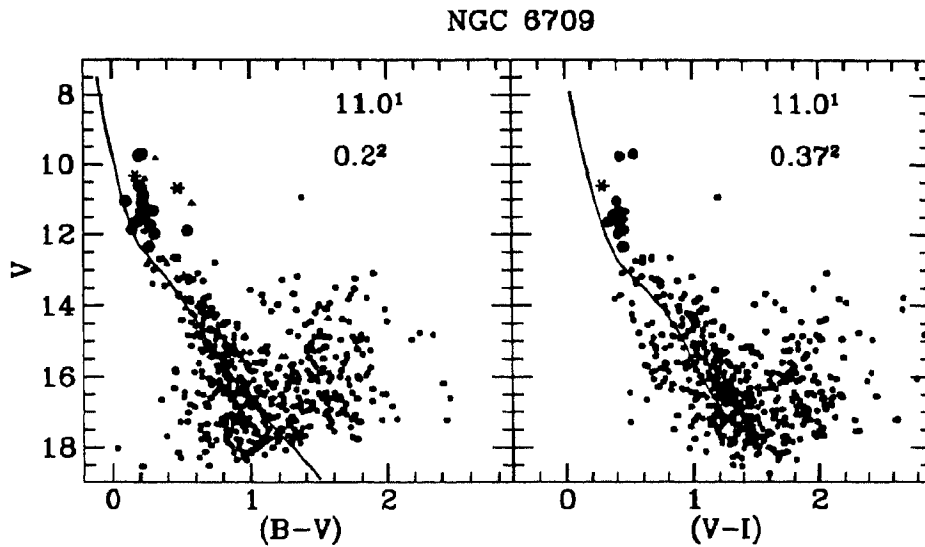
Figure 3.25: *The V vs (B—V) and V vs (V—I) are fitted with the ZAMS to estimate the used to find the reddening as explained in the text. The values of distance modulus are shown with superscript 1 and reddening with superscript 2.*

NGC 2383
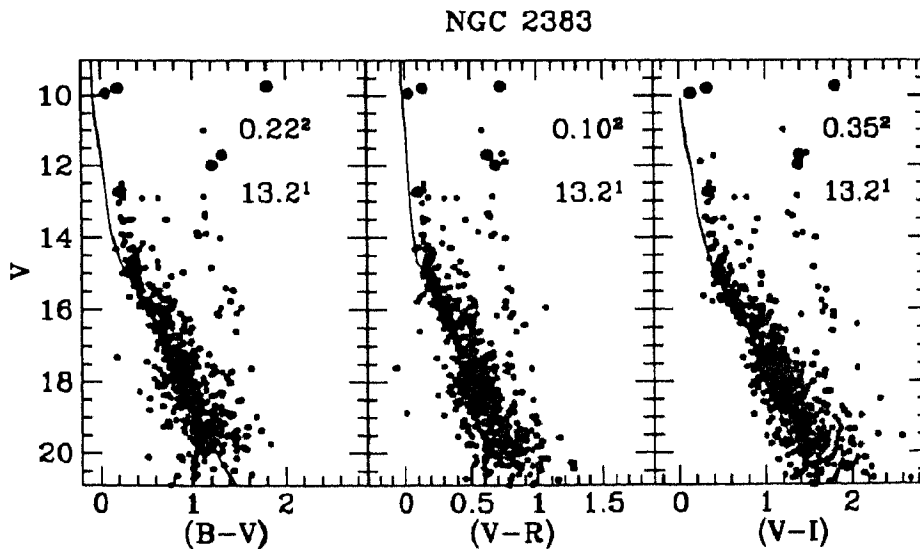
Figure 3.26: *The V vs (B—V), V vs (V—R) and V vs (V—I) CMDs are fitted with ZAMS. The distance modulus is shown with superscript 1 and the reddening with 2.*

NGC 6709 The V vs (B—V) and V vs (V—I) CMDs simultaneously fitted with

ZAMS to estimate the distance modulus as shown in Figure 3.25. We estimate

NGC 2384
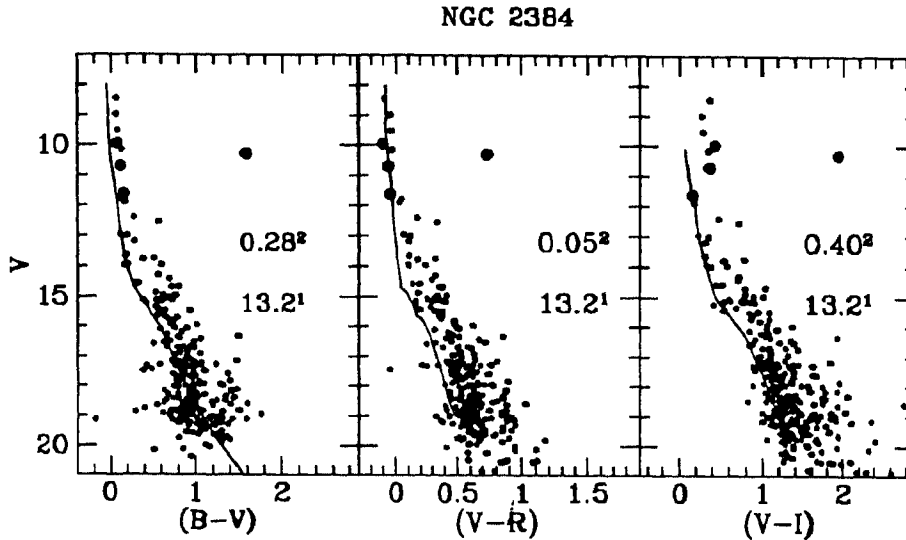
Figure 3.27: *The ZAMS is fitted to the cluster CMDs. The superscript 1 refers to the distance modulus and 2 refers to the reddening.*

a value of 11.0 mag for distance modulus and $E(B-V) = 0.20$ and $E(V-I) = 0.37$ as the reddening values. This will give rise to a value of 1.85 for $E(V-I)$ /$E(B-V)$. The value of A_V towards the cluster then becomes 0.62 mag. This will correspond to a value of 10.38 mag for $(V_0 - M_V)$ and 1190±175 pc for distance.

NGC 2383 The ZAMS are fitted simultaneously to the V vs (B−V), V vs (V−R) and V vs (V−I) CMDs, to estimate the distance modulus as 13.3 mag, as shown in the Figure 3.26. The reddening values estimated are 0.22 for $E(B-V)$, 0.10 for $E(V-R)$ and 0.35 for $E(V-I)$. Thus we find a value of 1.6 for $E(V-I)$ /$E(B-V)$ and 0.46 for $E(V-R)$ /$E(B-V)$. The interstellar extinction in this direction, A_V is found to be 0.68 mag, giving rise to a distance of 3340±490 pc to the cluster.

NGC 2384 The simultaneous fitting of ZAMS to the V vs (B−V), V vs (V−R) and V vs (V−I) CMDs estimate the distance modulus as 13.2 mag as shown in Figure 3.27. We obtain the reddening values as $E(B-V)$=0.28, $E(V-R)$ =0.05 and $E(V-I)$ =0.40. Then the ratio $E(V-I)$ /$E(B-V)$ = 1.43 and
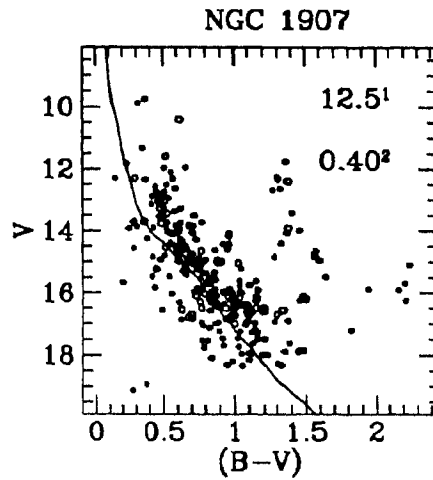
Figure 3.28: *The cluster CMD is fitted with ZAMS to obtain the reddening and distance. The estimated value of distance modulus is indicated by the superscript 1 and reddening by 2.*

$E(V-R)/E(B-V) = 0.18$. It can be seen that the brightest 6 stars in the CMD fall to the right of the ZAMS indicating that they are more reddened. This result is similar to that found in the $(U-B)$ vs $(B-V)$ plot. Thus the brighter stars are more reddened than the fainter MS stars. The visual extinction then becomes, $A_V = 0.87$ mag and the distance to the cluster is 2925 ± 430 pc.

NGC 1907 We determine the reddening and distance by fitting ZAMS as shown in Figure 3.28. This gives a value of 0.40 mag for $E(B-V)$ and 12.5 mag for the distance modulus. The value of A_V then becomes 1.24 mag and the distance 1785 ± 260 pc.

3.5.4 Method 3

We plot $(B-I)$ vs $(B-V)$ for NGC 1912, as shown in Figure 3.29 and fit a straight line using least square fit, iteratively removing the stars which are lying off by more than 3 sigma from the straight line. The value we get for β is 2.11 ± 0.02 and 0.13 ± 0.02 for C. This gives a value of 0.25 ± 0.03 mag for $E(B-V)$. In the case of NGC 6709, similar procedure is adopted and the value we get for
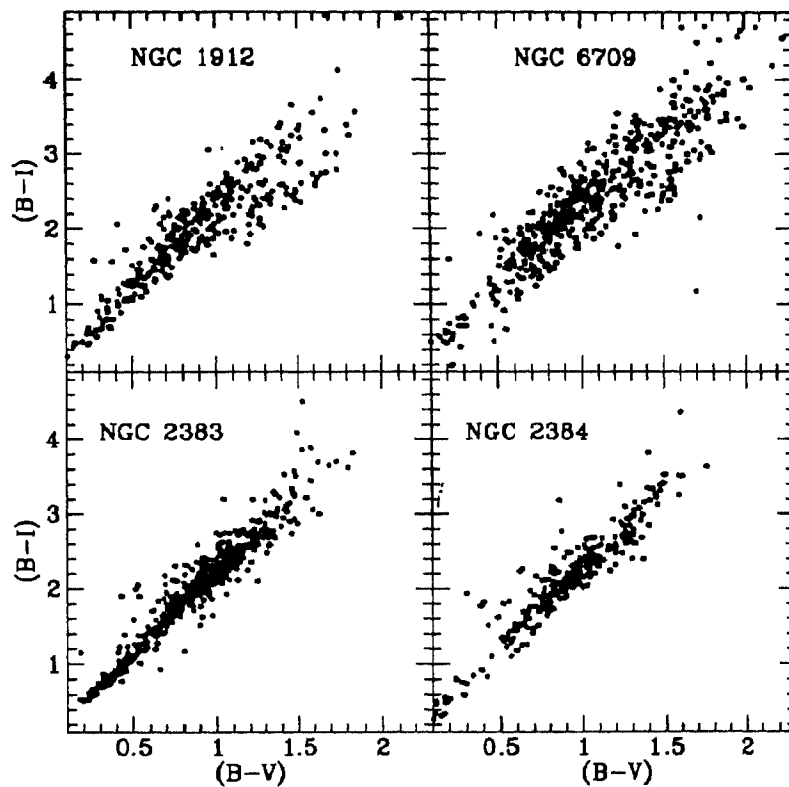
Figure 3.29: *The colour-colour plot of (B—I) vs (B—V) is shown here, which is used to find the reddening as explained in the text.*

β is 2.02±0.02 and 0.22±0.02 for C yielding a value of 0.35±0.03 for E(B−V). For, NGC 2383, we obtain a value of 2.13±0.02 for β, 0.11±0.01 for C. The value obtained for E(B−V) is 0.22±0.02 mag. The least square fit to the data of NGC 2384 gives a value of 2.02 ± 0.02 for β and 0.13 ± 0.02 for the y-intercept, C. This gives a value of 0.21±0.03 mag for E(B−V). In all the cases, the correlation coefficient of the least-square fit is ~ 98.0.

3.6 Spectral classification

The flux calibrated spectra of the stars observed are classified with the help of the digital spectral library from Jacoby et al. (1984). This library contains spectra of 161 stars between the spectral classes O to M covering the luminosity classes

Table 3.4: *Details of the Spectroscopic observations. All the observations are obtained from 1.02m telescope.*

Observing date	Cluster	# of stars
14th February 92	NGC 1912	8 stars
18th December 92	NGC 1912	3 stars
18th February 93	NGC 1912	6 stars
17th April 93	NGC 6709	4 stars
18th April 93	NGC 1912	1 star
26th April 93	NGC 6709	4 stars
26th June 93	NGC 6709	7 stars
20th January 94	NGC 2383	3 stars
6th February 94	NGC 2383	7 stars
5th February 94	NGC 2384	4 stars
4th June 94	NGC 6709	2 stars
26th June 94	NGC 6709	1 star

V, III & I. The spectra extend from 3510 to 7427 Å at a resolution of $\sim$ 4.5 Å and sampled at 1.4 Å interval. We have chosen 158 spectra of solar metallicity from the sample. The spectra given here are of individual stars and are corrected for interstellar reddening. The main advantage is that the spectra can be plotted along with the observed ones for a good comparison. The library spectra are normalised to 100 at 5450 Å , therefore the observed spectra are also normalised in the same way for comparison. All the spectra are observed with the 1.02m telescope and the summary of observation is tabulated in Table 3.4.

The estimated spectral type and luminosity class of the member stars in the clusters are used to estimate the values of reddening and distance to the clusters. We make use of the M_V , $(B-V)_0$ tabulation of Schmidt-Kaler (1982). From the photometric estimates of V and $(B-V)$, the values of $(V-M_V)$ and $E(B-V)$ are estimated. The error involved in the determination of $E(B-V)$ includes the error in the calibration of $(B-V)_0$, which is 0.04 mag, the error in the determination of the spectral type contributing an error of 0.05 mag in the determination of $(B-V)_0$ and the photometric error in $(B-V)$, which is 0.02 mag. The total error
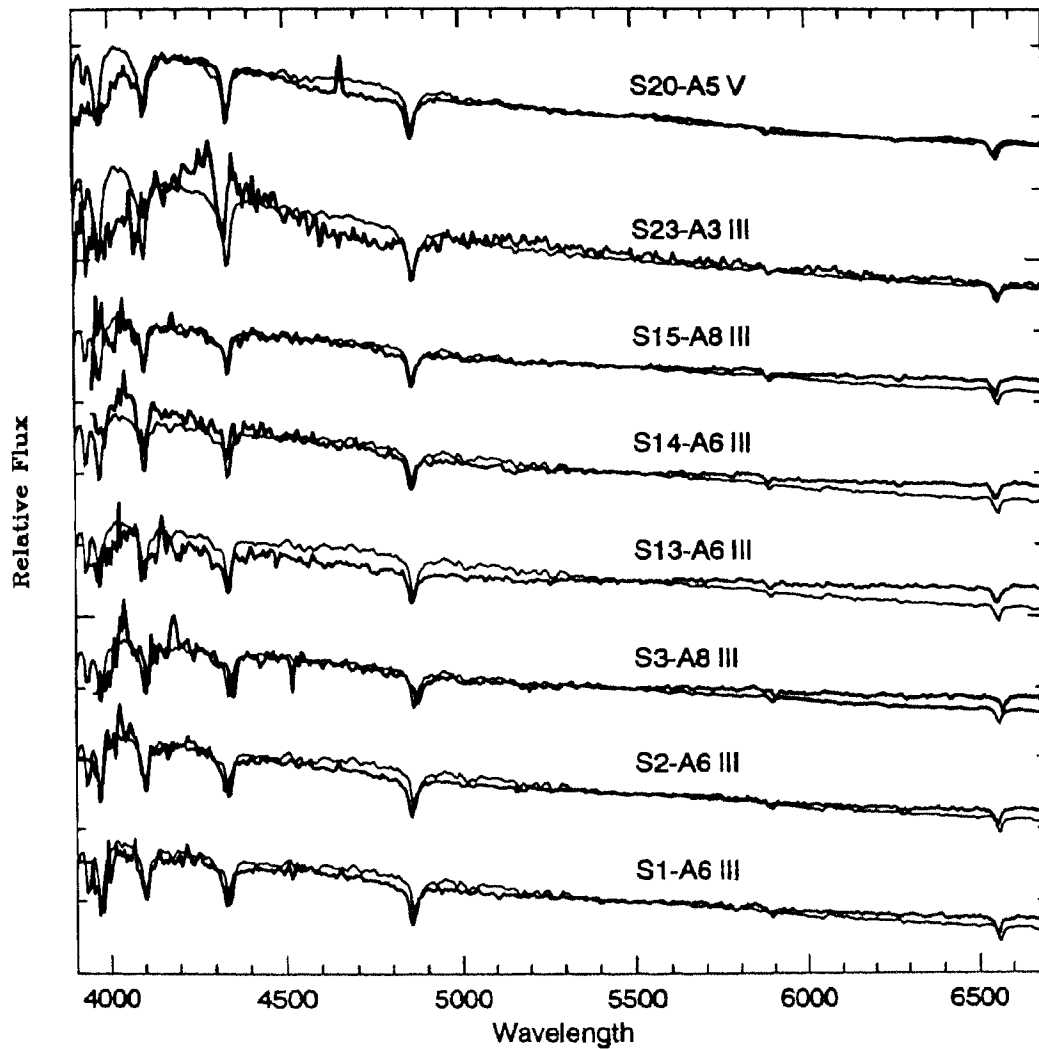
Figure 3.30: *The spectra of 8 stars in NGC 1912, along with the matching library spectra are shown. The thick line is the observed one and the thin line is the library spectra.*

is, $\sigma_{E(B-V)} \sim 0.07$ mag. The uncertainty in the estimated distance modulus consists of the photometric error in V, the uncertainty in the estimation of the luminosity class and the calibration error in M_V , which are 0.01 mag, 0.04 mag and 0.3 mag respectively. Therefore, the total uncertainty in the distance modulus
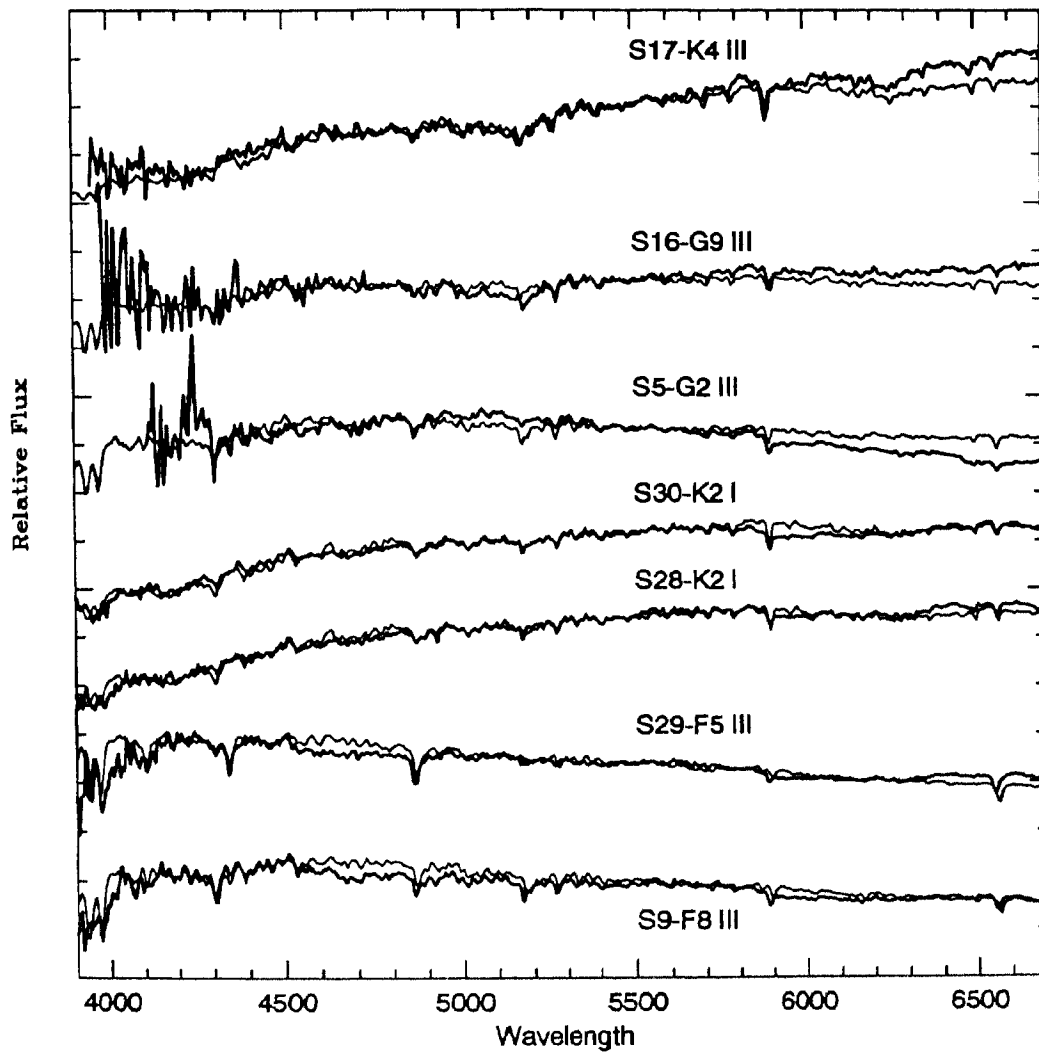
Figure 3.31: *Spectra for 7 stars in NGC 1912, see Figure 3.30 for details.*

is, $\sigma_{(V-M_V)} \sim 0.5$ mag.

NGC 1912 We have obtained spectra for 15 stars in the cluster. The observed spectra and the best fitting library spectra from Jacoby et al. (1984) are shown in Figures 3.30 and 3.31. The present classification is tabulated in Table 3.5. This

Table 3.5: *The results of spectral classification for the 15 stars in NGC 1912 are tabulated. Column one gives the present identification number and 2 gives the corresponding number in Mermilliod (1994). Present results are in column 3 and the spectral information from the literature are in column 4, where the superscript 1 refers to Hoag & Applequist (1965) and 2 refers to Sowell (1987). The V and (B−V) mag are tabulated in columns 5 and 6. Some values of V and (B−V) magnitudes are taken from Hoag et al (1961), they are marked with the † symbol. The M_V and (B−V)$_0$ values are taken from Schmidt-Kaler (1982) corresponding to the spectral type and the luminosity class and are given in columns 7 and 8. The estimated values of distance modulus (DM) and reddening are in column 9 and 10. The membership probability from Mills (1967) is shown in column 11.*

Star	hpd	Sp.Cl	Lit.	V	(B−V)	M_V	(B−V)$_0$	DM	E(B−V)	Prob
S20	16	A5V	−	10.54	0.25	1.95	0.15	8.59	0.10	0.61
S15	157	A8III	−	10.45	0.30†	1.2	0.25	9.25	0.05	0.61
S5	3	G2III	−	9.71	1.19	0.9	0.77	8.91	0.42	0.74
S23	29	A3III	−	10.47†	0.24†	0.5	0.08	9.97	0.16	0.42
S1	49	A6III	A2V[1]	10.62†	0.23†	0.9	0.19	9.72	0.04	0.53
S2	50	A6III	A0V[1]	10.24†	0.19†	0.9	0.19	9.34	0.00	0.47
S14	160	A5III	−	10.73†	0.16†	0.7	0.15	10.03	0.01	0.57
S9	16	F8III	−	10.27	0.65	1.24	0.54	9.03	0.11	0.0
S29	69	F5III	−	10.77	0.50	1.60	0.43	9.29	0.03	0.03
S13	164	A6III	−	11.34	0.23†	0.9	0.19	10.44	0.05	0.0
S3	31	A8III	−	11.34†	0.21†	1.2	0.25	10.14	0.00	0.25
S28	70	K2 I	G8III[2]	10.18	1.21					0.24
S30	194	K2 I	−	−						0.0
S16	292	G9III	−	−						0.0
S17	−	K4III	−	−						−

also contains identification numbers, the V and (B−V) magnitudes of these stars and their membership information and the spectral information already available. The estimated values of reddening and distance modulus are also tabulated. It can be seen that we get comparatively late spectral types and luminosity classes compared to the determination from Hoag & Applequist (1965) for the stars S1 and S2. Hoag & Applequist (1965) have used Hγ photoelectric photometry to determine the spectral information. The figure presented in their paper giving the dependence of Hγ on spectral type shows that the variation in Hγ strength across spectral type A is very small and also the turnover of the Hγ strength occurs in this spectral type. Therefore, Hγ strength is not a good parameter

to determine the spectral type near A. This may be the reason for the different results obtained here. In the case of the luminosity class, it is very difficult to differentiate between an A type MS and an A type giant when we are looking at the relative flux. The positions of the stars S1 and S2 in the CMD show that their identification as giants might be correct. Considering the results from the proper motion probability given in column 11, the first 7 stars in the table 3.5 are members. The distance modulus for these stars given in column 9, show a variation of 1.4 mag, and those of some of the non-members also happen to lie in the same range, tempting one to consider the stars S9, S29 and S3 as members. Star S13 has a high value for distance modulus and probably a non-member as also suggested by the proper motion data. The star S28 is also known as HD 35878 and its radial velocity has been determined as −1.0, which is close to the mean value of the radial velocity for the cluster. Our spectral classification finds that this has to be a foreground star, therefore we do not consider it as a member. As the library do not have spectra in between A3III and A6III and the spectra of S14 falls in between A3III and A6III, the star S14 is classified as A5III, though it is plotted with the A6III library spectra in the figure 3.30. Among the proper motion member stars, S20 and S5 have a low value for distance modulus compared to the rest of the members, though they have a high value of proper motion probability. Considering the remaining 5 of the 7 such members, the mean value of distance modulus is 9.7 mag. If all the stars, except S13 are considered for which distance modulus is estimated, the mean value becomes 9.4 mag. Considering all the stars except, S5, the mean value of the reddening is 0.06 mag.

NGC 6709 We have obtained spectra for 12 stars in the cluster. The spectra along with the best fitting library spectra are shown in the Figures 3.32 and 3.33. The derived spectral and luminosity class is also shown in the figure. The results in the tabular from can be seen in Table 3.6. This contains the identification number as per in Mermilliod (1994), HD number if available and the spectral information available in the literature. The Table 3.7 lists V and (B−V) magnitudes from photometry, the M_V and $(B−V)_0$ magnitudes according to the
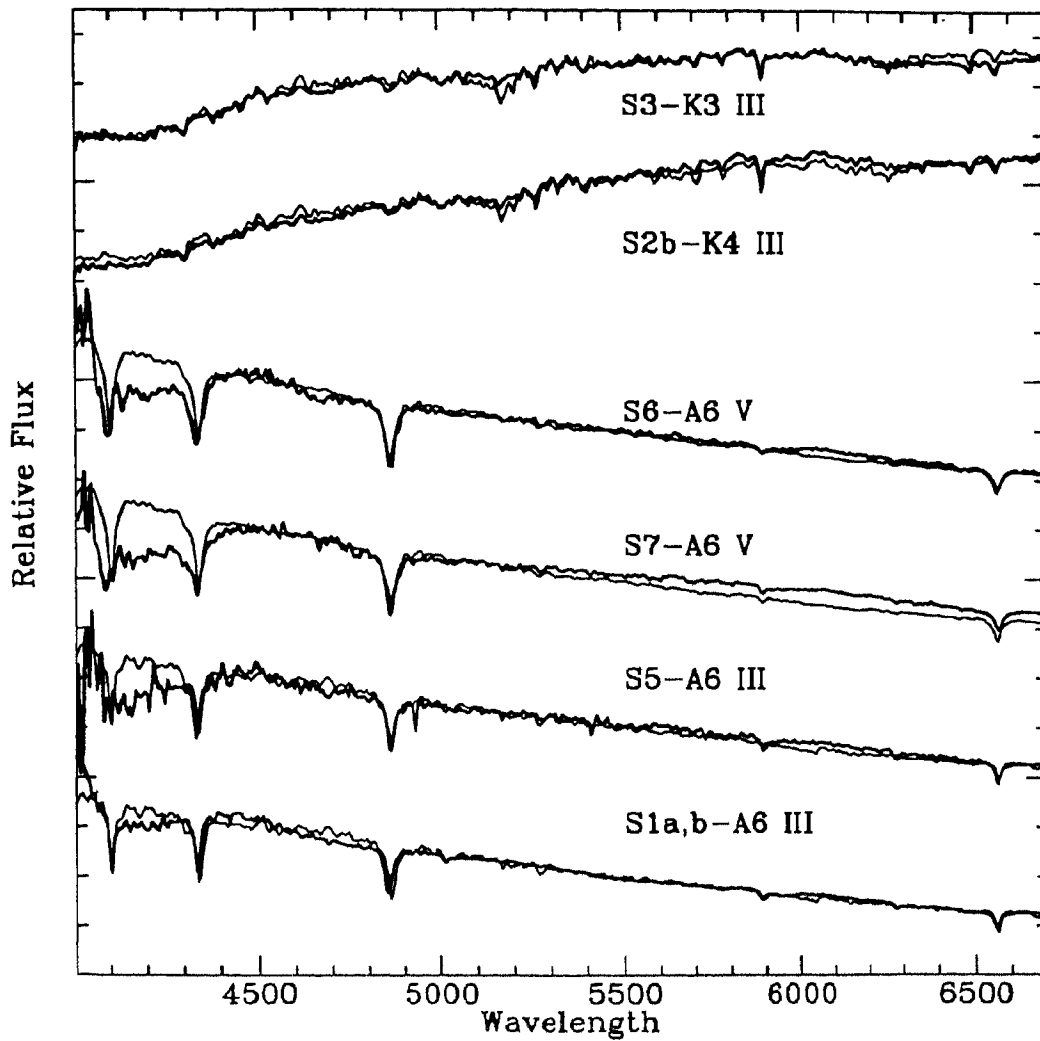
Figure 3.32: *The spectra of 6 stars in NGC 6709 are shown along with the best matching library spectra. The star number and the estimated spectral and the luminosity class are shown above each spectra.*

spectral and luminosity class and the estimated values of $(V-M_V)$ and $E(B-V)$. It also lists the proper motion probabilities and the radial velocities.

When we compare the spectral class as given in table 3.6, it is seen that the present determination estimates comparatively late spectral types as well as luminosity classes when compared with the estimations available. The analysis
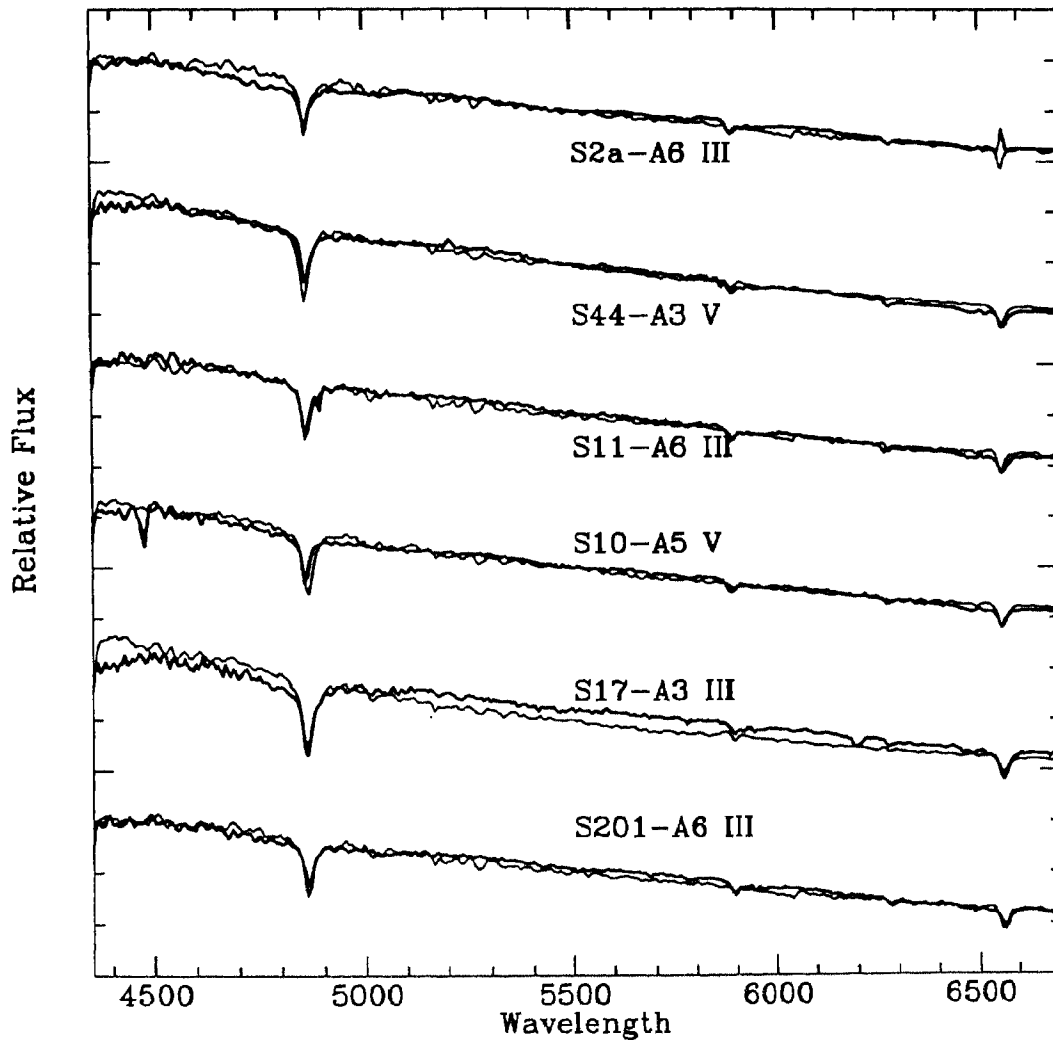
Figure 3.33: *The spectra for 6 stars in NGC 6709 are shown. See figure 3.32 for details.*

by Hoag & Applequist (1965) is based on Hγ photoelectric classification using equivalent width. The Hγ values may not be a good indicator for classification for stars in the spectral class A, as explained earlier. This may be the reason for the inconsistency. Moreover, the present analysis uses a standard library with a good coverage of all spectral types and luminosity classes. This may explain the discrepancies with respect to the other results. The radial velocity values given

Table 3.6: *The spectral classification for the observed spectra in NGC 6709 are tabulated. The second column refers to the identification number in Mermilliod (1994). Some stars are catalogued in the HD catalogue, their numbers are given in column 3. The spectral information from the literature for stars available are shown in the column 5. The references are given in the parenthesis, where 1 refers to Hoag & Applequist (1965), 2 refers to Young & Martin (1973) and 3 refers to Sowell (1987).*

Star	hpd	HD #	Sp.Cl	Lit.
S1a,b	–		A6 III	–
S2b	208		K4 III	K2Ib(3)
S3	303	229716	K3 III	G8 III/IV(3)
S5	293		A6 III	A0V(2)/B9V(1))
S7	–		A6 V	–
S6	291		A6 V	–
S201	201		A6 III	B9 V(1)
S10	372	229700	A5 III	A0 V(2)/A0 II–III(1)
S11	337	229715	A6 III	B9 V(1)
S44	413	229684	A3 V	B6 III(1)
S2a	209	174715	A6 III(Hα em)	–
S17	277		A3 III	–

are the average of the values available from Hayford (1932), Glushkova (1993) and Sowell (1987). The letter v denotes that the values obtained in various estimations are different and hence the radial velocity may be variable. The stars S2a and S2b lie close to each other and are noted as visual doubles by Jeffers et al. (1963). Schild & Romanishin (1976), in their study of Be stars in clusters, find that the stars, S5 and S2a as candidates. We do see Hα emission for S2a, but no Hα emission is seen for the star S5. Either the star has a varying emission such that this particular spectra does not show any emission or the star has ceased to have Hα emission. The second reason is possible as the present spectrum is taken after a span of about 30 yrs and this duration is long enough for the emission to disappear in Be stars. The spectra obtained of star S2a at Hα by Sowell (1987) shows that it is a shell star. We obtained three spectra of this star on different

Table 3.7: *The stars in NGC 6709 for which we have obtained spectra as in Table 3.6 are tabulated with their V and (B—V) magnitudes. The first star in Table 3.6 is not included as it is a combined spectra of two stars, S1a,b. The M_V and (B—V)$_0$ values are taken from Schmidt-Kaler (1982) corresponding to the spectral type and the luminosity class. The columns 6 and 7 tabulate the (V—M_V) and E(B—V). The membership probability from Hakkila et al. (1983) is given in column 8. Some values of V and (B—V) magnitudes are taken from Hoag et al. (1961), they are marked with the † symbol. The mean radial velocity is shown in the last column.*

Star	V	(B—V)	M_V	(B—V)$_0$	DM	E(B—V)	Prob	V_r
S201	10.60	0.20	0.9	0.19	9.70	0.01	0.65	
S10	10.33†	0.17†	0.7	0.15	9.63	0.02	0.85	−21.0v
S11	10.68	0.48	0.9	0.19	9.78	0.29	0.79	
S2a	9.70	0.21	0.9	0.19	8.80	0.02	0.84	
S5	10.92	0.11	0.9	0.19	10.02	0.00	0.40	
S2b	9.13	1.45	0.0	1.39	9.13	0.06	0.06	−11.2
S3	8.95	1.81	0.3	1.27	8.65	0.54	0.20	−14.0v
S7	9.81†	0.31†	2.1	0.18	7.71	0.13	0.0	
S6	10.58	0.25	2.1	0.18	8.48	0.07	0.0	
S44	9.85†	0.12†	1.5	0.08	8.35	0.04	0.0	+22.0
S17	10.93	0.08	1.2	0.08	9.73	0.0	0.0	

nights. At the present resolution, no shell feature is observed, though the Hα emission is present in all the spectra. Also, we classify the spectra as that of A6 spectral type and as a giant. This is consistent with its location on the cluster CMD. This star has a 12μ flux of 0.379 Jy, which corresponds to an IR excess of 0.316 (Sowell 1987).

The membership probability information from Hakkila et al. (1983) shows that only four of the observed stars (the first four in table 7) are members of the cluster. The distance modulus (DM) as given in the column 6 shows that the value is almost the same for the first 3 stars, but less for the fourth one. This star is a emission line star and hence one may not put much weight on its spectroscopic distance modulus, though it is a member. Among the non-members, S3, S7, S6 and S44 have lower value of distance modulus, while S2b, S5 and S17 have
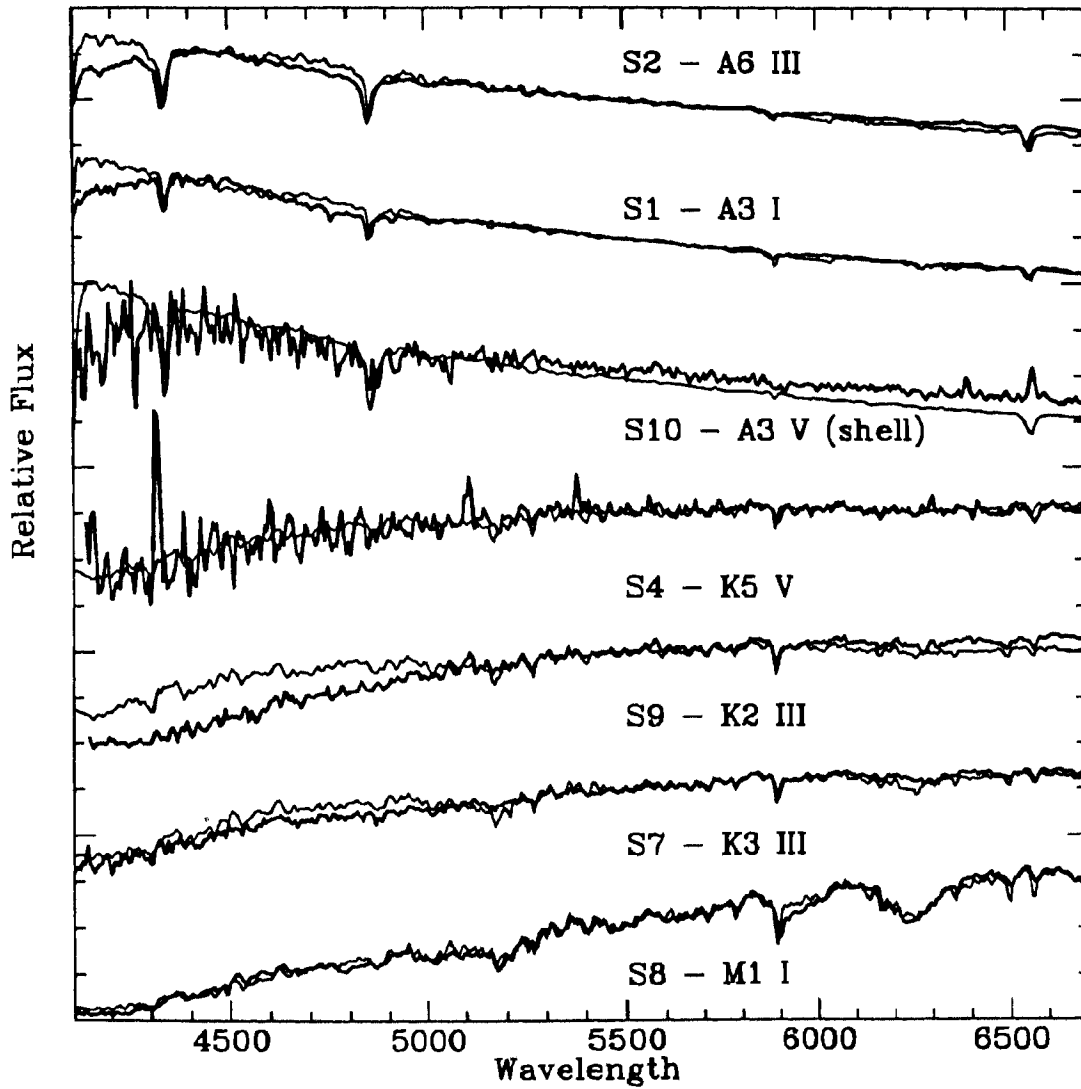
Figure 3.34: *The spectra of 7 stars in NGC 2383 are shown here. The best matching library spectra from Jacoby et al. (1984) are plotted together such that the bold line is the observed one and the thin line is the library spectra. The estimated spectral and luminosity class are shown near each spectra.*

distance modulus similar to that for the members. The star S5 can be classified as member, considering that its proper motion probability is 0.40 and the value

Table 3.8: *The spectral classification results for NGC 2383 are tabulated here. The star number given in the second column corresponds to that of Vogt & Moffat (1972). The third column contains the results of the present study, the symbol * refers to stars with two observed spectra and 's' refers to shell feature. The fourth column contains the classification available already, where the superscript 1 refers to Fitzgerald et al. (1979) and 2 refers to Michigan Catalogue of HD stars. The columns five and six give the V and (B−V) magnitudes from the photometry. The seventh and eighth columns contain the M_V and $(B−V)_0$ values corresponding to the spectral and luminosity class. The distance modulus (DM) is in column nine and reddening in ten.*

Star	#	Sp.Cl	Lit.	V	(B−V)	M_V	$(B−V)_0$	DM	E(B−V)
S1	1	A3 I*	B0 III[1]	9.94	0.07	−6.4	0.02	−	0.05
S2	2	A6 III*	A3 V[1] A9 V[2]	9.80	0.24	0.9	0.19	8.9	0.05
S7	7	K3 III	−	11.69	1.27	0.3	1.27	11.39	0.00
S8	8	M1 I*	K3 III[1]	9.73	1.80	−5.6	1.69	−	0.11
S9	9	K2 III	−	12.00	1.18	0.5	1.16	11.5	0.02
S10	10	A3 V(s)	−	12.76	0.22	1.5	0.08	11.26	0.14

of distance modulus close to that for the members. Therefore, considering these four stars as members, the mean value of the distance modulus becomes 9.8 mag and the reddening value is 0.08 mag.

NGC 2383 We have obtained spectra for 7 stars in this cluster. The spectra and the matching library spectra are plotted in Figure 3.34. The results of the spectral classification are tabulated in Table 3.8. Radial velocity is not available in the literature for any of the stars. The stars S1, S2 and S8 have been observed twice and in both cases the same spectral and luminosity class were obtained, as shown in table 3.8. The star 2 is designated as 58440 in the HD catalogue. The star S10 shows Hα in emission and shell feature in Hβ. The shell nature cannot be confirmed as we have only one good spectra, where the shell feature is seen, but we obtained two poor spectra (due to bad sky) which showed Hα in emission. As the stars S1 and S8 are classified as supergiants, they are very bright background stars. The star S2 has a very low value of distance modulus, indicating that it is

Table 3.9: *The results of spectral classification for NGC 2384 are presented here. The star numbers are same as in Vogt & Moffat (1972). The spectral information from the literature is given in column 3, where the superscript 1 refers to Fitzgerald et al. (1979) and 2 refers to Babu (1985). The estimated distance modulus (DM) and reddening are in columns 8 and 9 respectively. The last column gives the radial velocity, in the case of star 11, it is the average of 3 values. The values for stars 13 and 14 are taken from Liu et al. (1991).*

Star	Sp. Cl.	Lit.	V	(B−V)	M_V	$(B−V)_0$	DM	E(B−V)	rv
S11	B1.5 V	B3 IV[1] B3[2]	9.96	0.07	−2.8	−0.25	12.76	0.32	+57.5
S12	B3 V	B8[2]	11.63	0.16	−1.6	−0.20	13.23	0.36	−
S13	B1.5 V	B8[2]	10.70	0.11	−2.8	−0.25	13.50	0.36	+49.4
S14	K4III	A5[2]	10.29	1.58	0.0	1.39	10.29	0.19	+38.8

a foreground star and those of S7, S9 and S10 are very close to each other and can be considered as members. The mean spectroscopic distance modulus then becomes, 11.4 mag and reddening is 0.05 mag. The results from Vogt & Moffat (1972) are summarised below: S2 is a foreground star; S4 is either a background B star or a foreground G star; S7 and S9 are found to be background giants and S1 is a probable member; S8 is probably a K2 V star. The present CMD shows that star S1 cannot be a member. This is very evident from the well defined MS, turn-off and the large magnitude difference between the turn-off magnitude and that of S1. Similarly, S8 cannot be a member. On the other hand, S7 and S9 can be members, which can be seen while fitting the isochrones. Also, spectroscopically, stars S1 and S8 cannot be members and S7 and S9 can be considered as members. In the case of S2, we also find that it is a foreground star. The fact that S1 is considered as a member might be the reason for getting a lower value of distance modulus by Vogt & Moffat (1972). The present value is based on more number of stars and hence more reliable.

NGC 2384   The spectra of 4 stars along with the best matching library spectra are shown in Figure 3.35. The spectral and luminosity class are written along with the star number near the spectra. The results are tabulated in Table 3.9. Some
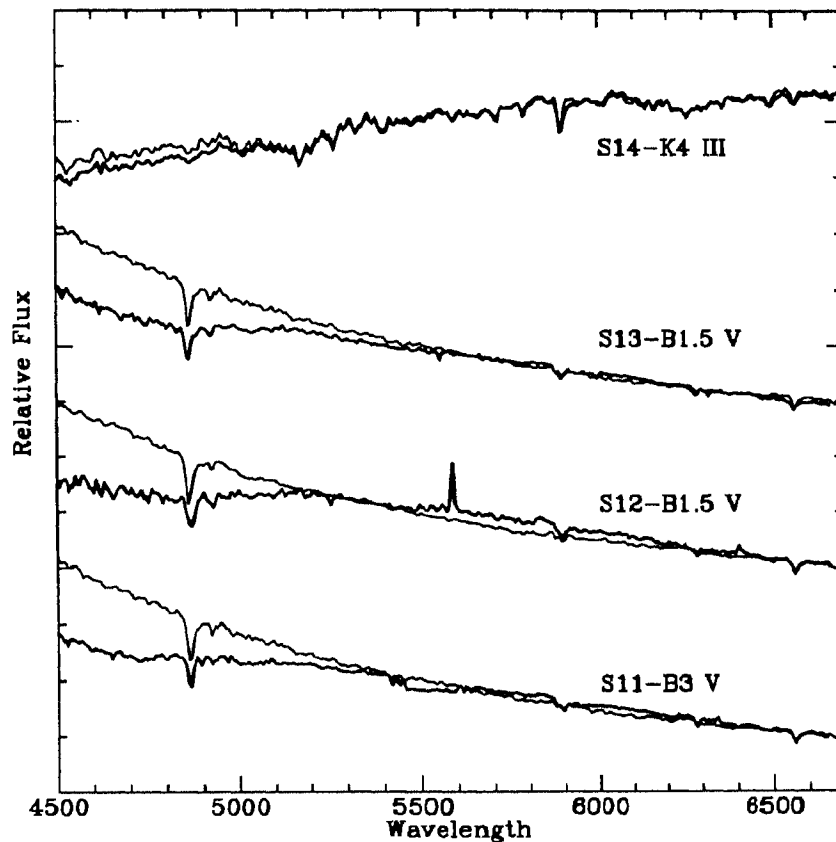
Figure 3.35: *The spectra of four stars in NGC 2384 are shown along with the best matching library spectra. The spectral and luminosity class of each star in indicated in the figure.*

problem in flux calibration of the spectra are seen in the blue region and hence the spectra are used only till 4500 Å in the blue end. The star numbers referred here are that of Vogt & Moffat (1972). The classification of S11 as B3 V is very similar to the classification in the literature. The stars S1 and S10 are identified as HD 58465 and HD 58509 respectively. From the radial velocity measurements (Liu et al. 1989), the star S10 is suspected to be a spectroscopic binary from its variable radial velocity. Hron et al. (1985) find that the stars S1, S2 and S10 have variable radial velocities. The star S11 has 4 determinations (Hron et al. 1985; Liu et al. 1989, 1991) and three of them give almost the same value, with mean value as

Table 3.10: *The results of the distance and reddening determinations of the open clusters under study are tabulated here.*

| Cluster | DM | | D | E(B−V) | | | |
| | Phot | Spec | Phot | 1 | 2 | 3 | spec |
	±0.3	±0.5		±0.05	±0.05		±0.07
NGC 1912	12.0	9.7	1810±265	0.20	0.23	0.25±0.03	0.06
NGC 6709	11.0	9.8	1190±175	0.20	0.20	0.35±0.03	0.08
NGC 2383	13.3	11.4	3340±490	−	0.22	0.22±0.02	0.05
NGC 2384	13.2	13.2	2925±430	0.20	0.28	0.22±0.03	0.36
NGC 1907	12.5	−	1785±260	−	0.40	−	

as 57.5 km/s. The average values of radial velocity for S1, S2, S8, S10 and S11 are similar indicating that these may be cluster members. The spectral classification of S11 and S12 show that they are MS stars and can be members. The star S14 has to be a foreground star with smaller reddening, distance modulus and radial velocity, as found by Vogt & Moffat (1972). Considering the stars S11, S12 and S13 as members, the mean distance modulus becomes 13.2 mag and the mean reddening is 0.36 mag.

3.7 Conclusions

The results of the distance and reddening determinations of the five clusters, NGC 1907, NGC 1912, NGC 2383, NGC 2384 and NGC 6709 are tabulated in Table 3.10. All the distances obtained here are larger than those given in Lyngå (1987) catalogue. The present distances are larger by 35%, 25%, 65%, 45% and 30% in the case of NGC 1912, NGC 6709, NGC 2383, NGC 2384 and NGC 1907 respectively. The present determinations are based on more number of stars in a wider range of brightness and also they are estimated with the help of the cluster CMDs not only in V vs (B−V) plane but also in V vs (V−I) and, V vs (V−R) in two cases. Therefore the present estimates can be considered as more accurate. On the other hand, the E(B−V) reddening values are same within errors, except in the case of NGC 6709, where the present reddening in less by 0.1 mag. It is to be noted that the determination using method 3 gives similar E(B−V) as in

Lyngå (1987).

The distance modulus to the clusters are determined using the photometric and spectroscopic data. It is seen that the spectroscopic distance modulus is systematically lower than that obtained from the photometric CMDs in the case of NGC 1912, NGC 6709 and NGC 2383. The differences between the photometric and the spectroscopic distance modulii are 2.3, 1.2 and 1.9 mag about the mean and the differences beyond the errors are 1.5, 0.4 and 1.1 mag for the clusters NGC 1912, NGC 6709 and NGC 2383 respectively. Therefore, there seems to be a real difference between the values obtained by the two methods. On the other hand, both the distance modulii are the same in the case of NGC 2384 and this might rule out the possibility of a systematic error in the spectral classification of the observed spectra. Similar discrepancy in the values of photometric and spectroscopic distance modulii have been noticed earlier by Hoag & Applequist (1965) and recently by Barbon & Hassan (1996).

The reddening towards the clusters are determined from the photometry using three methods. Except in the case of NGC 6709, the values obtained from all the three methods are same within errors. In the case of NGC 6709, the method 3 estimates a reddening larger by 0.15 mag when compared to the other two methods. The reddening values obtained using the method 2 are used for further analysis as it is derived from larger number of stars.

The reddening estimated from the spectra seems to be systematically lower than the values from photometry for the clusters, NGC 1912, NGC 6709 and NGC 2383, just like in the case of distance modulus. The difference between the $E(B-V)$ values from photometry and spectroscopy are 0.17, 0,12 and 0.17 mag about the mean and 0.05, 0.0 and 0.05 beyond the errors for the clusters NGC 1912, NGC 6709 and NGC 2383 respectively. There seems to be a little bit of discrepancy. The reasons for this can be many, for example, this can be due to a systematic error in the spectral classification, or a systematic error in the calibration of the library spectra, or due to the error in the flux calibration of the spectra. As we estimate consistent reddening values from the photometry, the spectroscopic reddening estimates are not considered.

From the spectra obtained in this study we could identify two stars with H_α

emission. One star is in NGC 6709 (star S2a), which is already known to have H_α emission and the other one is in NGC 2383 (star S10), which has been identified for the first time. The present resolution does not show any shell feature for the star S2a, as mentioned by Sowell (1987). The H_β profile of the star, S10 shows shell feature in one spectra, which needs to be confirmed. The CMDs of NGC 1912 show a large amount of spread in the (B—V) colour. This may be due to the presence of a large fraction of binaries, fast rotating stars or peculiar stars as seen in the case of NGC 2287 (Harris et al. 1993). Spectra of more stars in this cluster with better resolution is needed to identify the peculiar stars, if any.

In between the galactic latitudes $231° \leq l \leq 256°$ in the Galaxy, the interstellar absorption is small out to large distances. The reddening increases slowly to a distance of 1 kpc and beyond that it is nearly a constant reddening (E(B—V)=0.3 mag) out to more than 4 kpc (Isserstedt & Schmidt-Kaler 1964, Neckel & Klare 1980). This implies that nearly all reddening between 1 and 4 kpc is caused by local dust clouds lying within 1 kpc (see Vogt & Moffat 1972). In the present study, the clusters NGC 2383 and NGC 2384 lie in this region. We find the reddening to be 0.25 mag on an average to a distance of $\sim$ 3 kpc which supports the above statement.

Thus we find that the CMDs with more number of stars can give a better estimate of the cluster parameters like distance and reddening which is important for transferring the cluster CMD to the M_V vs $(B-V)_0$ plane, in order to compare them with the stellar evolutionary models.

Chapter 4

Test of stellar evolutionary models

This chapter[1] consists of four main sections. In the first section, we present the prescription for computing the synthetic CMD and an overview of the computer code. The different theoretical stellar evolutionary models used to compute synthetic CMD are described and the various inputs to the models are discussed. In the second section, the data presented in the last chapter for the five open clusters are used to test the models. The ages of these clusters are derived and synthetic CMDs are generated for each cluster using various models. The observed CMDs and the integrated luminosity functions (ILFs) are compared with the ones obtained from the synthetic CMDs. In the third section, we compare the observed CMDs and LFs of four young LMC star clusters with the models by means of synthetic CMDs and ILFs. The implications of the results obtained from the open clusters and LMC clusters are presented in the last section.

4.1 Introduction

The aim of this study is to compare the observational CMDs of star clusters with the stellar evolutionary models in order to identify the input mechanisms responsible for the observed features in the CMDs. The stellar evolutionary

---

[1]Part of the results presented here are published in Subramaniam & Sagar (1995), A&A, 297, 695

models output isochrones, which try to reproduce the observed features as seen in the cluster CMDs. The evolution of a star away from the MS after the hydrogen burning will not only depend on the inputs used in the models in these stages but also on those used in the MS phase and hence the isochrone which fits the turn-off, may or may not fit the rest of the evolutionary phases. Therefore, one tries to find the model whose isochrone reproduces all the features very similar to those observed, and this will throw light into the required values of luminosity and effective temperature in the different evolutionary stages to match the observed features. The shapes of the CMDs which the isochrones reproduce are subject to the treatment of the surface layers (Iben & Rood 1970) and the comparison of the isochrones with the cluster CMDs is essential for the calibration of the parameterised treatment of envelope convection.

Star counts play a much more important role in model testing, they come directly from the star counts and are connected to durations of stellar evolutionary phases, which in turn are quantities well rooted in the deep structure of the star. The above method does not give any clue to this parameter. The number of stars present in a particular evolutionary phase in a cluster CMD reflects how fast the star evolves in that phase (Renzini & Fusi Pecci 1988). This is based on the fact that if the phase is very fast, one would see very few stars there, like the Hertzsprung gap or if the phase is too slow most of the stars would be seen here, like the MS. Therefore, the number of stars one expects in a phase is proportional to the time-scale of evolution in that phase. Observationally, the ratio of number of MS stars present in the required magnitude bin to the stars in the He-burning phase can be computed from the luminosity function (LF) of the MS. Our aim is to get this from the stellar models. The method used is the synthetic CMD, which will populate the CMD using the isochrone having the same age as the cluster. Once the CMD is populated according to the time-scales predicted by the model, the normalised LF can be calculated. The ratio of the number of stars in the MS to the number of red giants is equivalent to the lifetime ratio of helium to hydrogen core burning. Therefore, the comparison of the MS luminosity function between the synthetic and the observed ones helps to identify the actual value of the ratio. Thus, the method of comparing the CMD and LF together is a more

powerful way of testing stellar models.

4.2   Synthetic CMD

The idea is to generate a CMD having the same age and chemical composition as the cluster, with the help of the evolutionary tracks of various masses as given by the stellar evolutionary models. The computer code developed for this purpose, populates stars along the isochrone according to the time-scales predicted by the models. We know that the observed cluster CMDs have scatter around the actual evolutionary path. As the synthetic CMD as well as the LF is used to compare with the observed ones, the factors which produce scatter in the MS as well as in the evolved region of the cluster CMDs have to be incorporated. The two main factor to be considered are the binary stars in the cluster and the observational photometric errors. The presence of binaries in a cluster produces width in the MS and scatter near the turn-off and in all the later evolutionary stages. The attempts to find the percentage of spectroscopic binary stars in open clusters indicate that it varies between 30–50% (Mermilliod & Mayor 1989 and Crampton et al. 1976). Such determinations are not available in the case of LMC clusters. Therefore, we assume around 30 % binaries in computing the synthetic CMD. The effect of binarity in the CMD is maximum when the ratio of their masses is close to one and therefore the mass ratio is chosen in the range of 0.75–1.25.

4.2.1   A description of the computer code

The computer code used to construct synthetic CMDs using evolutionary models is described below. The code described here is summarised in the form of a flow chart and is shown in Figure 4.1.

1. The first step is to distribute stars in a mass interval, using a relation for the initial mass function (IMF). The expression for the IMF is given by,

$$dN = AM^{-(1+x)}dM \qquad (4.1)$$

FLOW CHART FOR SYNTHETIC CMD

```
┌─────────────────────────────────────────────────┐
│ STARS ARE DISTRIBUTED ASSUMING A POWER-LAW       │
│ MASS FUNCTION WITH A CHANGEABLE SLOPE AND        │
│ UPPER AND LOWER MASS LIMITS USING  A             │
│ MONTE – CARLO METHOD                             │
└─────────────────────────────────────────────────┘
                       │
                       ▼
┌─────────────────────────────────────────────────┐
│ STARS ARE PAIRED TO PRODUCE THE REQUIRED         │
│ FRACTION OF BINARY STARS SUCH THAT THEIR         │
│ MASS RATIO IS IN THE RANGE 0.75–1.25             │
└─────────────────────────────────────────────────┘
                       │
                       ▼
┌─────────────────────────────────────────────────┐
│ THE STARS ARE THEN PLACED IN THE H–R DIAGRAM     │
│ TAKING THE VALUES OF LUMINOSITY AND              │
│ TEMPERATURE FROM THE MODELS                      │
└─────────────────────────────────────────────────┘
                       │
                       ▼
┌─────────────────────────────────────────────────┐
│ MAGNITUDES AND COLOURS ARE COMPUTED USING        │
│ BOLOMETRIC AND COLOUR–TEMPERATURE                │
│ RELATIONS                                        │
└─────────────────────────────────────────────────┘
                       │
                       ▼
┌─────────────────────────────────────────────────┐
│ INTEGRATED MAGNITUDES FOR BINARY STARS ARE       │
│ ESTIMATED AND THE OBSERVATIONAL ERRORS           │
│ ADDED TO THE COMPUTED  MAGNITUDES                │
│ AND COLOURS                                      │
└─────────────────────────────────────────────────┘
```

Figure 4.1: *The flow chart for the synthetic CMD.*

where dN is the number of stars in the mass interval dM and x is the mass function slope, the Salpeter (1955) value being, 1.35. The slope can be altered to any desired value. We use the random method to populate the adopted mass range, which naturally accounts for the stochastic nature of the mass function (Chiosi et al. 1989). Monte-Carlo method is used to distribute stars randomly in a mass interval for a given mass function slope.

The upper mass limit is set by the age of the cluster and the low mass end by the lower mass limit of the stellar model. The constant of proportionality can be fixed by the total number of stars to be produced or by the number of stars in a particular evolutionary phase or the number of stars in MS in a given magnitude range. Therefore the stars are populated until the required number of stars are obtained in the particular evolutionary phase chosen.

2. The stars thus produced can be assigned the age of the cluster intended to study. If the cluster CMD does not show any evidence of age spread, or if a single isochrone is able to fit the turn-off satisfactorily, then the same age can be assigned to all the stars. It is also possible to give an age spread to the masses, if we assume a spread in the formation time of the cluster members. This spread can either be a Gaussian with peak at the cluster age or a step function (Becker & Mathews 1983). We use the gaussian method to introduce the age spread among the stars.

3. Once the age and mass of a star is fixed, its luminosity, L and temperature T can be found from the stellar evolutionary model. The standard interpolation method is used to find the values of L and T for masses which fall between the given evolutionary tracks in the model. Thus all the stars can be placed in the H-R diagram.

4. The next step is to transfer stars from the theoretical plane to the observational plane. For this we use the colour-temperature relations and bolometric corrections from Kurucz (1979) and VandenBerg (1983) complemented with values form Johnson (1966) for the temperatures below 4000 K.

5. The method adopted for including the observational photometric errors is taken from Robertson (1974). A Gaussian distribution has been assumed for the errors with the standard deviation ΔB and ΔV given by, $\Delta B = a(B-b)^2$ and $\Delta V = c(V - d)^2$. The coefficients a, b, c and d are chosen to fit the observations where the errors increase with magnitude. The errors in magnitudes are used to find the error in the colour.

6. The stars are paired randomly to generate binaries, with the constraint that the ratio of their masses should fall in the range 0.75–1.25. This is done

as the next step after a star is generated and continued till the required percentage of binaries is met. The procedure works as follows: to each star of mass M_1 we associate a probability of being a member of a binary system with a companion of mass M_2 such that the mass ratio M_1/M_2 is confined within a given range. These two stars are then replaced by a single star whose flux in various pass bands is given by the sum of the fluxes of the component stars.

As soon as mass of a star is computed, it is assigned some age and its L and T values are determined from the models. Then its M_V and $(B-V)_0$ values are estimated. If the star is a binary, then the integrated magnitudes and colours are found. These values are given the errors in both magnitude and colour. This procedure is continued until the required number of stars are generated. Then the number of stars in the various magnitude bins in the MS are counted and the value is divided by the number of evolved stars in the chosen phase to get the normalised MSLF. The synthetic CMDs and the normalised MSLF are then compared with the observed cluster CMDs and MSLFs. The colour-temperature relations and the bolometric relations are used here. Each of these ingredients carries its own uncertainties and it is not uncommon that agreement can be enforced for several combinations of the parameters.

4.2.2   Inputs to stellar evolutionary models

The code described above needs the evolutionary tracks to compute the CMDs. Here, we discuss the various inputs to the models in which we are mainly interested. There are basically two schemes for stellar evolution, classical and core overshoot schemes. In the case of classical models, the boundaries of the convectively mixed cores are fixed at the limit $\nabla_{rad} = \nabla_{ad}$, called the Schwarzschild criterion, has been recognised to set a lower limit to the extension of convective cores. It is because, at the layer where the above condition is met, only the buoyancy force becomes vanishingly small, but not necessarily the velocity of the convective motion. Thus the convection has to penetrate (overshoot) into the surrounding stable layers. Though the problem can be stated in a simple form, its

formulation and the estimation of the efficiency are extremely complicated. The lack of a rigorous theory of convection remains undoubtedly one of the major deficiencies in the calculations of models. The question has been addressed in many papers and a discussion of the various treatments can be seen in Renzini (1987 and references therein). A common approach consists in adopting concepts and methods derived from the classical Mixing Length Theory (MLT). One generally assumes the mixing length, l, in the convective region to be proportional to the pressure scale height, $l = \alpha H_p$, where, α is the proportionality constant and H_p is the pressure scale height. If we characterise the overshooting length as d, the efficiency of mixing given by the ratio d/H_p. The assumed overshoot distance at the edge of the convective core greatly differs from one model to another, varying from 0 to 2 H_p.

Another input to the models is the opacity tables. Various tables of radiative opacity have been published by the Livermore group over the last few years, the two recent ones being from Rogers & Iglesias (1992, hereafter referred to as OPAL1) and from Iglesias et al. (1992, hereafter referred to as OPAL2). These modify the surface parameters of the stars significantly in comparison with the opacities from Los Alamos Opacity Library (LAOL) of Huebner et al. (1977). The new opacities are significantly higher than the LAOL around two temperatures, i.e. a few 10^5 K and about 1 10^6 K. For solar metallicities, the difference in opacity amounts to a factor of three and 20% respectively (cf. Bressan et al. 1993). The OPAL2 supersedes the previous OPAL1 because of the inclusion of the spin-orbit interaction in the treatment of Fe atomic data and the adoption of the recent measurements of the solar photospheric Fe abundance by Grevesse (1991) and Hannaford et al. (1992). Stothers & Chin (1991) show that in the structure calculations of evolutionary models, a large assumed metal abundance can remove the need for assuming significant amount of the overshooting of the core. At the same time Schaller et al. (1992) and Bressan et al. (1993) show that such an assumption has little effect on the lifetimes and lifetime ratios of the central H and He-burning phases. As we are looking for the comparison of the LFs which is same as the lifetime ratios, the choice of opacity tables is not very sensitive.

As the envelopes of the low mass stars and giants are convective, the value of the ratio l/H_p may affect the structure of the outer envelope and hence the model temperature and radius. An increase of the value l/H_p shifts the red giant branch to hotter temperatures with a very small effect on the luminosity (Becker 1981). VandenBerg (1991) discusses the effects of changing mixing length parameter on the morphology of the H-R diagram and stresses the importance of its calibration on some observable. The first and the most natural mixing-length calibrator is the Sun. The mixing-length parameter can then be fixed by demanding solar models to produce the solar radius.

4.2.3   Brief discussion of evolutionary models

We use four stellar evolutionary models consisting of two classical and two overshoot models, in this analysis. Both core overshoot models use the new opacity values. The Z value considered is 0.02 for all the models.

The differing input physics and computational techniques from model to model makes a direct comparison very difficult. The necessary homogeneity is provided by the Bressan et al. (1993) models as they include both classical and core overshoot models with all the other inputs remaining the same. The details of the models are given below:

a Model 1 given by Castellani et al. (1990) is a classical model. It covers a mass range of 0.8 to $20M_\odot$. This model is used to explain successfully the LF of NGC 2004 by Bencivenni et al. (1991) and NGC 1866 by Brocato et al. (1989). They have used old opacity tables (LAOL) for log T > 4 and at low temperatures opacities are taken from Cox & Tabor (1976). The evolutionary sequences are computed from zero-age main-sequence (ZAMS) to the thermally pulsing asymptotic giant branch (TPAGB) phase.

b Model 2 given by Schaller et al. (1992), cover a mass range of 0.8 $M_\odot$ to 120 $M_\odot$. They have used new opacities (OPAL1) supplemented by radiative opacities by Kurucz (1991) at temperatures below 6000 K. As a result of the increased values of opacities, the convection parameters l/H_p and the overshooting distance change with respect to their previous model given

by Maeder & Meynet (1989). The value of l/H_p is 1.6 ± 0.1. The ratio of overshooting distance to the pressure scale height, d/H_p, is 0.2 in the mass range 1.25 to 25 $M_\odot$. Mass loss is included for all the stellar masses throughout the H-R diagram.

c Model 3 given by Bressan et al. (1993) present evolutionary models in the mass range of 0.6 to 120 $M_\odot$. The evolutionary tracks extend from ZAMS to TPAGB phase for low and intermediate mass stars, and to the central carbon-ignition for higher masses. The opacities at temperatures between 6000 K and 10^8 K are taken from OPAL2. The opacities at lower and higher temperatures are taken from LAOL and Cox & Stewart (1970a, b) respectively. The value of l/H_p is taken as 1.63. The value of d/H_p is 0.25 for the mass range 1.0 to 1.5 $M_\odot$ and equals 0.5 for masses above. This value of 0.5 corresponds to the overshoot distance favoured by model 2 (Bressan et al. 1993). They have also included the effects of envelope overshooting at the bottom of the convective envelopes, by adopting a value of 0.7 for the envelope overshooting distance. The mass loss is included only for stars more massive than 12 $M_\odot$.

d Model 4 given by Bressan et al. (1993) is same as model 3 without incorporating the core overshooting but with all other inputs being the same. This set is available within the mass range 2.5–20 $M_\odot$.

4.3   Open clusters

The evolutionary studies of many open clusters have been attempted to identify the presence of the core overshoot and to identify the efficiency of mixing. Maeder & Mermilliod (1981) analysing clusters like the Pleiades noticed that the MS extends to too bright a luminosity to fit standard models and suggested a certain amount of overshoot of the core. There are also many recent works on old open clusters with turn-off mass less than $2M_\odot$ (Aparicio et al. 1990, Anthony-Twarog et al. 1991, Bergbusch et al. 1991 and Aparicio et al. 1993). The study by Castellani et al. (1992) on the CMDs of Hyades, Pleiades, Praesepe, NGC 2420, NGC 3680 and NGC 188 with the aid of classical models find that if the new

opacity, like LAOL is used, there is no need for the overshoot of the convective core. The studies of Aparicio et al. (1990) and Bertelli et al. (1992) find that the models with overshoot for stars in the mass range 1.5–2$M_\odot$ calculated by Bertelli et al. (1986a, b) overestimated the overshoot distance, whereas those by Maeder & Meynet (1989, 1991) calculated with a moderate amount of core overshoot suffered from an inconsistency in the evaluation of the lifetime. On the other hand, they suggested that a certain amount of overshoot is always required. In the case of old open clusters, both classical and overshoot models can lead to a reasonable fit of the CMDs as shown by Bertelli et al. (1993) and Carraro et al. (1994). However, looking at both the CMD and LF, several differences between the classical and overshoot models can be noticed (Alongi et al. 1993). Therefore the question regarding the need for the inclusion of core overshoot in stellar models is still open. We look at intermediate age open clusters to resolve this issue. The data of five clusters presented in the previous chapter are used for this study.

4.3.1 Observed CMDs

In order to identify the various sequences in the CMD, we have demarcated the region with only field stars and the region with the evolved stars in the V vs (B−V) CMDs as shown in Figure 4.2. On to the left of the slanting line lies the cluster MS. Here, the cluster MS stars along with the field stars are present. The right side contains only the field stars. The stars lying above the horizontal line are the candidate cluster red giants. The evolutionary features as seen in the individual clusters are described below.

(i) The cluster, NGC 1907 has a wide MS extending up to 12 mag in the brighter end and well populated up to the fainter limiting magnitude of 18 mag in V. The turn-off colour in (B−V) is ∼ 0.5 mag. The cluster turn-off clearly seen at V=12 mag means that one star seen around 0.7 mag brighter than the turn-off may be a blue straggler, if it is a member. The three stars (two filled circles and one open circle) which are brighter than 1 mag in V can only be field stars. The stars falling to the left of the ZAMS can
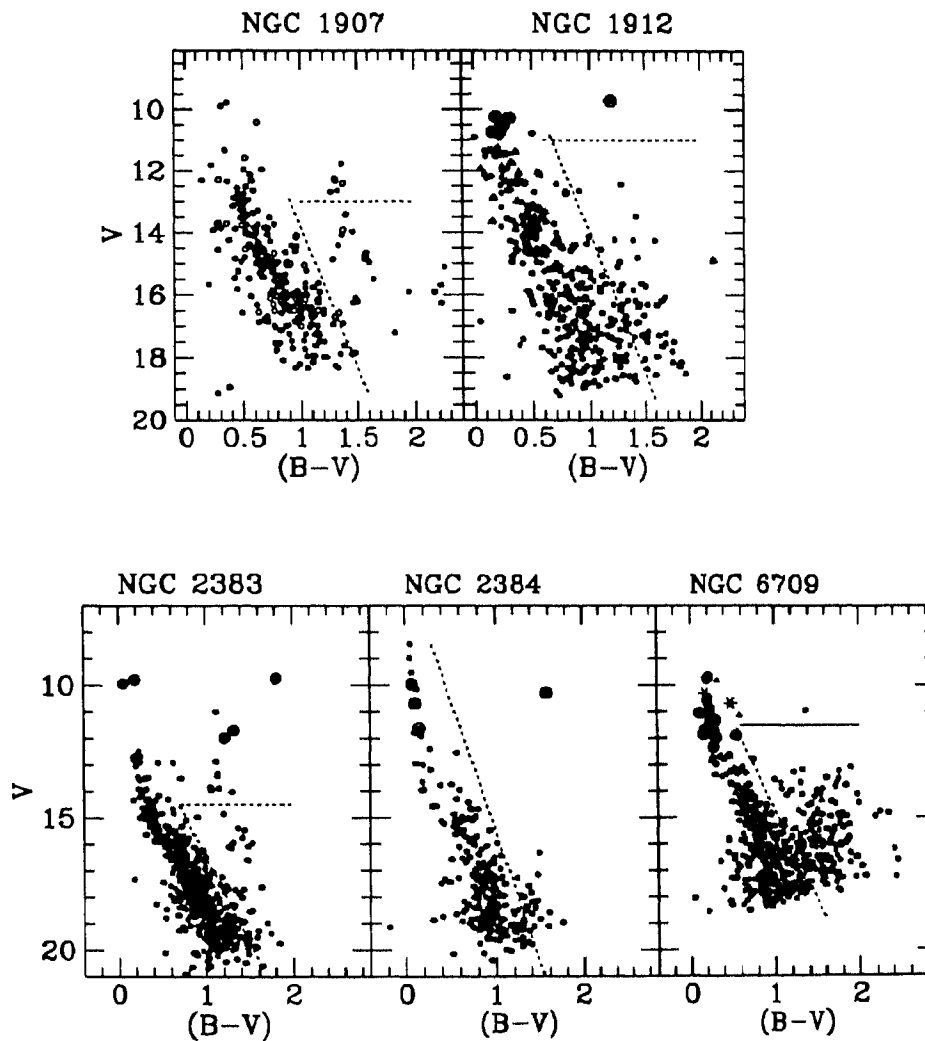
Figure 4.2: *The CMDs of five open clusters are shown here with the different regions identified.*

be assumed to be foreground stars. The scatter seen near the turn-off can also be produced by the presence of binaries, apart from the differential reddening and photometric errors. The clump of stars seen near V=12.5 mag and (B−V)=1.4 mag are the red giants. Though the red giant clump is seen, the red giant branch is not visible. The stars which lie below this clump and to the right of the MS are assumed to be field stars as the cluster is not young enough to have pre-MS stars in this region.

(ii) The cluster NGC 1912 has a very wide MS, which is more than what the variable reddening found in that region can account for. The MS extends up to 10 mag in V in the brighter end and up to 19 mag at the fainter end, which is the limiting magnitude in V. The data can be assumed to be complete up to 15 mag in V as the photographic data is also included. In this magnitude range, the stars are seen to be distributed in a clumpy fashion along the MS giving rise to gaps in between, which is also observed in the V vs (V−I) CMD. There is a large clump of stars lying 0.2 mag to the right of the MS near V=13.5 mag. Most of the stars in these clumps are proper motion members, which means that their presence need to be accounted for. The above mentioned features as well as the presence of stars on the right of the ZAMS indicate that most of the stars might be peculiar like fast rotators, binaries or stars with spots. There is only one star seen as a candidate for the red giant. The star seem to be too blue to be a red giant, though it is a member.

(iii) The cluster NGC 2383 has a well defined MS as seen in all the three CMDs. The turn-off is near V∼12.7, (B−V)∼0.2, (V−R) ∼0.1 and (V−I) ∼0.3 mag. The stars are seen populated continuously up to 14 mag in the MS and above this and up to the turn-off, only a few stars are seen. The scatter in the MS is less indicating that not many binary stars are present. The two bright stars around V=10 mag are non-members. The subgiant branch is seen more clearly in the V vs (V−R) CMD. The red giant clump seems to be extended in V mag, but the isochrone fitting as discussed later, shows that the the clump consists of the brighter 3 of the 7 stars at V=14 mag and (B−V)=1.1 mag. Three stars are also seen just above the clump. The two stars (with open circles around them) seems to lie in the red giant branch of the cluster. The bright star at V=9.7 mag and (B−V)= 1.8 mag is too bright to be a red giant and cannot be a member, this is evident from all the three CMDs.

(iv) The cluster NGC 2384 seems to be very young compared to the previous ones. The MS is extending up to ∼ 8.5 mag in V at the brighter end. There seems to be a gap in the MS below 15 mag in V, which is more clearly seen

in the V vs (V−R) and V vs (V−I) CMDs. The stars lying to the right of the MS at this V magnitude may be pre-MS stars. In that case, the stars lying fainter than 16 mag should mainly be field stars. The single star at V∼ 10 mag and (B−V) ∼ 1.6 mag cannot be a cluster member. There are no evolved member stars are seen in the CMD. The width of the fainter MS is very low indicating that the percentage of binary stars present is very low.

(v) The cluster NGC 6709 has a CMD mostly embedded in the field stars. The turn-off is around 9.5 mag in V, 0.2 mag in (B−V) and 0.3 mag in (V−I) . The photographic data is included up to 15.5 mag in V and the photoelectric data in the bright end. The MS is well populated between 10.5 mag and 12.0 mag in V in the bright end and three stars are seen above this at 9.5 mag. There seems to be a gap between 12.0 and 12.7, where only one star is present. There is again a gap between 13.0 and 13.5 mag in V. After V∼14 the MS is continuous, this may be due to the presence of more field stars in the fainter limit. The gaps mentioned above are also seen in the V vs (V−I) CMD. The clumpiness of stars in the MS is similar to that seen in the CMD of NGC 1912. There is only one candidate red giant star. As the data can be considered to be complete towards the brighter end, the cluster actually has only one red giant, if it is a member.

Gap in the MS

In three of the five clusters, gaps at various points in the MS of the CMDs are noticed. The details of the gaps found in the three cluster CMDs are given in Table 4.1. The probability for these gaps to be accidental is estimated using the method adopted by Hawarden (1975) and the probability values obtained are also tabulated. All the gaps listed in the table have very low probability to be accidental and hence are expected to be real gaps. The cluster MS of NGC 1912 is seen to be clumpy with many gaps and the prominent one is listed in the table 4.1, which lies a little below the MS turn-off. Another feature seen in this cluster MS is that, the stars near $M_V \sim 1.5$ seems to be shifted to redder (B−V) resulting in a gap in the MS and a clump of stars to the right of this, which are similar to the A-bend and A3-group found by Kjeldsen & Frandsen (1991). Two

Table 4.1: *The details of the gaps noticed in the MS of the three cluster CMDs are tabulated here.*

Cluster	M_V	$(B-V)_0$	width in		prob.
			M_V	$(B-V)_0$	
NGC 1912	−0.9	0.0	0.1	0.1	0.09
NGC 2383	−0.1	0.0	0.15	0.05	0.12
	0.35	0.05	0.05	0.05	0.08
NGC 6709	1.15	0.00	0.15	0.05	0.02
	1.5	0.1	0.1	0.1	0.04

gaps are noticed in NGC 2383, of which the first one may be the Mermilliod gap (Mermilliod 1976), but the $(B-V)_0$ values are differing by 0.1 mag. The first gap seen in the case of NGC 6709 is similar to the A-group and the second one is similar to the M11-gap (Kjeldsen & Frandsen 1991). The gap found in NGC 1912 and the second gap in NGC 2383 are not similar to any of the gaps mentioned in Kjeldsen & Frandsen (1991).

4.3.2   Luminosity functions

The MS luminosity functions are found for four clusters. The estimate of the field star density is not available for the cluster NGC 1907 and it is excluded from this analysis. The elimination of the field stars from the MS is done in two ways. For the clusters, NGC 1912 and NGC 6709, the field stars from the observed MS are eliminated using the proper motion data. In the case of NGC 1912, the MS up to 15 mag in V can be considered as devoid of field stars and for NGC 6709, the MS up to 14 mag in V is considered. The data is complete up to a magnitude of 16.0 in V, as seen from the results of the artificial addstar experiment for the cluster NGC 1912. As the clusters have similar crowding, the data for the rest of the clusters can also be assumed to be complete up to 16.0 mag in V. The next method is to observe a nearby region and find out the number of field stars in each magnitude bin and is a statistical method. The field region is observed only for the clusters NGC 2383 and NGC 2384. As the clusters lie very close to each
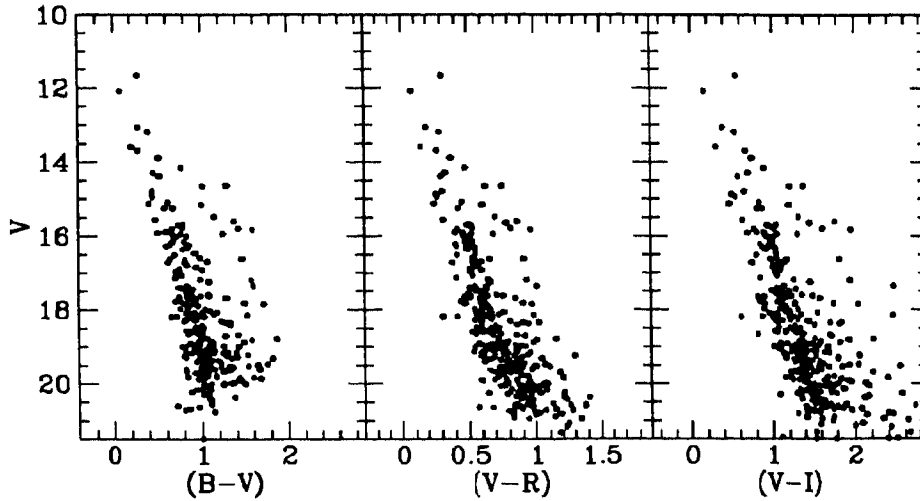
Figure 4.3: *The CMDs of the field region for the clusters NGC 2383 and 2384 are shown here.*

other the same region is considered as field to both the clusters. The CMD of the observed field region is shown in Figure 4.3. The CMDs show that most of the field stars are fainter than 15 mag in V and only a few stars are present brighter than this. This CMD can be used to eliminate the field star contamination in the CMDs of NGC 2383 and NGC 2384. In order to get the MSLF, the cluster stars which are in the MS, and below the turn-off are binned in V magnitude. After correcting for the difference in area between the cluster and the field regions, the number of stars obtained from the field region in each magnitude bin is subtracted from the number obtained from the cluster frame, which gives the actual number of cluster stars. The MSLF for the four clusters are shown in Figure 4.4. In the case of NGC 2383 and NGC 2384, the MSLF before the field star subtraction is also shown.

One expects the number of cluster stars to be increasingly more towards the fainter magnitudes, because of the nature of the mass function. The MSLF of NGC 1912 rises steadily as expected. In the case of NGC 2383, it rises in a jumpy fashion. There seems to be lesser number of stars in these clusters fainter than 15.5 mag. This cannot be an artifact due to incompleteness, as the crowding is
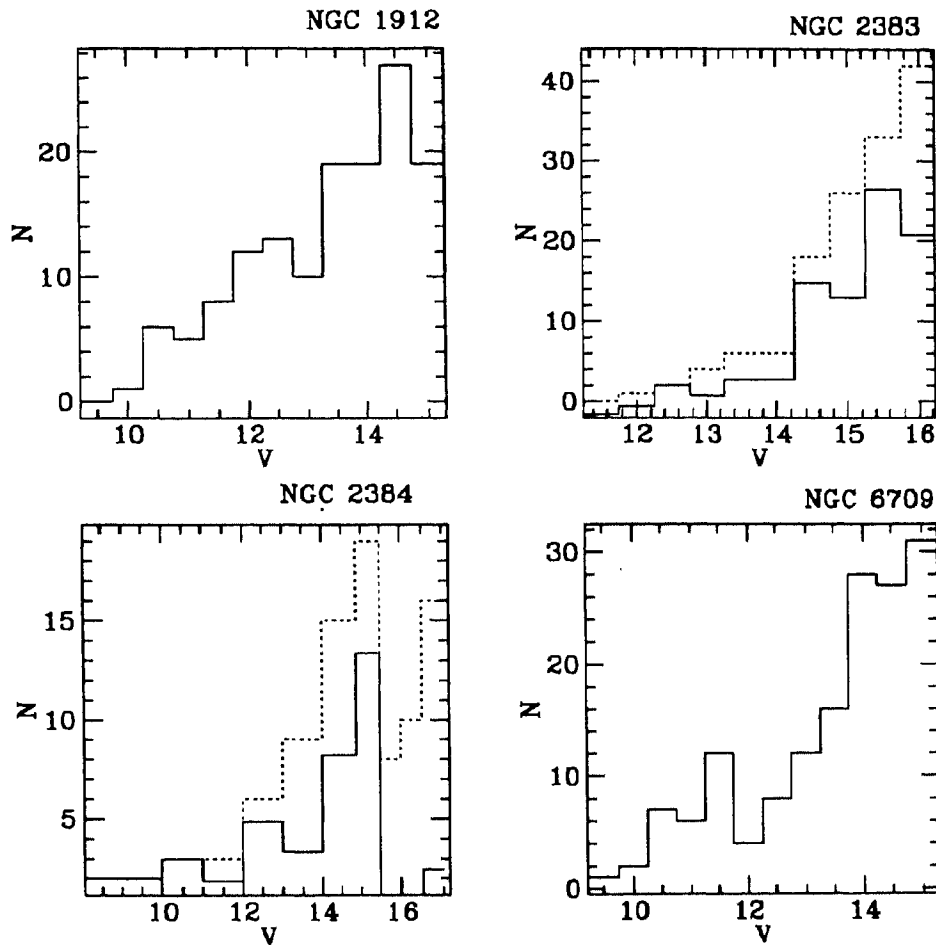
Figure 4.4: *The MSLF for the clusters NGC 1912, NGC 6709, NGC 2383 and NGC 2384 are plotted as continuous lines. The dotted lines show the MSLF before field star subtraction.*

very low at this magnitude. The most probable reason may be that, as the cluster is a few times 10^8 yr old, it might have lost the low mass stars due to dynamical evolution. In the case of NGC 2384, the initially rising MSLF falls after $V \sim 15$ mag. This point is mentioned in the previous section. The drop of the LF is very high indicating that the cluster MS ends here. The cluster is quite young to relax dynamically. If the stars below this V magnitude are in the pre-MS phase then one expects to see them to the right of the MS, just like the position of star 4 (see previous chapter). As no stars are seen in the pre-MS phase also, one

may conclude that the stars are formed only up to the mass corresponding to the limiting magnitude. The MSLF of NGC 6709 also shows a dip around 12 mag in V, but shows a steady rise beyond that. This decrease in the number of stars should be a real feature as the data is complete upto this brightness level.

4.3.3 Age determination

As the distance and reddening towards the clusters are estimated, we can place the cluster CMDs in the M_V vs $(B-V)_0$ plane. The age of the cluster is determined by comparing the cluster sequence with the isochrones from the models. The isochrones corresponding to the model 3 is obtained from Bertelli et al. (1994). The isochrones for the models 1 and 2 are computed. The isochrones are converted from the log $L/L_\odot$ vs log T_{eff} plane to the M_V, $(B-V)_0$ plane using colour-temperature relations and bolometric corrections from Kurucz (1979) and Vandenberg (1983) complemented with values given by Johnson (1966) for the temperatures below $4000^\circ K$. The isochrones are fitted to the cluster CMDs as shown in Figures 4.5 to 4.9. The ages of the clusters as found from the three models are tabulated in Table 4.2.

The isochrones for models 1 and 2 are constructed only in M_V vs $(B-V)_0$ plane. As the isochrones from model 3 are also available in the other two colours $(V-R)_0$ and $(V-I)_0$, these are fitted in the M_V vs $(V-I)_0$ for four clusters (except NGC 1907) and also in the M_V vs $(V-R)_0$ plane for NGC 2383 and NGC 2384. The isochrone of same age fits the CMDs in all the planes. The turn-off region of the clusters are well reproduced by all isochrones. As seen from table 4.2, except NGC 2384, the rest of the four clusters are of intermediate age. The overall morphology at the turn-off is same for the three models. The base of the red giant branch is extended more to the cooler side in the isochrones of model 3. This may be because of using different colour- temperature relations with respect to those used here. In the case of models 1 and 2, the isochrones of model 2 runs redder than those of model 1. The conversion problem is not here as the same relations are used, therefore this may be due to the difference in mixing length used in the calculation of envelope convection. The clusters where the red giant clump is seen, like NGC 1907 and NGC 2383, the isochrones need to go redder

Table 4.2: *The age (log τ) of the five open clusters as estimated from the three models are tabulated here.*

	log τ				
	NGC 1907	NGC 1912	NGC 2383	NGC 2384	NGC 6709
Model 1	8.45	8.2	8.45	7.1	8.35
Model 2	8.6	8.4	8.6	7.2	8.5
Model 3	8.6	8.4	8.6	7.3	8.5
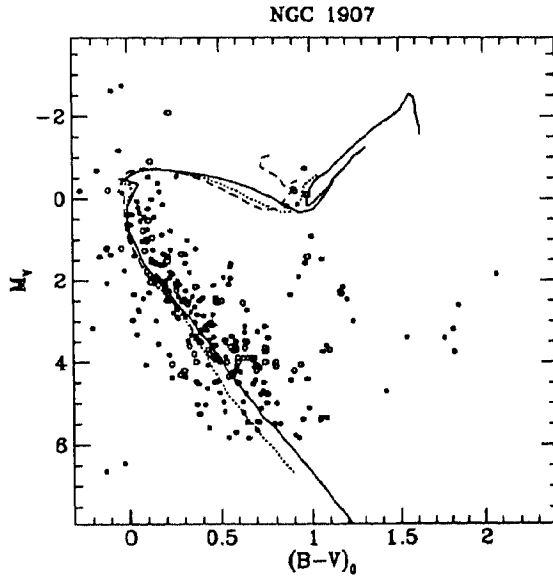
Figure 4.5: *The isochrones are fitted to the cluster sequence of NGC 1907, for distance and reddening as given in the previous chapter. The continuous line is the one from Model 3, the dotted one from Model 2 and dashed line is Model 1.*

in the case of model 1. As mentioned above, the difference between classical and overshoot models are not very clear from this comparison. One point to be noticed is that the isochrones of models 2 and 3 fit the MS well for the estimated values of reddening. In the case of model 1, the isochrones are falling bluer in $(B-V)_0$ than the cluster sequence as well as the other isochrones. We have shifted the model 1 isochrones by 0.03 mag in $(B-V)_0$ to the red to match the sequence. The classical model, model 1 finds younger age for the clusters compared to the
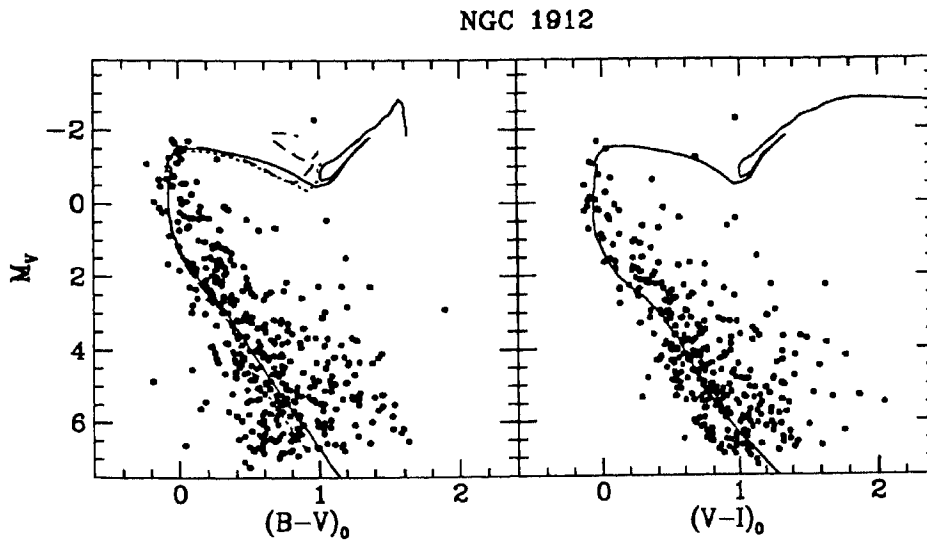
NGC 1912

Figure 4.6: *Isochrones are plotted to match the CMDs of the cluster NGC 1912, see figure 4.5 for details.*
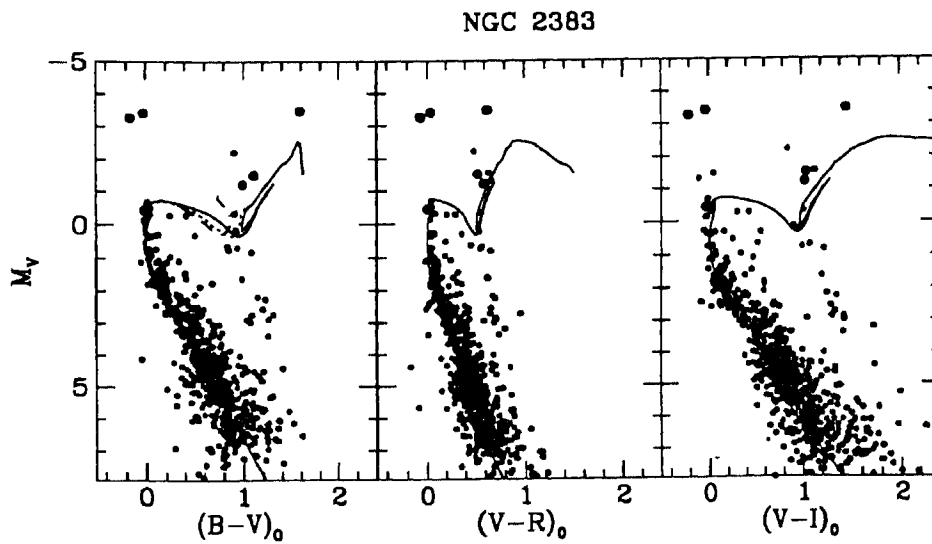
NGC 2383

Figure 4.7: *Isochrones are plotted to match the CMDs of the cluster NGC 2383, see figure 4.5 for details.*

overshoot models. In the case of older four clusters, models 2 and 3 find the same age. For the younger cluster, NGC 2384, model 3 finds older age compared to model 2. The present age determinations for NGC 1907 and NGC 1912 are very
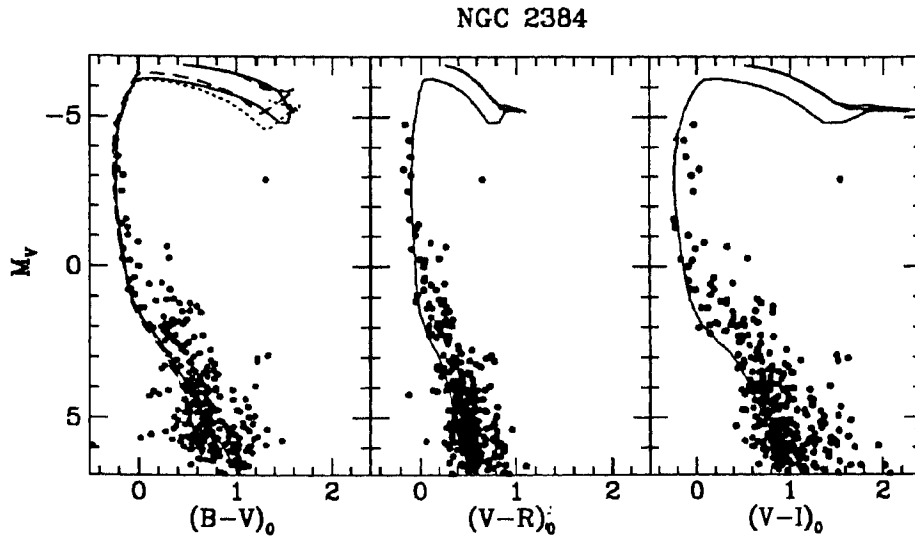
NGC 2384

Figure 4.8: *Isochrones are plotted to match the CMDs of the cluster NGC 2384, see figure 4.5 for details.*

NGC 6709

Figure 4.9: *Isochrones are plotted to match the CMDs of the cluster NGC 6709, see figure 4.5 for details.*
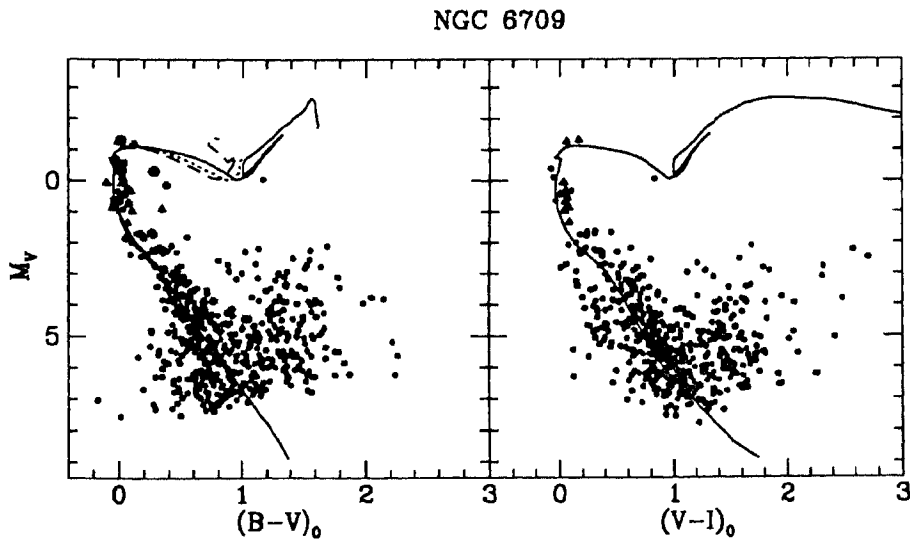
close to the values given in Lyngå (1987). In the case of NGC 2383, the present determination shows that the cluster is much older than the previously estimated value. Also, the clusters NGC 6709 and NGC 2384 turns out to be older than

the ages given in Lyngå (1987).

4.3.4 Synthetic CMDs and LFs

The synthetic CMDs are obtained using the first three models. The fourth one cannot be used here, as the lowest mass for which the track is available is 2.0 $M_\odot$. The number of stars in the brighter part of the MS is used for fixing the proportionality constant in the mass function. The number of evolved stars are not used because the number is very small. We first compare the features in the CMDs as predicted by the models with the observed ones and then the ILF.

Comparison of features

The synthetic CMDs put stars along the evolutionary path which the model predicts. A comparison between the observed and the synthetic CMDs will help in identifying the model which reproduces evolutionary track closest to the observed one. We take a look at the individual clusters below.

NGC 1907 This cluster seems to have a decent number of red giants. There are six candidate red giants in the cluster, but no kinematic information is available on their membership. The synthetic CMDs using models 2 and 3 produces the clump, and in the case of model 1, the stars are rather scattered near the clump. Another feature is that the model 1 tries to produce stars in the subgiant phase and in the inert helium-core phase, which are not observed. The observed width of the MS (excluding the wide scatter) can be reproduced when the observed error and $\sim$ 30 % binaries are included in the input for the synthetic CMD.

NGC 1912 This cluster has one red giant star and another in the subgiant phase. All the three models seem to produce more number of red giants when the Salpeter value is used for the mass function slope. The model 1 produces 3 stars in the evolved phase for x=2.0 and the models 2 and 3 produce 2 and 3 stars each for x=1.7. There are about 9 stars seen at the top of the observed MS, which lie along the isochrone. None of the models have been

able to produce these stars. These lie in the fast evolutionary phase of the isochrone. These stars may be contact binaries or candidate blue stragglers.

NGC 2383 This cluster has a red giant clump consisting of three stars and two stars in the subgiant branch. These can be considered as members. As seen in the case on NGC 1907, the clump is not well reproduced by model 1. The model 2 has a little bit of scatter in the clump, but model 3 produces a very compact clump. The models 1 and 2 produce one subgiant star, whereas no subgiants are produced by model 3. The required number of stars seen at the top of the observed MS is not obtained in any of the synthetic CMDs, only lesser number of stars are produced. The approximate number of stars in the clump are produced for the Salpeter value of x.

NGC 2384 This cluster is the youngest among the open clusters studied here. When the age as estimated by the isochrone fitting is used to make the synthetic CMDs, the stars at the top of the MS are not populated. We try to populate them by lowering the age of the cluster. The synthetic CMDs are made using model 2 for an age of 3.2 Myr and x=1.0, model 3 for an age of 8 Myr and x=0.8 and model 1 for an age of 3.2 Myr and x=1.0. Though a few stars are seen in the CMDs using models 1 and 2, the CMD using model 3 populates almost the observed number of stars. Thus the cluster is younger in age and seems to have a shallower slope for the mass function.

NGC 6709 This cluster has only one candidate for red giant, which we consider as a member. The synthetic CMDs are constructed with values of x steeper than the Salpeter value of x. The models 1 and 3 put 4 stars in the evolved phase for x=2.0, whereas model 2 puts 2 stars for a value of x=1.7. Therefore, the cluster has a steeper value of x compared to the Salpeter value. Again the three stars seen at the top of the observed MS is not generated in the synthetic CMDs.

The synthetic CMDs which closely reproduce the observed features are shown in Figure 4.10. The model used to construct the CMD is shown along with the name of the cluster. In general, the evolved parts of the CMDs are better reproduced by the models 2 and 3, which include the effects due to core overshoot. The stars
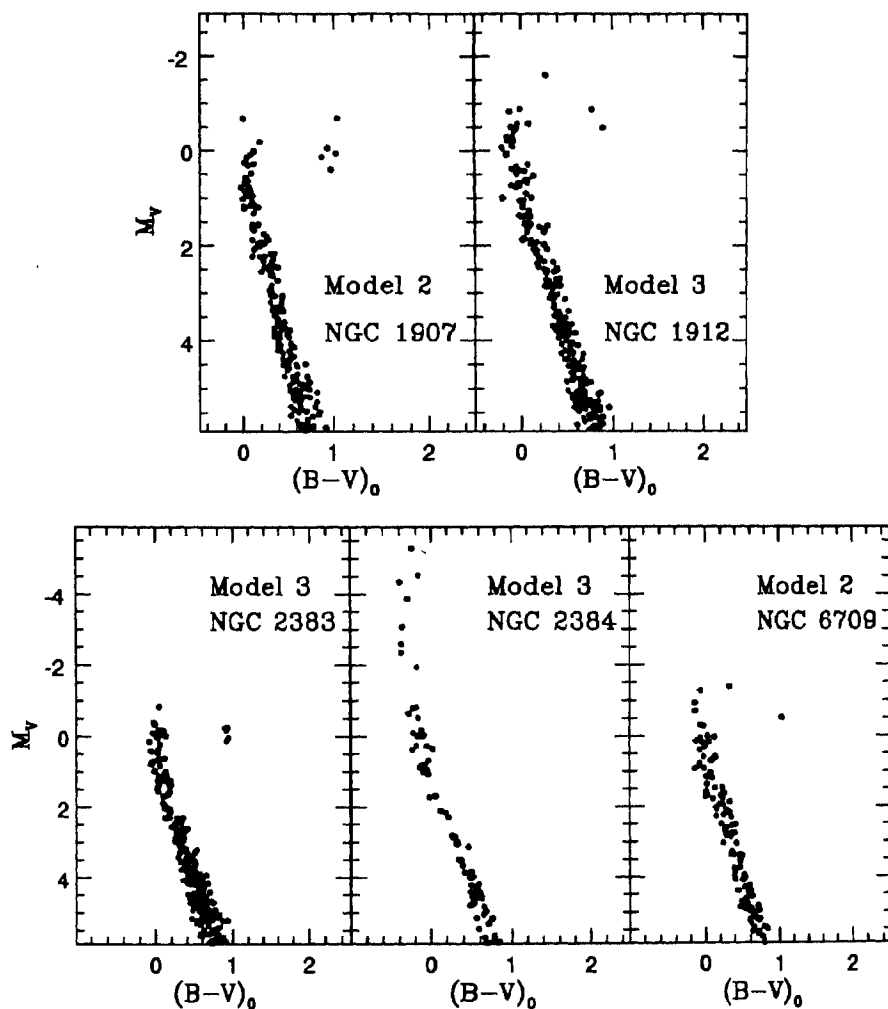
Figure 4.10: *The synthetic CMDs which reproduce the observed features are shown here. The model used to produce the synthetic CMD is shown.*

which are seen at the top of the cluster MS are not populated in the synthetic CMDs. One star among this group in NGC 1912 is observed spectroscopically and shows giant nature. This may indicate that these stars are in the normal phase of evolution and hence the evolutionary time-scales need to be corrected to produce stars in this region. The nature of the rest of the stars also have to be confirmed. Another possibility is that some of these stars may be contact

Table 4.3: *The values of x and percentage of binary are tabulated here which are used as inputs to construct the synthetic ILFs shown in Fig. 4.11.*

Cluster	mass range	Model 1		Model 2		Model 3	
		x	binary	x	binary	x	binary
NGC 1912	3.9–1.7	2.0	30	1.7	30	2.0	30
NGC 2383	3.1–1.7	1.3	20	1.3	30	1.3	25
NGC 2384	14.0–2.0	1.0	0	1.0	0	0.8	0
NGC 6709	3.4–1.7	2.0	20	1.7	45	2.0	35

binaries and candidate blue stragglers, in which case they are not in the normal evolutionary phase.

Comparison of ILFs

Chiosi et al. (1989) show that the integrated luminosity function (ILF) of main sequence (MS) stars normalized to the number of evolved stars can be used to differentiate among different evolutionary scenarios, since it is just the ratio of core H to He burning lifetimes which is very much affected by the mixing scheme used. Here we compare the observed ILFs of MS, normalised to the number of evolved stars with those estimated from the synthetic CMDs. This is not attempted in the case of NGC 1907, as the estimates of field star contamination are not available.

The synthetic CMDs are constructed for varying values of the MF slope, x, and the ILFs are calculated in each case. The results for the four clusters are shown in Figure 4.11 and are tabulated in Table 4.3. The values of the percentage of binary stars used are also given in the table.

The ILF of NGC 1912 is best matched by the ILF computed from the model 2, with a slope x=1.7. The ILFs computed from the models 1 and 3 computed with x=2.0 follow closely, within the error of the observed ILF. Though the distinction between the ILFs computed from different models is not much, the model 2 ought to be preferred. Also, the cluster mass function slope seems to be 1.7, which is steeper than the Salpeter value. In the case of NGC 2383, the ILFs from all
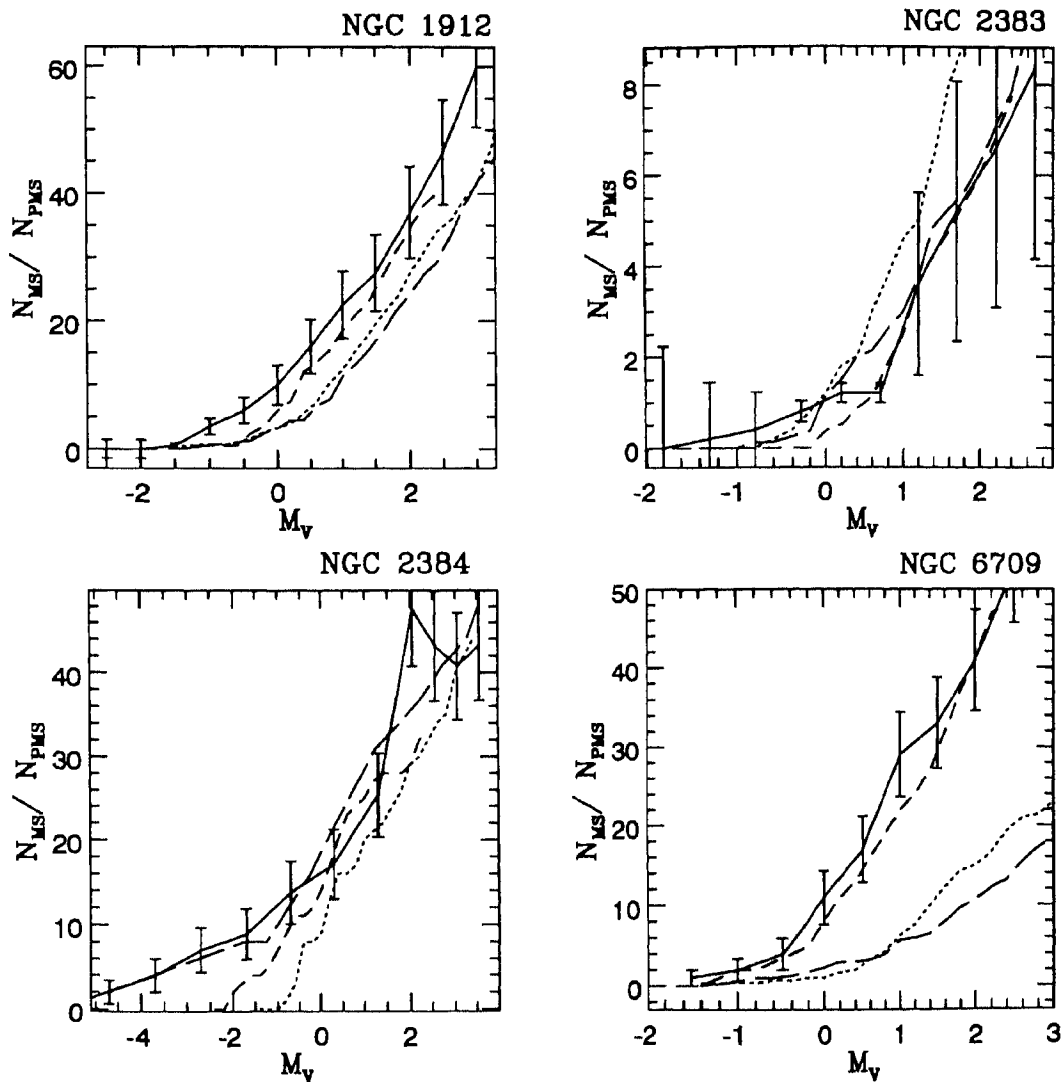
Figure 4.11: *The synthetic ILFs are compared with the observed ILFs. The continuous line is the observed one, model 1 is the dotted line, model 2 is the short dashed line and model 3 long dashed line. The details of the synthetic CMDs used to calculate the plotted ILFs are tabulated in Table 4.3.*

the three models come close to the observed one for a value of 1.3 for x. The ILF computed from the model 1 deviates at the fainter limits and the ILFs from models 2 and 3 are very similar. The distinction between the overshoot models is not possible in this case, but the overshoot models have to be preferred. The

Table 4.4: *The turn-off masses for the clusters as obtained from the three models are tabulated here. The lifetime ratio τ_{He}/τ_H corresponding to the masses are also tabulated.*

Cluster	Model 1		Model 2		Model 3	
	M_{TO}	τ_{He}/τ_H	M_{TO}	τ_{He}/τ_H	M_{TO}	τ_{He}/τ_H
NGC 1912	3.9	0.321	3.35	0.210	3.5	0.225
NGC 2383	3.15	0.390	2.8	0.246	2.9	0.297
NGC 2384	14.34	–	11.6	0.098	11.3	0.062
NGC 6709	3.4	0.379	3.0	0.245	3.2	0.262

cluster mass function is similar to the Salpeter value of 1.35. The age of the cluster NGC 2384 from the synthetic CMD is much lower than that obtained from the isochrone fit. Also, in order to populate the brightest part of the MS, shallower value of x is used. The models 1 and 2 are not able to produce a synthetic CMD close to the observed one, in the brighter end. The synthetic ILFs from all the three models match in the fainter end of the observed ILF. The mass function slope for the cluster is 1.0, which is shallower than the Salpeter value. For the cluster NGC 6709, the observed ILF, is matched by the ILF computed from model 2. The other two models do not come close even within the error. The important point to be noted here is that, the number of evolved star observed in one and hence the observed ILF is normalised using this number. The statistical error is equal to the value itself and this can make the ILFs of all the three models agree with the observed ones within errors. The mass function used for model 2 is 1.7 and still steeper values for the other two models. The cluster mass function is thus x=1.7. The error involved in estimating the slope of the mass function, x is ~ 0.15.

The results obtained from the comparison of the ILFs can be directly converted to the comparison of the ratio of the evolutionary time-scales. The turn-off mass of the clusters corresponding to the age estimated from the models are tabulated in Table 4.4. The ratio of the helium core burning to hydrogen core burning lifetimes corresponding to these masses are also tabulated in the table.

It can be seen that the cluster ages estimated using the classical model, model 1 is younger and the turn-off mass, M_{TO} heavier than the overshoot models. Though the two overshoot models, models 2 and 3 estimate the same ages for the older clusters, the M_{TO} given by model 2 is lighter than that given by model 3. Also, the value of the lifetime ratio τ_{He}/τ_H is smaller in the case of model 2 compared to model 3. The comparison of ILFs show that the model 2 is to be preferred marginally to model 3. This may indicate that the smaller of the two lifetime ratios presented by the overshoot models is to be preferred.

As seen above, the number of stars observed in the evolved phase of the cluster CMD is very less to make the results statistically significant. The errors in the observed ILFs can be reduced if the number of stars in the evolved phase is large. This can be achieved by using the CMDs of populous clusters in the LMC.

4.4 Young LMC star clusters

The CMDs of young MC star clusters are a very good testing ground for the stellar evolutionary models in order to discriminate among the possible evolutionary scenarios of high mass to intermediate mass stars. Since clusters in the MCs are rich, they populate almost all the evolutionary phases and also occupy regions of the age and metallicity domain which are not populated in our galaxy. They therefore extend the range of comparison between models and observational data. Furthermore, their study is mandatory for the understanding of star clusters in external galaxies where only integrated properties can be observed.

A detailed comparison of evolutionary models with the narrow and well defined stellar sequences in the CMDs of MC star clusters could not be done till recently, because most of the earlier CMDs (cf. Sagar & Pandey 1989, Seggewis & Richtler 1989) are based on either photographic or electronographic observations which are, in general, not only restricted to bright stars (V~17–18 mag) but also limited in accuracy. However, the advent of modern detectors and software for doing accurate photometry in crowded regions have recently made such work possible. For example, Chiosi et al. (1989) analyzed the BV CCD data of the cluster NGC 1866 to disentangle classical stellar evolutionary models from that incorporate

overshooting of the convective core. They conclude that substantial overshooting ought to occur in stars with mass of about 5 $M_\odot$. Vallenari et al. (1991) also support the above fact on the basis of an analysis of the CCD data of NGC 2164. Bencivenni et al. (1991) while analyzing the similar data for the cluster NGC 2004 conclude that their models based on classical theory can very well explain the number of stars present in the various evolutionary phases. Stothers & Chin (1992) find that in the mass range 4–15 $M_\odot$, very little or no overshooting of the core is needed to reproduce the observed features of the blue populous clusters, NGC 330 and NGC 458 in the Small Magellanic Cloud. Thus, the question regarding the necessity for including the effects due to overshooting of the convective cores needs to be addressed. Here, we address this by comparing synthetic CMDs and luminosity functions (LFs) obtained from the models with the homogeneous set of data consisting of observed CMDs and LFs of the four LMC star clusters namely, NGC 1711, NGC 2004, NGC 2164 & NGC 2214. The four clusters considered span a wide range in age, thus have a range in turn-off masses.

4.4.1 Observational data

The data for the clusters NGC 1711, NGC 2004, NGC 2164 & NGC 2214 are taken from Sagar et al. (1991). The data were obtained at the f/8.5 Cassegrain focus of the 1.54m Danish telescope at the European Southern Observatory, La Silla, Chile using a RCA CCD chip of 320×512 pixel in size where one pixel corresponds to 0.47 arcsec. Since the data for the field region of NGC 2164 in Sagar et al. (1991) is not very deep, we have taken those from Vallenari et al. (1991).

4.4.2 Observational CMDs and LFs

The CMDs of the clusters analyzed here are presented in Sagar et al. (1991). These CMDs need to be corrected for data incompleteness and field star contamination before they can be compared with models. We use the statistical method of subtracting field stars. The first step towards this goal is to define a cluster

Table 4.5: *Coordinates of cluster center (X_c, Y_c), annuli of selected rings in pixels and $E(B-V)$ values in mag for the clusters are given.*

Cluster	X_c	Y_c	Selected annuli		$E(B-V)$
			Ring 1	Ring 2	
NGC 1711	140	242	$50 \le R < 115$	$115 \le R < 200$	0.09
NGC 2004	150	407	$45 \le R < 115$	$115 \le R < 200$	0.09
NGC 2164	132	237	$45 \le R < 110$	$110 \le R < 180$	0.10
NGC 2214	171	231	$45 \le R < 110$	$110 \le R < 200$	0.07

region which can be considered as cluster representative, but suffering less from the above defects. The next task is to determine the incompleteness of the data and adopt a suitable method to remove the field stars from the CMDs.

4.4.3   Selection of the cluster region

The idea is to find an annular ring best representing the cluster but suffering less from data incompleteness and stellar crowding. The cluster center is derived iteratively by calculating the average x and y positions of stars within 150 pixels from an eye estimated center, until it converges to a constant value. As the crowding is maximum near the center we expect the data to be least complete near the central region. An error of a few arcsec is expected in locating the cluster center. We consider the region where the data completeness factor (CF) is < 30 % (defined in Sagar & Richtler 1991) as the central region and exclude this circular region from our further analysis. This serves as the inner boundary for the required cluster region. The outer boundary is identified from a plot of stellar density as a function of the distance from the cluster center. The limits of the annular region best representing the cluster are given in Table 4.5. Since incompleteness varies also within this region, we divide it into two rings, namely, ring 1 and ring 2.

4.4.4 Data incompleteness correction

The procedure to quantify the stellar completeness factor CF in photometry is described in detail in Sagar & Richtler (1991). The completeness factor Λ_i at a point $(V_i, (B-V_i))$ in V, (B–V) diagram will be mainly controlled by that CF value of B and V CCD frames where completeness is less, i.e., the value of Λ_i cannot be larger than the smaller value of the pair $(CF(V_i), CF(B_i))$; where $CF(V_i)$ and $CF(B_i)$ are the completeness values at the brightness V_i and B_i in the V and B CCD frames respectively. Consequently, we have used,

$$CF(V_i, (B-V)_i) = min(CF(V_i), CF(B_i)),$$

for the data incompleteness correction in our analysis. The exact value of the incompleteness correction to be applied in the V vs (B–V) plane is still debated. Mateo (1988) used the product of the CF in V and B passbands, which is seen to overestimate the actual incompleteness value. Sagar & Richtler (1991) argued that the two frames were not independent and that the multiplicative assumption of Mateo (1988) could not be justified. Instead, as the spatial distribution of stars in the frames is the same and the magnitude distribution is slightly modified, the completeness at a given point in the CMD would be mainly controlled by the lesser of the two completeness factors. These two methods are seen to estimate the two extremes of data completeness (Mateo 1993). Banks (1995) find that the method adopted by Sagar & Richtler (1991) gives the best results within a few percent accuracy and is to be preferred to the incompleteness method adopted by Mateo (1988). The completeness values for all regions are taken from Sagar & Richtler (1991), except for the field region of NGC 2164, where they are from Vallenari et al. (1991). The value of $CF(B_i)$ is generally less than that of $CF(V_i)$ except in a few cases.

For applying the incompleteness correction to get a complete CMD, the CMDs for the rings 1 and 2 are constructed separately. Then the CMD of each ring is divided into a number of boxes having a width of 0.2 mag in V and 0.1 mag in (B–V). The Λ_i for the mean values of B_i and V_i for i^{th} box is found using the above relation. The actual number of stars in the ith box is then calculated as $N_{ci} = (N_{oi})/\Lambda_i$, where N_{oi} is the observed number of stars in the ith box. Now,

the extra number of stars in the ith box, $\triangle N_i$, given by, $\triangle N_i = N_{ci} - N_{oi}$, is then randomly distributed inside the box. In this way the stellar incompleteness is corrected for both the rings and then the CMD of the rings are combined to obtain a complete CMD for the chosen cluster region. The same technique is applied to the field region without dividing it into different rings since the data incompleteness does not depend on position here.

4.4.5 Correction for field star contamination

We have used the zapping technique described by Mateo & Hodge (1986) to remove the field stars from the cluster CMD after accounting for the difference in the areas of field and cluster regions considered. In this method, for each star in the CMD of the field region, the nearest star in the CMD of the cluster region is identified and removed. The maximum box size for such an identification is varied and finally fixed at $V \sim 1$ mag and $(B - V) \sim 0.5$ mag. This box size is not related to the one used for the completeness correction. Lupton et al. (1989) have measured the radial velocities of some stars in NGC 2164 and NGC 2214 and identified a few of them either as galactic foreground stars or LMC field stars. We have therefore removed them from our further analysis. In this way, we get a cluster CMD ready to be compared with the theoretical evolutionary models.

4.4.6 Observed CMDs

For the four clusters under study, Figure 4.12 shows the observed CMDs corrected for photometric incompleteness and field star contamination. For comparing the number of stars present in different stellar evolutionary phases, the CMDs are divided into three parts consisting of MS stars, bright red giants (BRGs) and faint red giants (FRGs). The BRGs are the evolved stars of the cluster and the FRGs are the intermediate age core helium burning stars of the LMC field. Even after the field star subtraction using zapping technique we do find some FRGs, which we reject assuming them as the left out field stars. Here we discuss the various features of the final cluster CMDs and the main sequence LFs.

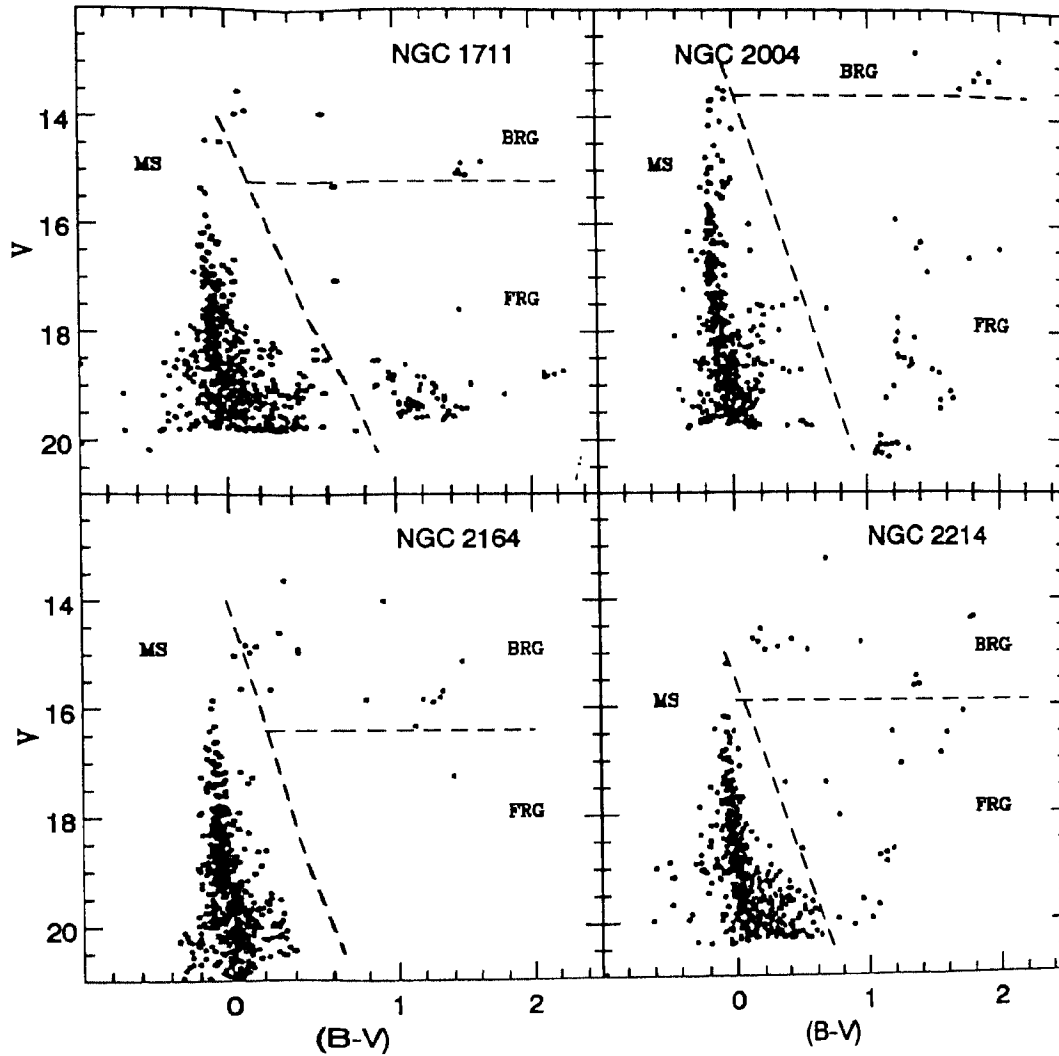Figure 4.12: *The cluster CMDs after completeness correction and field star subtraction are shown here. The regions occupied by MS stars, BRGs and FRGs are also shown.*

(i) NGC 1711 has a well populated MS ($\sim$590 stars) up to $V \sim 16$ and some stars are seen scattered up to 14.2 magnitude. A total of 10 BRGs are distributed between 0.0 and 2.0 mag in (B–V). The red clump of BRGs are at a (B–V) value of 1.6.

(ii) NGC 2004 is the youngest of the clusters considered here, having a well populated MS of ~520 stars continuous up to $V \sim 13.5$ mag. There are six BRGs confined to a very small range in brightness, $14.5 \leq V \leq 15.25$ but with somewhat larger range in their colours, $1.3 \leq (B-V) \leq 2.0$.

(iii) The brightest MS star in NGC 2164 has $V \sim 14.5$ mag and $(B-V) \sim -0.1$. Then there are no MS stars up to $V \sim 15$ mag. Below that the cluster MS is well populated with ~530 stars. The 16 BRGs are seen scattered between -0.1 and 1.4 mag in $(B-V)$.

(iv) The cluster MS of NGC 2214 containing ~550 stars is well populated up to $V \sim 16$ mag. The V magnitude difference between the brightest and the next brightest MS star is ~0.8 mag. The 14 BRGs are populated between -0.1 and 1.3 mag in $(B-V)$.

4.4.7 Luminosity functions of the MS stars

The LFs for the MS stars are calculated from the CMDs using a bin width of 0.2 mag in V. The resulting LFs for the clusters under study are shown in Figure 4.13, where the effects of correction of photometric incompleteness as well as of the field star contamination are also indicated. Despite the incompleteness correction, the luminosity functions seem to be complete only for stars brighter than $V \sim 19.5$ mag. We have fitted a straight line to the log N vs V plots using the least squares regression. The value of the slopes are 0.16 ± 0.03, 0.19 ± 0.04, 0.15 ± 0.03 and 0.16 ± 0.02 for the clusters NGC 1711, 2004, 2164 & 2214 respectively. This indicates that the slopes of their mass functions are similar which is in agreement with the results given in Sagar & Richtler (1991).

4.4.8 Determination of age of the clusters

To determine the age of the clusters, we fit the isochrones obtained from the stellar evolutionary models to the M_V vs $(B-V)_O$ CMDs of the clusters obtained from their V, $(B-V)$ CMDs. We adopt a value of 18.6 for the distance modulus to the LMC based on the studies of cepheid variables in LMC (Viswanathan 1985, Caldwell & Coulson 1985, Walker 1987, Welch et al. 1987, 1991). The reddening
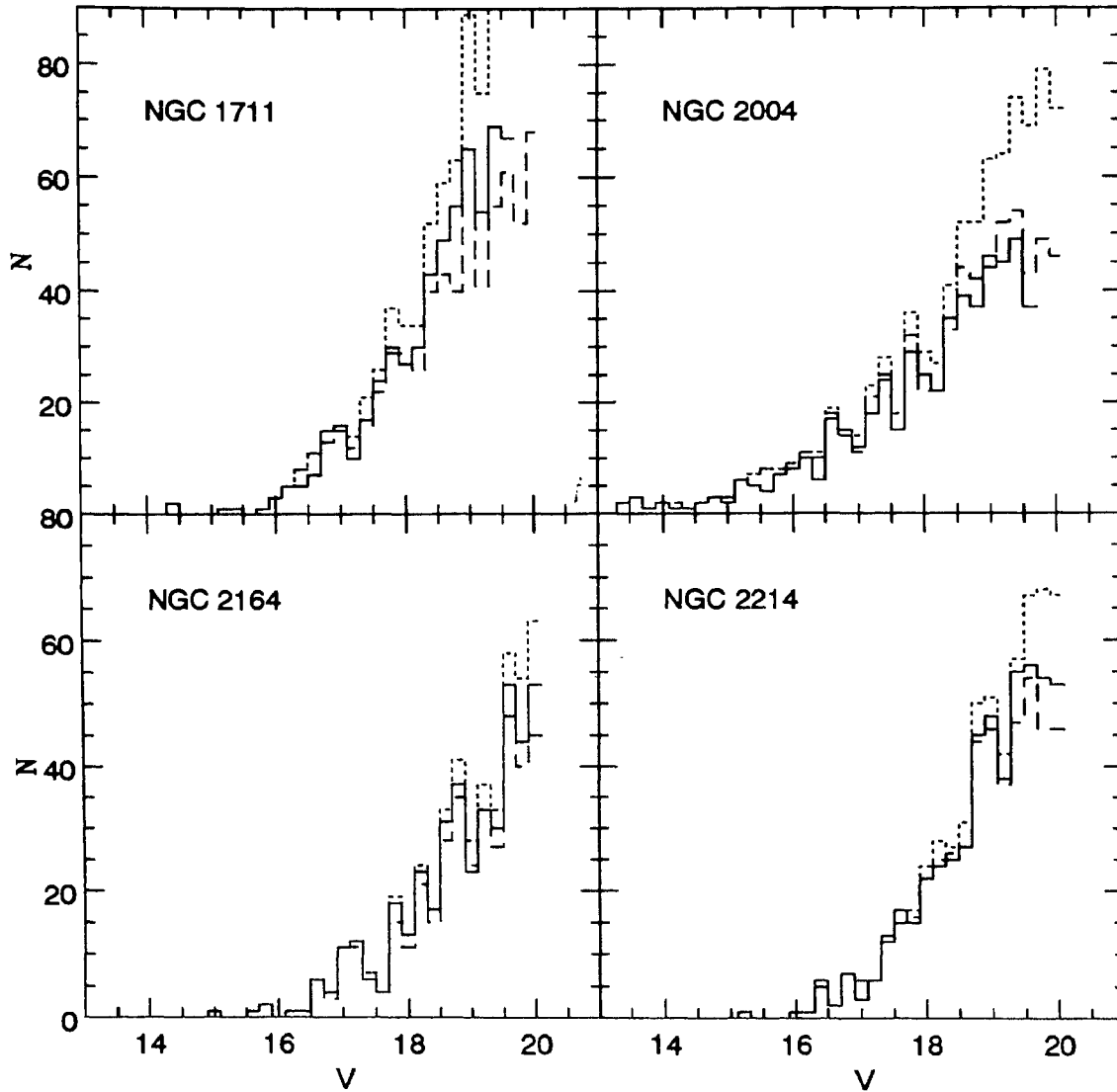
Figure 4.13: *The MSLF of the four clusters are plotted in solid lines. The LFs from the raw data are indicated in dashed lines, whereas the LFs from the data after completeness correction (before field star subtraction) is shown in dotted lines.*

values used are given in the Table 4.5. For NGC 1711, the E(B—V) value is taken from Mateo (1988) and for others from Cassatella et al. (1987). We assume the extinction in V as 3.1 × E(B—V). The isochrones fitted to the CMDs of the clusters under study are shown in Figure 4.14.

Table 4.6: *Age and turn-off mass of the clusters determined from the models.*

Cluster	Ages in Myr from models				Turn-off masses in $M_\odot$ from models			
	1	2	3	4	1	2	3	4
NGC 1711	22	28	35	23	9.7	8.3	8.3	9.4
NGC 2004	12	14	18	12	14.3	12.3	11.4	13.7
NGC 2164	35	50	60	38	7.5	6.4	6.4	7.2
NGC 2214	37	50	60	40	7.3	6.4	6.4	7.0

The ages and the turn-off masses obtained from different models are given in Table 4.6, which indicate that they depend strongly on the evolutionary models used. Isochrones with core overshoot make the object older but the turn-off mass lighter while those without make the cluster younger but the turn-off mass heavier. The ages and the turn-off masses of the clusters derived from the two classical models agree very well with each other. This may indicate that use of new opacities in models has not changed the hydrogen burning time scales significantly. Amongst the core overshoot models, model 3 makes the object oldest, even though the overshoot amount is the same as in model 2. However, both the core overshoot models yield the same turn-off masses. We also notice that the red giant stars are generally best fitted by the core overshoot models. The isochrones produced from the classical models could not reach the observed red end of the giant branch. Bencivenni et al. (1991) using the model 1 found an age of 8 Myr for the cluster NGC 2004, but using the same model we find an age of 12Myr. We find that an age of 8 Myr predicts the BRGs roughly 1 mag brighter than the observed ones, instead a 12 Myr isochrone fits the red giants better though it falls short by $\sim$ 0.25 in (B−V) mag.

4.4.9 Comparison of observed CMDs with synthetic CMDs

In order to compare the theoretical stellar evolutionary models with present observations, we produced synthetic CMDs from the models. We compare the features
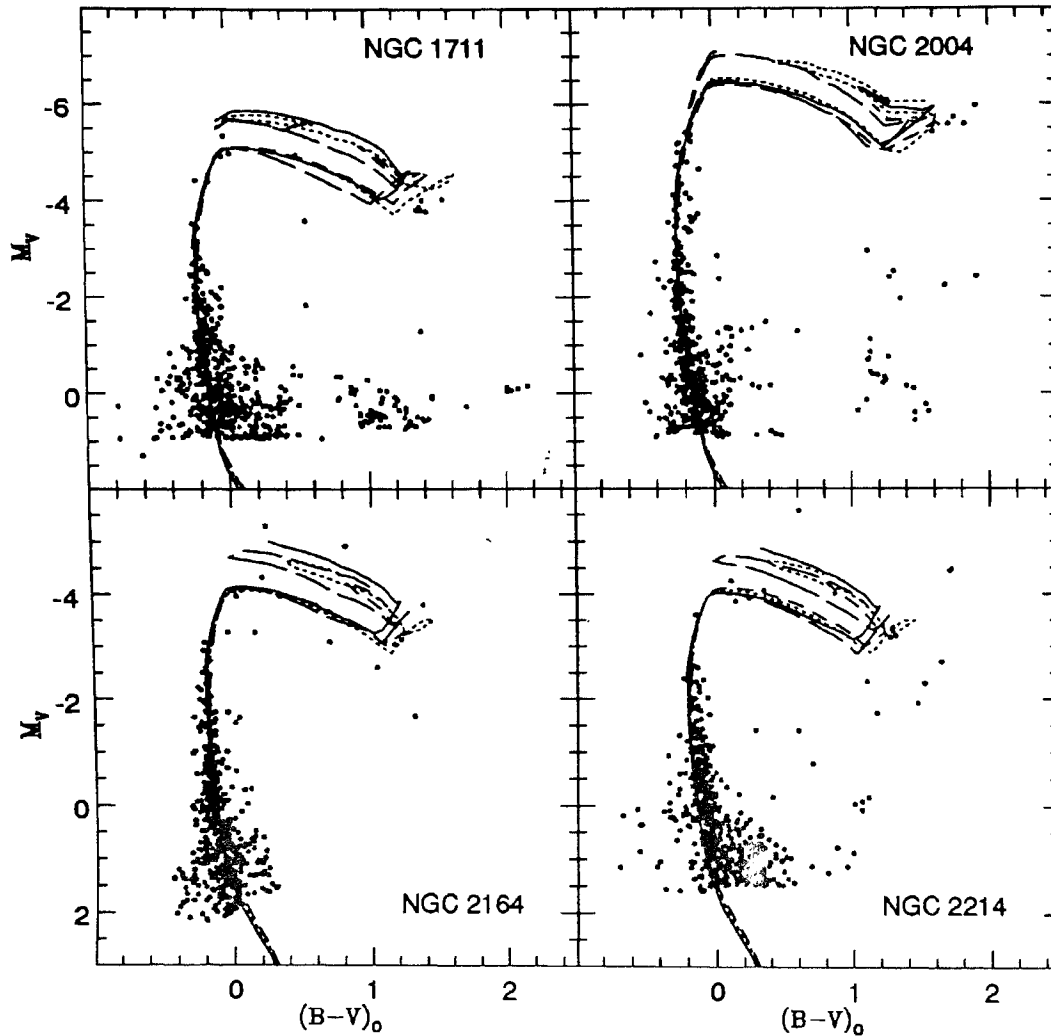
Figure 4.14: *The determination of the age by isochrone fitting for the four clusters are shown here. The continuous line represent model 1, dotted line model 2, short dashed line model 3 and long dashed line model 4.*

as well as the ILF of the observed CMDs with the synthetic ones.

4.4.10 Comparison of features

Here, we compare the features of the synthetic CMDs with the observed ones. The synthetic CMDs for the clusters which are best matching with the observation

Table 4.7: *The observed features of the cluster CMDs are compared with the ones predicted by the models from the synthetic CMDs. In the table, (a), (b), (c) and (d) denote the M_V of the MS tip, M_V of the faintest BRG, number of blue supergiants and the (B—V) value of the reddest BRG respectively. The last column gives the error in the values obtained from models.*

cluster	quantity	observed	Values from models				
			1	2	3	4	error
NGC 1711	(a)	−4.5	−4.0	−3.6	−4.0	−3.9	± 0.2
	(b)	−3.8	−4.5	−4.5	−4.4	−4.3	± 0.1
	(c)	1	2	4	0	3	
	(d)	1.55	1.3	1.7	1.65	1.34	± 0.2
NGC 2004	(a)	−5.5	−4.0	−4.75	−4.6	−4.2	± 0.1
	(b)	−4.45	−5.8	−5.6	−5.35	−5.0	± 0.1
	(c)	0	0	2	0	4	
	(d)	1.9	1.65	1.63	1.45	1.40	± 0.2
NGC 2164	(a)	−3.3	−3.0	−3.3	−3.4	−3.6	± 0.3
	(b)	−3.0	−3.8	−3.2	−3.1	−3.4	± 0.1
	(c)	1	0	6	0	5	
	(d)	1.38	1.23	1.47	1.46	1.24	± 0.1
NGC 2214	(a)	−3.6	−3.3	−3.3	−3.4	−3.1	± 0.3
	(b)	−3.2	−3.5	−3.5	−3.1	−3.3	± 0.1
	(c)	0	2	4	0	4	
	(d)	1.3	1.0	1.48	1.2	1.25	± 0.1

are shown in Figure 4.15. The absolute magnitude of the MS tip, the absolute magnitude of the faintest BRG, the (B—V) value of the reddest BRG and the number of blue supergiants predicted by the models and the values obtained from the observed CMDs are tabulated in Table 4.7.

Models 2 and 4 predict blue supergiants in all the clusters which is contrary to the observation, while models 1 and 3 produce almost none in their synthetic CMDs. In all the clusters the evolved part of the CMD is more closely reproduced by model 3. It is interesting to note that even though the amount of overshooting of the convective core is the same in models 2 and 3, the number of blue super giants and the evolved parts of the CMDs are better matched with model 3. This
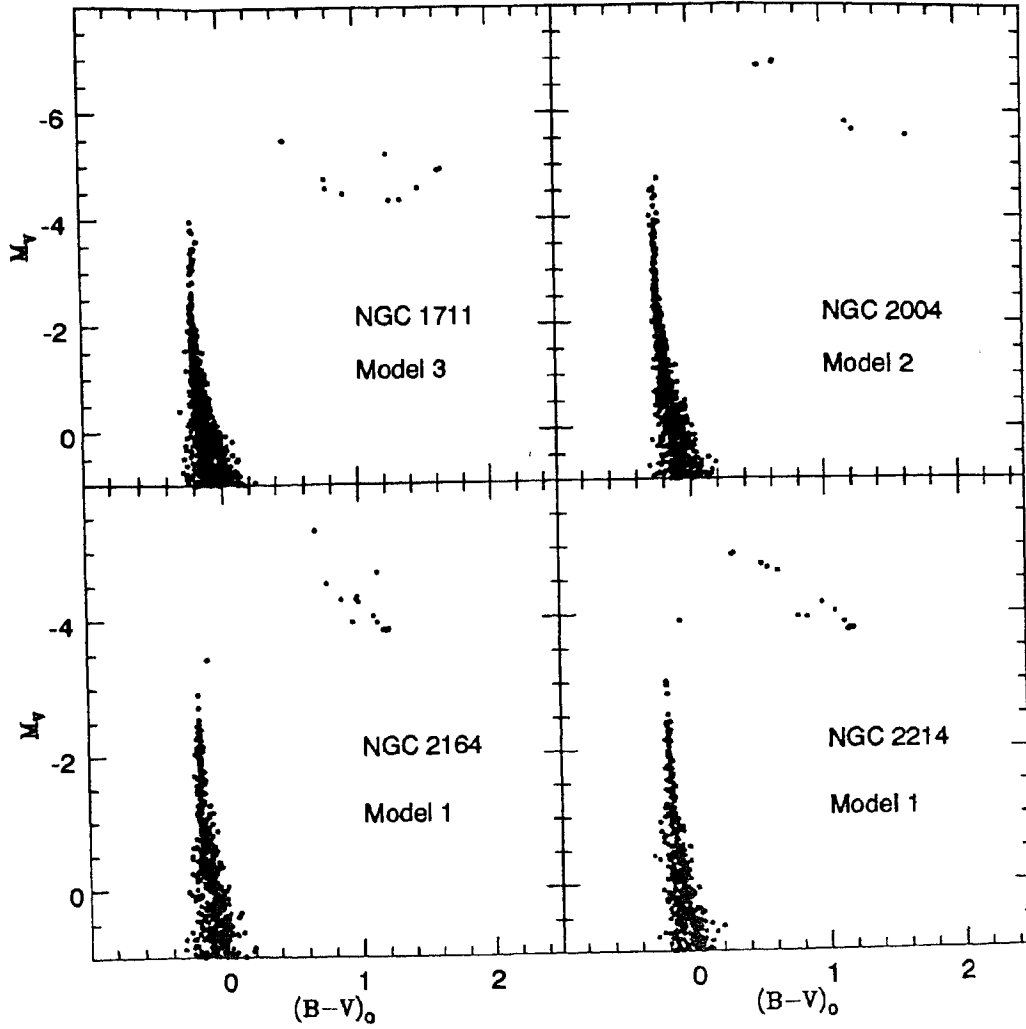
Figure 4.15: *The synthetic CMDs those match the observation for $x=1.35$ and binary fraction of 30% for the four clusters are shown here. The models from which the CMDs are made are also shown.*

may be due to the differing input physics and computational techniques involved in the two models.

In the cluster NGC 2004, the brighter end of the MS is not populated up to the observed value by any of the synthetic CMDs. Therefore we tried to populate the MS up to the observed tip by adopting an age spread. This gives rise to a
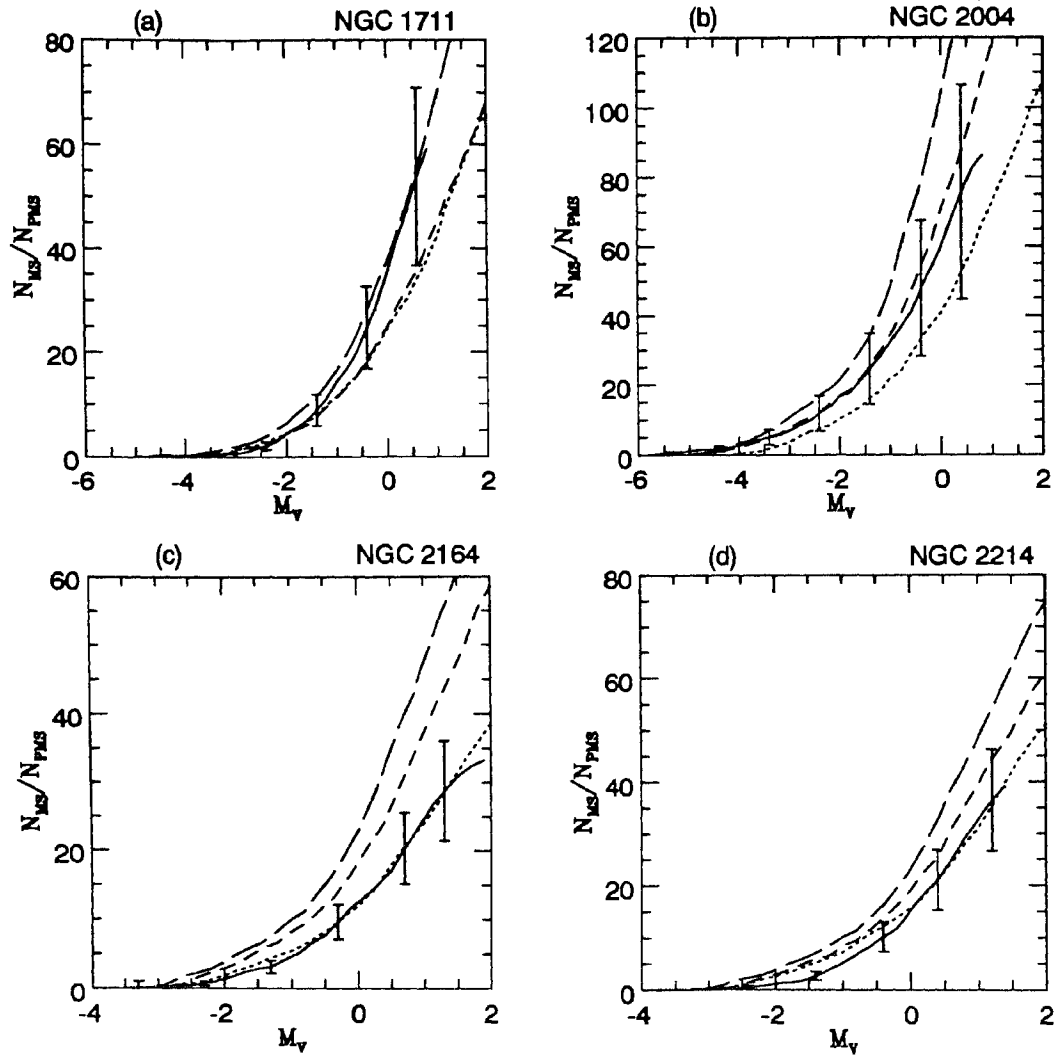
Figure 4.16: *The ILFs for the four clusters are plotted here. The continuous line indicate the observed ILFs. The dotted line represent the ILFs from model 1, short dashed line from model 2 and long dashed line from model 3. The error bars indicate the statistical error at the magnitudes shown for the observed ILF. The synthetic ILFs are constructed for x=1.35 and a binary fraction of 30%.*

spread out BRG population, both in M_V and $(B - V)_O$, which is contrary to what is observed. In order to populate the MS up to observed bright end, an age 6 Myr less than that obtained from BRGs is needed, in all the models. This may indicate that the stars which populate the tip of the MS are 6 Myr younger

than the BRGs. Bencivenni et al. (1991) has assigned an age of 8 Myr to this cluster using model 1 and still find a group of 10 stars lying above the observed bright end o the MS. They attribute such an evidence to the occurrence of binary accreting systems.

4.4.11   Comparison of observed ILFs with simulated ILFs

We derive the ILF normalized to the number of evolved stars for these clusters from the observed data as well as from synthetic CMDs constructed using different evolutionary models and compare them in Figure 4.16, for the Salpeter value of mass function slope (x=1.35) and an assumed binary fraction of 30%. The observed ILF depends on the number of evolved stars present in the sample. In order to minimize the effects of data incompleteness and stellar crowding in the cluster sample, it is restricted to the outer annular region. It is assumed that such a sample has the same proportion of stars in all mass ranges. This assumption is valid except in the case of NGC 1711 where slight mass segregation among the MS stars has been found (cf. Subramaniam et al. 1993). Also stochastic nature in the star formation if present can also affect the number of observed evolved stars.

Since model 4 is available only for masses $\geq 2\ M_\odot$ it is not possible to compare the ILFs from this model with the observed ones, instead we compare the ratio of the core He to H burning lifetimes. An inspection of figure 4.16 indicates that different models produce best fits for different clusters. In order to see the effects

Table 4.8: *The values of x which produces the best fit between synthetic and observed ILFs for a binary fraction of 30% for different models.*

cluster	x value for models		
	1	2	3
NGC 1711	1.90	1.60	1.35
NGC 2004	1.65	1.35	1.25
NGC 2164	1.35	1.13	1.05
NGC 2214	1.35	1.25	1.10

Table 4.9: *The value of binary fraction which produces the best fit between the observed and synthetic ILFs for the Salpeter mass function slope (x=1.35) for different models.*

Cluster	value of the binary fraction for models		
	1	2	3
NGC 1711	–	50%	30%
NGC 2004	50%	30%	0%
NGC 2164	30%	20%	–
NGC 2214	30%	20%	5%

of uncertainties in the value of x and binary fraction we have varied one of these two parameters keeping the other constant. The results of such an exercise are summarized below:

(i) For a given model, the value of binary fraction is fixed at 30% and the value of x was changed to get the best fit between observed and synthetic ILFs. The values of x for the best fits are tabulated in Table 4.8.

This table indicates a general trend that the model 1 needs steeper whereas model 3 needs flatter mass function slope. The value most deviating from the Salpeter value is for NGC 1711 in the case of model 1. Hence, it can be seen that with values of x not very different from Salpeter's value, the various models are able to fit the observed ILFs.

(ii) For a given model, the value of x is fixed at 1.35 (Salpeter's value) and the binary fraction is varied to get the best fit. The values of binary fraction are varied between 0 to 50% and the results are tabulated in Table 4.9.

In some cases, the change in binary fraction could not bring the synthetic ILFs closer to the observed one. These are given as blanks in the table. It can be seen that to obtain the best fit some models require rather extreme values of binary fraction.

Thus it can be seen that the comparison of ILFs does not show a clear picture

Table 4.10: *The values for the ratio of the helium to hydrogen burning lifetime is listed for different solar masses.*

Mass	τ_{He}/τ_H			
	Model 1	Model 2	Model 3	Model 4
7.0	0.169	0.109	0.071	0.146
9.0	0.144	0.099	0.063	0.111
12.0		0.098	0.062	0.087
15.0		0.096	0.065	0.093

as to which model is to be preferred. Since the ILFs reflect the ratio of the H to He-burning lifetimes, the values of He to H-burning lifetime ratios for the turn-off masses of the clusters as given by the models are tabulated in Table 4.10.

For a cluster, these values are very different, while the turn-off masses from the models are not very different (see table 4.6). One striking point being, both the classical models give very similar values for the ratio. Hence, it is difficult to find out the value of the ratio which is fitting the observation, mainly because of the uncertainty in the value of the mass function slope. Similar conclusion has been arrived at by Chiosi et al. (1994) while analyzing the SMC cluster NGC 330.

4.5 Conclusions

We have compared the CMDs and LFs derived from two homogeneous sets of data, one set comprising of four open clusters with turn-off masses in the range 2.8–4.0 $M_\odot$ and $\sim$ 12 $M_\odot$ and the second set comprising of the four LMC star clusters having turn-off masses in the range 6–15 $M_\odot$ with the synthetic ones produced using the stellar evolutionary models from Castellani et al. (1990), Schaller et al. (1992) and Bressan et al. (1993). Therefore, this study covers the range of intermediate to high mass stars.

Two of the old open clusters, NGC 1912 and NGC 6709 show clumpiness in the MS of their CMD. The reason for this is not known. It is important to know

the reason as most of the stars in these cluster MS happen to lie in the clumps. More photometric and spectroscopic observation of some stars in these clumps are needed to find presence of high rotation or spots etc., which might help in understanding the nature of these stars. In the case of open clusters and the LMC clusters, the stars seen at the very bright end of the MS were not populated in the synthetic CMDs of classical as well as the overshoot models. If these stars are in the normal evolutionary phase, then the evolutionary time-scale have to be modified to produce stars in this region. More observations are needed to identify the nature of these stars as to whether they are peculiar stars like accreting binaries etc.

In general, the features of the observed CMDs are well reproduced by overshoot models. In the lower mass range considered, the distinction between the two overshoot models couldn't be made. The model 3 is preferred to model 2 in the case of the higher mass range. As far as the lifetime ratios are concerned, a clear cut picture does not emerge from the present analysis. The analysis of the LMC clusters show that the fine tuning of the percentage of binary stars and the slope of mass function can bring the synthetic ILFs of all the models to match the observed ILFs. This procedure is not attempted in the case of open clusters because of the poor number statistics. Though the model 2 seems to have the vale of τ_{He}/τ_H close to the observed one, the statistical uncertainty pushes the values of the other two models also within the errors of the observed one.

Another point to be noticed is that, for ages $> 10^8$ yr, the model 2 and model 3 estimates the similar ages, whereas for younger clusters, model 2 estimates a younger age when compared to model 3. For old clusters, when the models 2 and 3 estimate similar ages, model 2 estimates a lower turn-off mass and τ_{He}/τ_H ratio compared to model 3. In the case of younger (LMC) clusters, the model 3 has the lower M_{TO} and τ_{He}/τ_H. Though the models use the same amount of core overshooting, they seem to differ differently in the lower and the higher mass ranges considered.

The slopes of the mass function for the four LMC clusters studied here, have been determined by Sagar & Richtler (1991). The present estimates of the mass function slopes for the clusters are similar to the values obtained by Sagar &

Richtler (1991) within errors.

The main results of the present investigation are:

1. Classical models make the clusters younger but the turn-off masses slightly heavier in comparison to the models incorporating the overshooting of the convective core.

2. In general, the overshoot models reproduce the observed features when compared to the classical models. Stellar evolutionary models with core overshoot given by Bressan et al. (1993) reproduce the observed features of CMDs best in the case of the higher mass range studied here.

3. The synthetic ILF derived from a model strongly depends on the value of the mass function slope, and lightly on the binary fraction whereas the observed ILFs are affected by the uncertainty in the number of evolved stars. Hence the comparison of the synthetic with the observed ILFs does not favour any model specifically. In order to constrain the models from the comparison of the synthetic ILFs with the observed ones, reliable estimates of mass function slope, binary fraction are desired.

4. The ILFs comparison can limit the values of the mass function slopes to a certain extent. The open clusters NGC 1912 and NGC 6709 have x=1.7±0.15, NGC 2383 has x=1.3±0.15 and NGC 2384 has x=1.0±0.15. The LMC clusters, except NGC 1711 have x close to 1.3±0.15. A steeper slope of mass function is obtained for NGC 1711, this may be because of the slight mass segregation seen in the cluster.

Chapter 5

Probable binary open star clusters in the Galaxy

5.1 Introduction

The[1] open clusters are mostly found in the spiral arms of the Galaxy. These clusters are formed in the molecular cloud complexes, which delineate the spiral arms. Molecular clouds which are the formation sites of young open clusters are known to form more than one star cluster in their lifetime. It is more than likely that some of the clusters formed from a single parent molecular cloud survive as bound objects, even after the disruption of the cloud. A probable site for finding Galactic double or binary clusters in the Galaxy may be the spiral arms where the density of open clusters is high. Optical sky surveys such as the Palomar Observatory Sky Survey (POSS) reveal a large number of closely located clusters, when seen projected on the plane of the sky. The actual physical association of even a few of these clusters has important implications on the evolution of open clusters. Star clusters born as binaries could either survive as such for their entire lifetime, or get disrupted by the Galactic tidal field. A few clusters with small separations could probably even merge in a few million years.

The total number of open clusters known in our Galaxy is ~ 1400. Of these, the only well established double or binary cluster is h&χ Persei (NGC 869 & NGC 884), which consists of the two rich, young clusters located at a distance

---

[1]Part of the chapter can be seen in Subramaniam et al. (1995), A&A, 302, 86

of more than 2 kpc from the sun. The existence of other possible double clusters and cluster complexes has been proposed earlier (Pavloskaya et al. 1989), but not been seriously looked into. On the other hand, the Magellanic Clouds (MCs) are widely believed to have a number of binary clusters and these have been studied in some detail (Bhatia 1990 and references therein). The MCs are at a distance of $\sim$ 50–60 kpc and this makes the identification of the double star clusters easier, as the candidacy is established from the closeness of their projected positions on to the plane of the sky. This method of determining candidate members for double star clusters in our Galaxy is not however feasible. Since we are looking at the Galaxy from inside, the distance to the clusters should also be taken into account. The distances are estimated for five open clusters in the present study and of these, NGC 1912 & NGC 1907 and NGC 2383 & NGC 2384 are at the same distance. Also these two pairs lie very close to each other in the sky. In this chapter, we examine existing catalogues of open cluster data and suggest pairs of clusters located closely enough in space, to be considered as possible binaries or double clusters. Tidal disruption time-scales for the identified double clusters are estimated.

5.2 Open cluster data and analysis

The catalogue of open clusters by Lyngå (1987) has been used for the analysis. This contains around 1400 clusters and $\sim$ 400 of these have known distances.

As the distribution of the open clusters in the Galaxy is highly non-uniform and concentrated along the spiral arms, a statistical analysis based on the projected separation on the plane of the sky cannot be done without appropriate weightage. However, the distribution cannot be modeled accurately and hence the above method may not be very reliable. Therefore, we have restricted our analysis to those open clusters with distances known. Within the resulting database of 416 clusters, we find the distance of the nearest neighbour for each cluster. This is done by finding the angular separations between two clusters, $\Delta\theta$ and assuming the distance to be the mean of the two cluster distances, thus the separation is equal to $\Delta\theta \times d$. We have allowed for a 20% error in the distances given in the catalogue. A cluster pair is termed as a binary cluster if their separation

is ≤ 20 pc. The average separation between open clusters as determined from the cluster formation rate given by Battinelli & Capuzzo-Dolcetta (1991) is around 100 pc assuming a typical cluster lifetime of $2\ 10^8$ yr. This implies less than 1% probability of finding a cluster within 20 pc by chance or random fluctuations in the spatial density of clusters. Besides, a typical giant molecular cloud has an extent of 20 pc and clusters with separations smaller than this have a higher chance of being physically associated. Thus we form a list of 18 candidate binary clusters as listed in Table 5.1. We have excluded clusters of dubious nature and OB associations. A search of existing literature has been made for other cluster parameters such as age, mass, radial velocity etc.

5.2.1 Two cluster pairs

The present set of data obtained for the five open clusters as given in the chapter 3, has two of the 18 pairs given in Table 5.1. They are NGC 1907 & NGC 1912 and NGC 2383 & NGC 2384. These two pairs are discussed below. The distances and reddening to these four clusters are determined in Chapter 3. The cluster parameters as estimated in the present study and supplemented from the literature are listed in Table 5.2. The distances are estimated using the same method and hence the errors given in the table are relative errors.

NGC 1907+NGC 1912 The clusters NGC 1907+NGC 1912 lie in the constellation of Auriga. The two clusters as seen in the Palomar chart are shown in Figure 5.1. The present distance estimates are larger and the reddening estimates are very close to the values given in the catalogue. With the new distance, the separation between the clusters become 18.8 pc. There is a difference of 0.12 mag in reddening between these two clusters and is primarily because of the foreground Taurus-Auriga cloud, which gives rise to differential reddening in this direction. This is evident from the cluster region as seen in the Palomar chart. The present age estimates show that the two clusters have similar ages. Available metallicity and the radial velocity estimates find similar values for the clusters. These facts strengthen the arguement that the two clusters might be born from the same cloud nearly at the same time.

Table 5.1: *List of candidate binary clusters with known parameters*

| Cluster name	lon.	lat.	distance	log age	rad.vel	A_V	separation(pc)	log τ_{tidal}
King 14	120.72	0.36	2600	7.2	–	1.71	8.64	8.54
NGC 146	120.87	0.49	2900	7.10	–	2.16		
NGC 869	134.63	–3.72	2200	6.75	–40	1.68	18.93	7.00
NGC 884	135.08	–3.6	2300	6.5	–	1.68		
NGC 1513	152.6	–1.57	820	8.63	–	1.77	19.00	7.15
NGC 1545	153.36	0.17	800	8.29	–15	1.08		
NGC 1907	172.62	0.30	1380	8.64	+1	1.41	14.12	7.62
NGC 1912	172.27	0.70	1320	8.35	–3	0.72		
NGC 1981	208.09	–18.98	400	–	+28	–	19.38	7.15
Coll 70	204.98	–17.44	430	–	–	–		
Basel 8	203.79	–0.12	1300	–	–	–	7.17	8.95
NGC 2251	203.60	0.13	1550	8.48	–7	0.72		
NGC 2383	235.26	–2.44	2000	7.4	–	0.81	5.84	9.36
NGC 2384	235.39	–2.41	2000	6.0	+31	0.93		
Haff 18	243.11	0.44	6900	6.0	–	–	15.76	6.90
Haff 19	243.04	0.52	6900	6.8	–	–		
Pismis 6	264.81	–2.87	1600	7.5	+30	1.20	12.97	7.94
Pismis 8	265.08	–2.63	1400	7.5	+63	2.22		
NGC 3247	284.59	–0.35	1400	7.7	–	0.96	15.53	7.68
IC 2581	284.60	0.01	1660	7.0	–6	1.29		
Hogg 10	290.80	0.10	2200	6.3	–	1.38	3.9	10.36
Hogg 11	290.89	0.14	2300	6.8	–	0.96		
Basel 18	307.20	0.20	1556	8.2	–	–	11.04	8.37
Coll 271	307.09	–1.62	1600	7.8	–	0.96		
NGC 6152	332.93	–3.14	1030	–	–	–	14.00	7.91
NGC 6208	333.69	–5.82	1000	9.0	–	0.54		
NGC 6383	355.68	0.05	1380	6.65	–2	0.78	6.06	9.59
Tr 28	355.98	–0.26	1500	8.3	–	2.22		
NGC 6755	38.55	–1.7	1500	7.6	+57	3.55	12.45	8.16
NGC 6756	39.067	–1.69	1650	7.7	–	4.41		
NGC 6996	85.46	–0.47	500	–	+10	1.92	11.88	8.15
Coll 428	86.21	–1.41	480	–	–	–		
NGC 7031	91.32	2.26	1000	7.8	–	2.46	16.60	7.48
NGC 7086	94.41	0.20	1200	7.9	–	2.07		
NGC 7429	108.95	0.28	1920	–	–	–	18.15	7.20
Mark 50	111.36	–0.20	2250	7.0	–81	2.58		
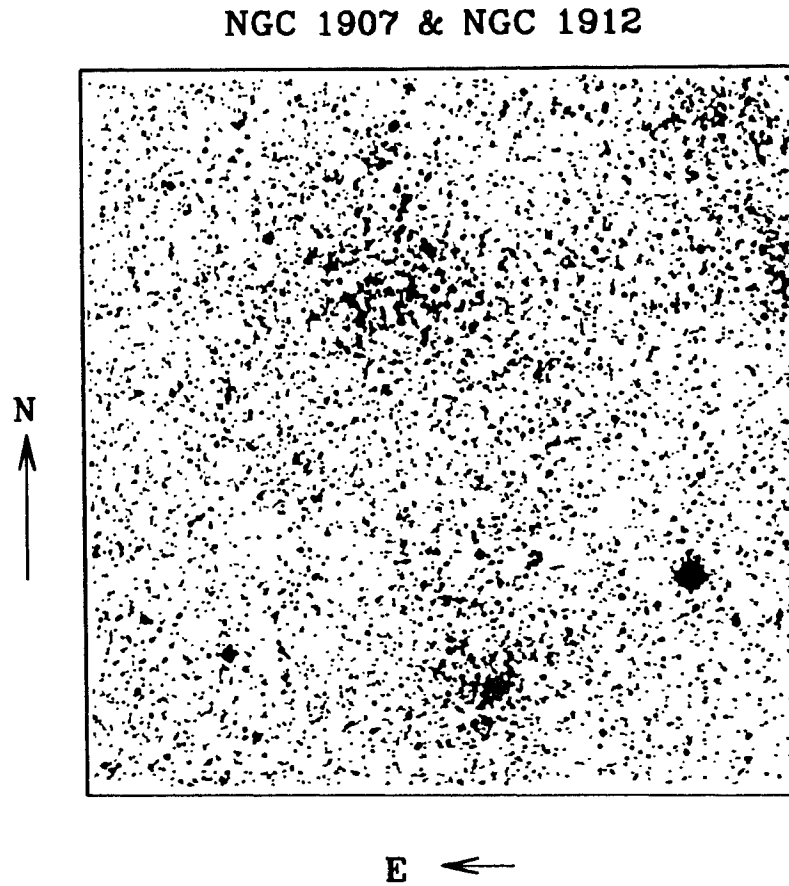
NGC 1907 & NGC 1912

Figure 5.1: *The combined region of NGC 1907+NGC 1912 is shown here. NGC 1912 lies towards the north and NGC 1907 towards the south in the figure.*

NGC 2383+NGC 2384 These two clusters lie in the constellation of Canis Major. The clusters as seen in the SERC charts are already shown in Figure 3.3. Vogt & Moffat (1972) have commented on these two clusters and they find that they lie in two different arms and they are close in the sky,

Table 5.2: *The parameters of four clusters are tabulated here. The metallicity values are taken from the literature .*

Cluster	Distance	E(B−V)	Log Age	Metallicity	separation	log τ_{tidal}
	pc	mag			pc	
NGC 1907	1785±80	0.40	8.6	−0.10	18.8	
NGC 1912	1810±80	0.23	8.4	−0.11	18.8	7.0
NGC 2383	3340±155	0.22	8.6	−	9.2	
NGC 2384	2925±135	0.28	7.3	−	9.2	8.4

just because of projection. The present analysis find that these two clusters lie close to each other, at a distance different from the one given in the catalogue. The separation between the clusters now becomes 9.2 pc. The reddening values are very similar. There are no metallicity and radial velocity estimates available. The present age estimates show that these two clusters have different ages. The cluster NGC 2384 is very young, having almost all the stars on the MS. This indicates that these clusters are not born together.

5.3 Tidal disruption

The open clusters in the Galaxy are distributed close to the Galactic plane with a scale height of only 70 pc. They are hence subjected to a strong tidal field due to differential rotation in the Galaxy. The lifetime of a cluster is in fact determined by the tidal field and is disrupted typically after a few 10^8 years. The influence of the galactic tidal field is stronger on the binary/double cluster due to its larger extent and could potentially disrupt the pair in its early stages and the pair may not remain bound for even a fraction of the cluster lifetime. The tidal disruption times for each candidate cluster pair has been estimated using the impulse approximation as in Bhatia (1990). They calculate the disruption time by equating the energy input by the galactic tidal field to the binding energy of the pair. The expression for disruption time is given by

$$t_{tidal} = \frac{4G^{1.5}(m_1 * m_2)}{(m_1 + m_2)^{0.5}(d^2\omega/dr^2)a^{4.5}}$$

where a is the separation, m_1, m_2 are the masses of the clusters and the $d\omega/dr$ is the tidal acceleration. The Galactic rotation curve determined empirically (see Bowers & Deeming 1984) has been used to obtain the acceleration and this is fairly accurate at the cluster galactocentric distances. The separation, a, used here is that determined from the mean cluster distance. It should be noted that for a precise evaluation of the tidal time-scale, the *true* physical separation should be used, for which better distance estimates to the clusters are required. Masses for some of the clusters are available in literature. Most of these are, however, luminous mass estimates which are systematically lower than the dynamical masses of the clusters (Battinelli et al 1994). We have assumed a common mass of $5 \cdot 10^3$

$M_\odot$ for all clusters. We believe that this assumption is not too bad, as t_{tidal} varies only weakly with mass, its strongest dependence being on the separation between the clusters. The separation and tidal disruption times for each pair are also tabulated in Table 5.1. With the new distance estimates for the two pairs, NGC 1907+NGC 1912 and NGC 2383+NGC 2384, the tidal disruption time-scale, log t_{tidal} becomes 7.0 and 8.36 respectively.

5.4 Discussion

The candidate binary clusters (18 pairs in number), have been proposed on the basis of their spatial proximity. Other parameters like age, extinction, radial velocities etc. provide additional information on their binarity. Clusters of similar ages suggest a common origin whereas similar radial velocities further strengthen their closeness. Table 5.1 gives the ages and radial velocities for the clusters in our list, where available (Mermilliod 1994). It is seen that there is only one pair in our sample, NGC 6383+Tr 28, where the members have widely disparate ages, suggesting that most of our candidates could be of a common origin. Radial velocity measurements are not available for both clusters of a pair, except for NGC 1907+NGC 1912 and Pis 6+Pis 8. The radial velocities of Pis 6 and Pis 8 do not match suggesting that these two clusters may not be physically close. NGC 1907 and NGC 1912, on the other hand, have similar radial velocities indicating that they are probably physically associated. It is to be noted that the two disparate pairs, Pis 6+Pis 8 and NGC 6383+Tr 28, are the only ones with extinction values differing by more than one magnitude. The catalogue has data taken from different sources and hence the data is not homogeneous. This gives rise to problems like different reliability for the same parameter for different clusters. We have obtained homogeneous data for 2 pairs listed in table 5.1. The estimates of the cluster parameters for the pair NGC 1907+NGC 1912 strengthens its candidacy. The new estimates show that they have very similar values for distance and age, which makes them a good candidate for binary cluster, but the tidal time-scale for the pair is less than their age, which might suggest that the clusters are not gravitationally bound. In the case of the pair NGC 2383+NGC 2384, their ages show that they cannot have a common origin. The separation between the clusters in the line of sight is 415 pc about the mean and $\sim$ 200 pc beyond errors.
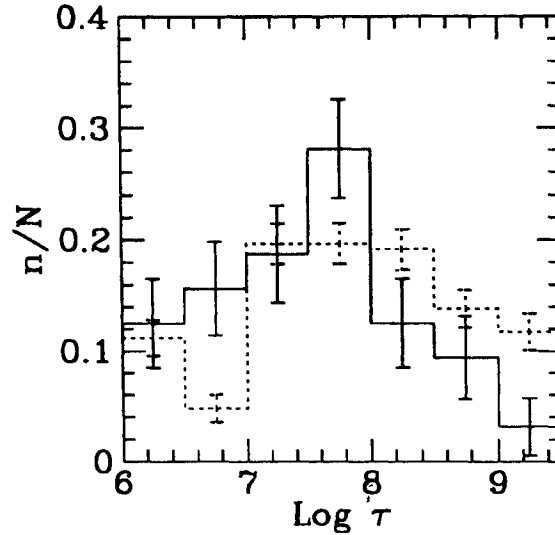
Figure 5.2: *Histogram of cluster ages (log τ) for binary (solid line) and single clusters (dashed line) from the sample. The number of clusters in each bin have been normalized with respect to the total number in the two categories.*

Therefore, the separation between the clusters is (200 pc) only 1.5 times the error in distance estimation. Thus, the clusters can be considered to be at the same distance. Also, the tidal time-scale is similar to the age of the cluster, indicating that they may be physically associated.

Thus we find 16 pairs of clusters from the cluster sample. These constitute about 8% of our sample of 416 clusters. It is to be noted that similar fractions of clusters are found to be in binary systems in the Magellanic Clouds (11% in the LMC and slightly less in the SMC, Hatzidimitriou & Bhatia 1990).

Further the distribution of separations between clusters in a pair, shows an apparent peak for the LMC ($\sim$ 6 pc) and the SMC ($\sim$ 11 pc). No such preferred separation is observed in Galactic clusters. A comparison of the frequency distribution of ages of the clusters in a pair with that of single clusters in our Galaxy (Figure 5.2) shows that the two differ, especially for larger ages. It is seen that the pairs are preferentially younger and the distribution falls off sharply for ages longer than $Log\tau \geq 8$. This result probably implies that older cluster pairs do not survive the disruptive influence of the Galactic tidal field and molecular cloud encounters. Similar distributions are found for the LMC and the SMC with 'binary

clusters apparently following the young rather than old clusters' (Hatzidimitriou & Bhatia 1990).

A comparison of the cluster disruption time scales with the mean age of a cluster pair, shows that except for three pairs, all others have consistently larger τ_{tidal} than their mean age. This further strengthens the supposition that the clusters may be physically associated. It is to be noted that the time-scale for tidal disruption as calculated here, is not valid for the system NGC 869+NGC 884 (h+χ Persei). In the calculation of τ_{tidal}, it is assumed that the separation between the clusters is larger than the sum of their radii and this assumption does not hold for this pair. For a proper analysis on binary cluster stability, merger time scales should also be computed. These, however, involve detailed numerical N-body simulations which have not been attempted.

We thus find that 8% of our sample are probable members of binary systems. Were the distances to all the clusters known, there would be many more candidates within our limiting separation of 20 pc. This indicates that binary clusters are probably a common occurence in the Galaxy as well and are potentially interesting objects which could provide valuable information on the dynamics of groups of stellar systems. The presence of double or binary clusters with small separations ($\sim$ 20pc) also has implications on the star-forming processes in the Galaxy. This indicates that star-formation in a molecular cloud (extent $\sim$ 20pc) is not restricted to a single region in the cloud but probably takes place in two or more concentrations. Examples of such multiple cluster formation sites are the Chamaeleon I cloud (Hartigan 1993) and the young open cluster NGC 2264 (Mathieu 1986, Sagar et al. 1988 Lada et al. 1993) which show the presence of two central cores. The open cluster OCL 556 (Haffner 3) also shows the presence of two distinct concentrations (Babu 1985). Though only the tidal disruption times have been computed above, it should be noted that merging is an equally important end state for a binary cluster. Clusters with large disruption times are more likely to merge in times short compared to a cluster lifetime.

5.5 Conclusions

Binary clusters are believed to be common in the Magellanic Clouds, but the only known binary cluster in the Galaxy is the h&χ Persei. We propose the

existence of more double clusters of which some may be physically associated and unlikely to be disrupted by the Galactic tidal field during their lifetime. From a sample of 416 clusters for which distances were known, we find 16 pairs, which implies that 8% of the clusters are members of binary systems. The present observations show that the pair NGC 1907+NGC 1912 is a good candidate for binary cluster. The fraction of clusters in pairs and the age distributions are found to be similar to those in the Magellanic Clouds. The cluster pairs may get disrupted by encounters with molecular clouds or due to the Galactic tidal field, or merge if the separations are very small. The presence of a companion cluster could greatly influence the dynamical evolution of either member of the pair and such studies could prove very interesting. Further, the possible existence of double clusters with small separations indicates that star-forming activity in molecular clouds takes place in two or more regions at the same time.

Chapter 6

Conclusions

The scope of the present work is to compare a set of homogeneous data with the theoretical stellar evolutionary models. The work is dealt with in detail in the previous chapters. The main conclusions and the prospects of future work are presented here.

The photometric observations of five and spectroscopic measurements of individual stars in four open clusters are used in this study. This is supplemented by the photometric data of four LMC star clusters. The photometric and spectroscopic observations are used to find the reddening and distance to the cluster. It is seen that the photometric reddening estimates are very similar to the values obtained before. On the other hand, the spectroscopic observations estimate a lower value for the reddening. Also, the spectroscopic distance modulii are systematically lower than the values obtained from photometry. In the case of NGC 2384, the spectroscopic reddening turns out to be larger than the photometric value because, these values were found from the more reddened members of the cluster. In this cluster, the brightest few members seem to be more reddened than the rest of the members of the cluster. These are the B-type stars and the extra reddening may be due to any surface activity or high rotation. The present spectroscopic observations reveal the presence of an H_α emission star in NGC 2383 for the first time. The distance measurements to all the five clusters studied turns out to be more by $\sim$ 30 % than the earlier estimates. The present photometry reaches a limiting magnitude $\sim$ 20.0 in V, whereas, all the previous estimates were limited to the brighter part of the CMD. Therefore the present distance estimates are more accurate. The CMDs of two clusters show the pres-

ence of clumpiness in their MS. The spread in the color may be due to binarity, rotation or surface activity.

The galactic open clusters have only small number of stars in the evolutionary phases, giving rise to poor number statistics, while the LMC clusters are richer in stars and hence are better from the statistics point of view. The observed CMDs of five open clusters and four LMC clusters are used to compare with the theoretical stellar evolutionary models from Castellani et al. (1990), Schaller et al. (1992) and Bressan et al. (1993). This comprises two classical and two overshoot models. The comparison is brought out with the help of isochrones from the models, synthetic CMDs constructed using a code and ILFs computed from the CMDs. Four of the five open clusters are of intermediate age. The classical model from Bressan et al. (1993), could be used only in the case of young LMC clusters as the lowest mass available from this model is close to the turn-off masses of the intermediate age open clusters. Only two of the intermediate age clusters show the presence of the red giant clump in their CMDs. The other two have only one star as a candidate for the red giant. The isochrones from the models are used to estimate the ages of the clusters. The classical models estimate younger ages for the cluster, while the overshoot models estimate comparatively older ages. This is expected as the overshooting of the convective core increases the lifetime of a star on the MS. In the case of the intermediate age clusters, models 2 and 3 estimate similar ages, whereas for younger clusters, model 3 estimates older ages in comparison to model 2. The point to be noted is that these two models use the same amount of overshooting from the core. For the young clusters, the ages determined by the classical models are similar, though model 1 estimates younger values compared to model 4.

A computer code is used to construct the synthetic CMDs from the evolutionary models. These synthetic CMDs are then used to estimate the ILFs of the MS. Of the five open clusters, only four have field star estimates. Therefore the comparison of LFs are limited to four open clusters. The clusters studied here have a range of turn-off mass from 2.8–4.0 $M_\odot$ (three intermediate age open clusters) and 6.0–14 $M_\odot$ (one young open cluster and four LMC clusters). Therefore the evolutionary features discussed are corresponding to the stars in these mass ranges. The comparison of the observed and the synthetic CMDs show that, in the case of intermediate age clusters, the overshoot models are able to reproduce

the evolutionary sequences as seen in the observed CMDs. The distinction between the two overshoot models could not be made. The classical model 1 tries to populate stars in subgiant branch contrary to the observation. In the case of younger LMC clusters, model 3 fits the observation the best. Models 2 and 4 predict blue supergiants, while 1 and 3 produce none in their synthetic CMDs, similar to what is observed.

All the four intermediate age open clusters show the presence of a few stars at the top of the MS. Though these stars lie along the isochrones computed from the above models, none of the models are able to populate these stars in their synthetic CMDs. This can be seen in the plot where the observed and the computed ILFs are compared. There can be two reasons to this. One is that these stars are not in the normal phase of evolution, for example, if they are contact binaries or accreting binaries, then they do not follow the path of the evolution of a single star. The other reason is that, if these stars are single normal stars, then the models need to change their time-scales of evolution in order to incorporate these stars. The spectra of one such star in NGC 1912 shows giant nature, but the resolution is not enough to find any abnormality in the spectra. High resolution spectroscopic observations of these stars are required to resolve the issue. Again, in the case of very young clusters, NGC 2004 and NGC 2384, the synthetic CMDs are unable to populate the brightest stars in the MS. In the case of NGC 2004, an age younger by 6 Myr compared to the age of the red giants had to be adopted for populating this region. Bencivenni et al. (1991) also find similar case with this cluster and express the possibility of these stars being accreting systems. The cluster NGC 2384 does not have any evolved stars and hence the brightest MS stars have to be relied upon to estimate the age. The synthetic CMDs require an age less by $\sim$ 8 Myr from the isochrone estimate to populate this region.

The ILF of the MS, normalised to the number of red giants is equivalent to the ratio of time-scales of core helium burning to core hydrogen burning. Therefore, the comparison of the ILFs computed from the synthetic CMDs with the observed ones helps in identifying the actual observed value of the ratio. In the case of intermediate mass stars, the value of the ratio estimated from the model 2 seems to come very close to the observations. On the other hand, for different values of mass function slope, the other models also seem to have the ratio within the observational error. This behaviour is seen in the case of high mass stars also.

Changing the percentage of binary stars in the synthetic CMDs can also bring the synthetic ILFs close to the observed ones, to a certain extent. Though the ILF comparison is expected to bring out the correct lifetime ratio, it is very sensitive to the mass function slope used and the percentage of binary stars to a lesser extent. Therefore, the present analysis is not capable of identifying the correct value of the lifetime ratio.

The comparison of the ILFs can be used to constrain the mass function slope. In the case of open clusters, the slope of the mass function, x is found to be 1.7 ± 0.15 in the case of NGC 1912 and NGC 6709, 1.3 ± 0.15 in the case of NGC 2383 and 1.0 ± 0.15 in the case of NGC 2384. Therefore, two clusters are seen to have steeper, one shallower and one close to the Salpeter value of mass function slope. The mass function estimates seems to be model dependent and the values quoted here are the ones falling close to the Salpeter value. Similarly, in the case of LMC clusters also, the value of x is seen to be model dependent. The estimates for the LMC clusters are for stars in an annular region avoiding the cluster center. The mass function slopes seems to be close to the Salpeter value for NGC 2004, NGC 2164 and NGC 2214. On the other hand, for NGC 1711, the slope seems to be steeper, this may be due to the slight mass segregation seen in the cluster.

Binary clusters are believed to be common in the Magellanic Clouds, but the only known binary cluster in the Galaxy is the h+χ Persei. We propose the existence of more double clusters of which some may be physically associated and unlikely to be disrupted by the Galactic tidal field during their lifetime. From a sample of 416 clusters for which distances were known, we find 16 pairs, which implies that 8% of the clusters are members of binary systems. The present observations show that the pair NGC 1907+NGC 1912 is a good candidate for double cluster as they are close enough in the line of sight and are of very similar age to have born together. On the other hand, the new distance estimates of NGC 2383+NGC 2384 show that these clusters are physically close within the errors of distance estimates. The present age estimates of this pair shows that these have very different ages so that they could not have been born together.

References

Alongi M., Bertelli G., Bressan A., Chiosi C., Fagotto F., Greggio L., Nasi E., 1993, A&AS 97, 851

Ambartsumian V.A., 1947, Stellar Evolution and Astrophysics (Armenian Academy of Sciences)

Anthony-Twarog B.J., Heim E.A., Twarog B.A., Caldwell N., 1991, AJ 102, 1056

Aparicio A., Alfaro E.J., Delgado A.J., Rodriguez-Ulloa J.A., Cabrera-Cano J., 1993, AJ 106, 1547

Aparicio A., Bertelli G., Chiosi C., Garcia-Pelayo J.M., 1990, A&A 240, 262

Babu G.S.D., 1985, Ph.D. Thesis

Banks T., Dodd R.J., Sullivan D.J., 1995, MNRAS 274, 1225

Barbaro G., Pigatto L., 1984, A&A 136, 355

Barbon R., Hassan S.M., 1996, A&AS 115, 325

Battinelli P., Brandimarti A., Capuzzo-Dolcetta, 1994, A&AS 104, 379

Battinelli P., Capuzzo-Dolcetta, 1991, MNRAS 249, 76

Becker S.A., 1981, A&AS 136, 355

Becker S.A., Mathews G.J., 1983, ApJ 270, 155

Becker W., 1963a, ZA 57, 117

Becker W., 1963b, ZA 58, 202

Becker W., Stock J., 1954, ZA 43, 1

Bencivenni D., Brocato E., Buonanno R., Castellani V., 1991, AJ 102, 137

Bergbusch P.A., VandenBerg D.A., Infante L., 1991, AJ 101, 6

Bertelli G., Bressan A., Chiosi C., 1992, ApJ 392, 522

Bertelli G., Bressan A., Chiosi C., Angerer K., 1986a, A&AS 66, 191

Bertelli G., Bressan A., Chiosi C., Angerer K., 1986b, in The Ages of star clusters, ed. F.Caputo, Mem.SAI. 57, 427

Bertelli G., Bressan A., Chiosi C., Fagotto F., Nasi E., 1994, A&AS 106, 275

Bertelli G., Bressan A., Chiosi C., Mateo M., Wood P.R., 1993, ApJ 412, 160

Bhatia R.K., 1990, PASJ 42, 757

Böhm-Vitense E., 1992, Introduction to Stellar Astrophysics, Vol.3

Bowers R.L., Deeming T., *Astrophysics II*, 1984, Jones & Barlett Publishers, Inc. Boston

Bressan A., Fagotto F., Bertelli G., Chiosi C., 1993, A&AS 100, 647

Brocato E., Buonnano R., Castellani V., Walker A., 1989, ApJS 71, 25

Burki G., 1977, A&A 57, 135

Caldwell J.A.R., Coulson I., 1985, MNRAS 212, 879

Carraro G., Chiosi C., Bressan A., Bertelli G., 1994, A&AS 103, 375

Cassetella A., Barbero J., Geyer E.H., 1987, ApJS 64, 83

Castellani V., Chieffi A., Straniero O., 1992, ApJS 78, 517

Castellani V., Chieffi A., Straniero O., 1990, ApJS 74, 463

Chevalier C., Ilovaisky S.A., 1991, A&AS 90, 225

Chiosi C., Bertelli G., Meylan G., Ortolani S., 1989, A&A 219, 167

Chiosi C., Maeder A., 1986, ARA&A 24, 329

Chiosi C., Vallenari A., Bressan A., Deng L., Ortolani S., 1994 A&A 293, 710

Collinder P., 1931, Ann. Lund. Obs. 2

Cox A.N., Stewart J.N., 1970a, ApJS 19, 243

Cox A.N., Stewart J.N., 1970b, ApJS 19, 261

Cox A.N., Tabor J.E., 1976, ApJS 31, 271

Crampton D., Hill G., Fisher W.A., 1976, ApJ 204, 502

Fitzgerald M.P., Luiken M., Maitzen H.M., Moffat A.F.J., 1979, A&AS 37, 345

Gorti U., Bhatt H.C., 1995, MNRAS 272, 61

Glushkova E.V., Rasorguev A.S., 1991, Sov. Astron. Lett. 17, 13

Glushkova E., 1993, priv. comm.

Grevesse N., 1991, A&A 242, 488

Hagen G.L., van den Bergh S., 1974, ApJ 189, L103

Hakkila J., Sanders W.L., Schroder R., 1983, A&AS 51, 541

Hannaford P., Lowe R.M., Grevesse N., Noels A., 1992, A&A 259, 301

Harris G.L.M., Fitzgerald M.P.V., Mehta S., Reed B.C., 1993, AJ 106, 1533

Hartigan P., 1993, AJ 105, 1511

Hassan S.M., 1984, in Astronomy with Schmidt-type telescope, p.295

Hatzidimitrou D., Bhatia R.K., 1990, A&A 230, 11

Hawarden T.G., 1971, Observatory 91, 78

Hayford P., 1932, Lick. Obs. Bull. 16, 53

Hiltner W.A., 1956, ApJS 2, 389

Hoag A.A., 1966, Vistas in Astronomy 8, 139

Hoag A.A., 1965, Vistas in Astronomy 8, 139

Hoag A.A., Applequist L. 1965, ApJS 12 215

Hoag A.A., Johnson H.L., Iriarte B., Mitchell R.I., Hallam K.L., Sharpless S., 1961, Publ. US. Nav. Obs. 17, 347

Hron J., Maitzen H.M., Moffat A.F.J., Schmidt-Kaler T., Vogt N., 1985, A&AS 60, 355

Huebener W.F., Merts A.L., Magu N.H., Agro M.F., 1977, Los Alamos Scientific Laboratory Report LA-6760-M

Iben I.Jr., Rood R.T., 1970, ApJ 159, 605

Iglesias C.A., Rogers F.J., Wilson B.G., 1992, ApJ 397, 717

Isserstedt J., Schmidt-Kaler T., 1964, ZA 59, 182

Jacoby G.M., Hunter D.A., Christian C.A., 1984, ApJS 56, 257

Janesick J., Blouke, M., 1987, S&T 74, 238

Jeffers H.M., van den Bos W.H., Greeby F.M., 1963, Publ. Lick Obs. vol. 21, part 2

Johnson H.L., 1966, AR&AA 4, 193

Johnson H.L., 1961, Low. Obs. Bull. 5, N8

Johnson H.L., Morgan W.W., 1953, ApJ 117, 313

Joner M.D., Taylor B.J., 1990, PASP 102, 1004

King I.R., 1979, in Star Clusters, IAU Symp. 85, ed. J.E. Hesser, 137

King I.R., 1971, PASP 83, 199

Kjeldsen K., Frandsen S., 1991, A&AS 87, 119

Kurucz R.L., 1991, in Stellar Atmospheres: Beyond classical models, NATO ASI Series C, Vol. 341

Kurucz R.L., 1979, ApJS 40, 1

Lada , C.J., 1991, in The Physics of Star Formation and Early Stellar Evolution, eds C.J. Lada, N.D. Kylafis, 339

Lada C.J., Young E.T., Greene T.P., 1993, ApJ 408, 471

Liu T., Janes K.A., Bania T.M., 1991, ApJ 377, 141

Liu T., Janes K.A., Bania T.M., 1989, AJ 98, 626

Lupton R.A., Fall S.M., Freeman K.C., Elson R.A.W., 1989, ApJ 347, 201

Lyngå G., 1987, Calalogue of open star cluster data.

Lyngå G., 1979, in Star Clusters, IAU Symp. 85, ed. J.E. Hesser, 13

Maeder A., 1974, A&A 32, 177

Maeder A., Mermilliod J.-c., 1981, A&A 93, 136

Maeder A., Meynet G., 1991, A&AS 89, 451

Maeder A., Meynet G., 1989, A&A 210, 155

Mateo M., 1993, in The globular cluster - Galaxy connection, ASPCS. 48, eds.
    G. H. Smith & J. P. Brodie., 387

Mateo M., 1988, ApJ 331, 281

Mateo M., Hodge P., 1986, ApJ 311, 133

Mathieu R.D., 1986, Highlights Astron. 7, 481

Mathieu, R.D., 1983, Ph.D.Thesis, Univ. of California, Berkeley.

Mayya Y.D., 1993, PhD. Thesis

Mayya Y.D., 1991, JAA 12, 319

McCaughrean M., Rayner J., Zinnecker H., 1991, MmSAI. 62, 715

Mermilliod J.-c., 1994, Calalogue of open cluster data (Computer readable form)

Mermilliod J.-c., 1981, A&A 97, 235

Mermilliod J.-c., 1976, A&A 53, 289

Mermilliod J.-c., Mayor M., 1989 A&A 288, 618

Mills G.A., 1967, J. Obs. 50, 179

Natali F., Natali G., Pompei E., Pedichini F., 1994, A&A 289, 756

Neckel Th., Klare G., 1980, A&AS 42, 251

Pavlovskaya E.D., Filippova A.A., 1989, Sov. Astron. 33, 6

Phelps R.L., Janes K.A., 1994, ApJS 90, 31

Phelps R.L., Janes K.A., 1993, AJ 106, 1870

Penny A.S., Dickens R.J., 1986, MNRAS 220, 845

Piskunov A.E., 1976, Nauch. Informatsii 22, 47

Renzini A., 1987, A&A 188, 49

Renzini A., Fusi Pecci F., 1988, ARA&A 26, 199

Rieke G.H., Lebofsky M.J., 1985, ApJ 288, 618

Robertson J.W., 1974, ApJ 191, 67

Rogers F.J., Iglesias C.A., 1992, ApJS 79, 507

Ruprecht J., 1966, Bull. Astron. Inst. Czech. 17, 33

Sagar R., Myakutin V.I., Piskunov A., Dluzhnevskaya O.B., 1988, MNRAS 234, 831

Sagar R., Pandey A., 1989, A&AS 79, 407

Sagar R., Pati A.K., 1989, Bull. Astron. Soc. India 17, 6

Sagar R., Piskunov A.E., Myakutin V.I., Joshi U.C., 1986, MNRAS 220, 383

Sagar R., Richtler T., 1991, A&A 250, 324

Sagar R., Richtler T., de Boer K.S., 1991, A&AS 90, 387

Salpeter E.E., 1955, ApJ 121, 161

Scalo J.M., 1986, Fundamentals of Cosmic Physics, 11, 1

Schaller G., Schearer D., Meynet G., Maeder A., 1992, A&AS 96, 269

Schild R.E., 1983, PASP 95, 1021

Schild R.E., Romanishin W., 1976, ApJ 204, 493

Schmidt K.H., 1963, Astron. Nach. 287, 41

Schmidt-Kaler T., 1982, in Landolt-Börnstein, Group VI, Vol 2b, Stars and Star Clusters (Berlin: Springer-Verlag)

Seggewis W., Richtler T., 1989, in: Recent Developments of Magellanic Cloud Research: A European Colloquium, eds., K.S.de Boer, F.Spite, G.Stansiska, published by Observatoire de Paris, p.45

Shapley H., 1918, PASP 30, 42

Sowell J.R., 1987, ApJS 64, 241

Spitzer L.Jr., Hart M.H., 1971, ApJ 164, 399

Stetson P.B., 1987, PASP 99, 191

Stetson P.B., Davis L.E., Crabtree D.R., 1989, in CCDs in Astronomy, ASPCS. 8, ed. Jacoby G.H., 289

Stothers R.B., Chin C.-w., 1992, ApJ 390, 136

Stothers R.B., Chin C.-w., 1991, ApJ 381, L67

Strobel A., 1991, ApJ 376, 204

Subramaniam A., Sagar R., Bhatt H.C., 1993, A&A 273, 100

Taff L.G., 1974, AJ 79, 1280

Tarrab I., 1982, A&A 109, 285

Trumpler R.J., 1930, Lick Obs. Bull. 14, 154

Trumpler R.J., 1925, PASP 37, 307

Trumpler R.J., Weaver,H.P., 1953, Statistical Astronomy, Univ. California Press,
    Berkeley, p.358

van den Bergh S., 1991, ApJ 369, 1

van den Bergh S., Lafontaine, A., 1984, AJ 89, 1822

Vallenari A., Chiosi C., Bertelli G., Meylan G., Ortolani S., 1991, A&AS 87, 517

VandenBerg D.A., 1991, in The Formation and Evolution of Star Clusters,
    ASPCS. 13, ed. K.A.Janes, 183

VandenBerg D.A., 1983, ApJS 51, 29

Vasilevskis S., 1962, AJ 67, 699

Visvanathan N., 1985, ApJ 288, 182

Vogt N., Moffat A.F.J., 1972, A&AS 7, 133

Walker A.R., 1987, MNRAS 225, 627

Welch D.L., Mateo M., Côté P., Fischer P., Madore B.F., 1991 AJ 101, 490

Welch D.L., Mclean R.A., Madore B.F., McAlary C.w., 1987, ApJ 321, 162

Wielen R., 1984, in Dynamics of Star Clusters, IAU Symp. 113, eds. J. Goodman
    & P. Hut, 449

Wielen R., 1975, in Dynamics of Stellar Systems, ed. A. Hayli, p.119

Wielen R., 1971, A&A 13, 309.

Young A., Martin A.E., 1973, ApJ 181, 805